ANALYSIS OF METAL-CLAD TM-PASS POLARIZERS USING THE METHOD OF LINES

by

MUHAMMAD AJMAL KHAN

A Thesis Presented to the
DEANSHIP OF GRADUATE STUDIES

In Partial Fulfillment of the Requirements
for the Degree

MASTER OF SCIENCE

IN

ELECTRICAL ENGINEERING

KING FAHD UNIVERSITY
OF PETROLEUM AND MINERALS

Dhahran, Saudi Arabia

February 2001

KING FAHD UNIVERSITY OF PETROLEUM AND MINERALS

DHAHRAN 31261, SAUDI ARABIA

DEANSHIP OF GRADUATE STUDIES

This thesis, written by

MUHAMMAD AJMAL KHAN

under the direction of his Thesis Advisor and approved by his Thesis Committee, has been presented to and accepted by the Dean of Graduate Studies, in partial fulfillment of the requirements for the degree of

MASTER OF SCIENCE IN ELECTRICAL ENGINEERING

THESIS COMMITTEE

Dr. Hussain A. Al – Jamid (Chairman)

Dr. Mahmoud M. Dawoud (Member)

Dr. Husain M. Masoudi (Member)

Department Chairman

Dean of Graduate Studies

Date

Dedicated

to

my beloved mother

and

to the memory of my late father.

Acknowledgements

In the beginning, I must thank Allah the Almighty and the Most Merciful for His blessings throughout my life in general and in the course of this thesis in particular.

I am grateful to King Fahd University of Petroleum and Minerals for supporting my M.S. studies and this research work.

I would like to pay a high tribute to my thesis advisor Dr. Hussain A. Al-Jamid for his invaluable guidance and helpful ideas throughout this thesis work. His appreciation and words of encouragement gave a new life to my efforts in hard times. I am also indebted to him for his valuable time, efforts and his continuous support and inspiration. I am also grateful to him for providing me some of his own computer programs. At the later stages, he helped me a lot in writing my thesis.

I would also like to express my deep appreciation to my committee members, Dr. Husain M. Masoudi and Dr. Mahmoud M. Dawoud, for their constant help and encouragement.

I am thankful to Dr. Samir A. Al-Baiyat, Chairman Electrical Engineering Department for establishing an excellent graduate research laboratory in our department.

I am thankful to my parents for their love, guidance and support.

I am thankful to my friend M. Nadeem for his guidance throughout my thesis work. I am also thankful to my friends Fareed and Ahmar Shafi for their moral support and guidance. I am also thankful to my friend Wasif for the help in LaTeX. Thanks are also due to my friends Rafay, Rais, Shafayat, Junaid, Kashif, Moin, Faisal, Saad, Majid and Atif.

Contents

List of Tables

List of Figures

Nomenclature

English Symbols

$\mathbf{E}$	electric field vector, volts/meter
$\mathbf{H}$	magnetic field vector, amperes/meter
N	diagonal matrix of refractive-index squared at mesh grids
I	identity matrix
B	Phase Parameter
P	time-averaged power per unit length in the y-direction, watts/m
Q	matrix of the eigen-value equation
n	refractive index
k_o	free space wavenumber, radians/meter
h	mesh size, meter
d	thickness of a layer, meter
b	buffer layer thickness, meter
L	length of metal-clad section, meter

L_{gr}	length of grating section in the polarizer, meter
L_S	spacing between metal-clad and grating section, meter
j	$\sqrt{-1}$
t	time, sec
$\mathbf{A} \cdot \mathbf{B}$	scalar (dot) product of vectors **A** and **B**
$\mathbf{A} \times \mathbf{B}$	vector (cross) product of vectors **A** and **B**

Greek Symbols

ψ	general field component of the **E** or **H** field
Ψ	general field component of the **E** or **H** sampled field, column vector
ϵ_o	free space permittivity, $4\pi \cdot 10^{-7}$ Vs/Am
ϵ_r	relative permittivity
μ_o	free space permeability, $8.8541 \cdot 10^{-12}$ As/Vm
μ_r	relative permeability
$\omega = 2\pi f$	angular frequency, rad/sec
α_m	mth modal field coefficient
β	propagation constant. radians/meter
λ	wavelength, meter
∇	nabla operator, $\frac{\partial}{\partial x}\hat{a_x} + \frac{\partial}{\partial y}\hat{a_y} + \frac{\partial}{\partial z}\hat{a_z}$
∇^2	Laplace operator, $\frac{\partial^2}{\partial x^2} + \frac{\partial^2}{\partial y^2} + \frac{\partial^2}{\partial z^2}$

Abbreviations

TE	Transverse Electric

TM	Transverse Magnetic
MOL	Method of Lines
PML	Perfectly Matched Layer
BPM	Beam Propagation Method
ABC	Absorbing Boundary Condition
PER	Polarizer Extinction Ratio
PIL	Polarizer Insertion Loss
FOM	Polarizer Figure of Merit
n_{eff}	Modal Effective Index
λ_B	Bragg Wavelength
Re	Real part of a complex number
Im	Imaginary part of a complex number

Subscripts

A_x, A_y, A_z	x, y, z components of a vector $\mathbf{A}$
$\psi_0, \psi_{\pm 1}, \psi_{\pm 2}$	sample number of field ψ
$\psi_{0\pm}, \psi_{1\pm}, \psi_{2\pm}$	field immediately to the left or to the right of a sample point

Superscript

ψ'	first derivative of ψ
ψ''	second derivative of ψ
ψ'''	third derivative of ψ

ψ''''	fourth derivative of ψ
ψ'''''	fifth derivative of ψ
ψ''''''	sixth derivative of ψ
β''	mode attenuation, N_p/μm
${n_{eff}}'$	real part of the effective index
${n_{eff}}''$	imaginary part of the effective index
A^*	complex conjugate of A

THESIS ABSTRACT

Name: MUHAMMAD AJMAL KHAN

Title: ANALYSIS OF METAL-CLAD TM-PASS POLARIZERS USING THE METHOD OF LINES

Degree: MASTER OF SCIENCE

Major Field: ELECTRICAL ENGINEERING

Date of Degree: FEBRUARY 2001

The polarizers are important elements of integrated optical circuits. In this research work, two types of metal-clad TM-pass polarizers, transmission mode polarizer and reflection mode polarizer, are studied. In the first type, the TM polarized waves are transmitted with low-loss, while TE polarized wave are transmitted with very high loss. The second type of polarizer has corrugations in its structure. It functions by reflecting TM waves with low-loss, while the reflected TE polarized waves are highly attenuated. The reflection and transmission spectra of the reflection mode polarizer are calculated for different high-index buffer layer thicknesses, different number of grating periods, different groove depths and different length of metal-clad section. The Method of Lines (MOL) with the Cascading and Doubling Algorithm is applied to model the multi-layer waveguide structure with periodic corrugations. Higher-order approximations of the second derivative ($\partial^2/\partial x^2$) operator with appropriate interface conditions are used. The Perfectly Matched Layer (PML) absorber is used to absorb the radiated fields due to the presence of longitudinal discontinuities.

Keywords: Optical Waveguides, Waveguide Gratings, Metal-clad Waveguides, Method of Lines (MOL), Higher-Order Approximations, Perfectly Matched Layer (PML), TM-Pass Polarizer, TE-Pass Polarizer, Reflection Mode Polarizer, Transmission Mode Polarizer.

Master of Science Degree

King Fahd University of Petroleum and Minerals, Dhahran.
February 2001

الاسم: محمد أجمل خان
عنوان الرسالة: دراسة مستقطب الموجة المغطى بمعدن باستخدام طريقة الخطوط
الدرجة: ماجستير في الهندسة الكهربائية

تعتبر المستقطبات إحدى العناصر المهمة في مجال الدوائر البصرية المصغرة. نقوم في هذا البحث بدراسة نوعان من المستقطبات المغطاة بمعدن والتي تقوم بالسماح للموجات الكهرومغناطيسية ذات المجال المغناطيسي العرضي (Trasnverse Magnetic, TM) بالنفاذ بينما لا تسمح بنفاذ الموجات ذات المجال الكهربائي العرضي (Transverse Electric, TE) . النوع الأول من هذه المستقطبات يقوم بنقل موجات TM بخسارة صغيرة بينما يقوم بنقل موجات TE بخسارة عالية جداً. أما النوع الثاني من المستقطبات فانه يحتوي على حزوز بالإضافة للمعدن. هذا النوع من المستقطبات يسمح بارتداد موجات TM بخسارة صغيرة بينما يقوم برد موجات TE بخسارة عالية جداً. بالنسبة للنوع الثاني من المستقطبات نقوم بحساب طيف المرور وكذلك طيف الارتداد في الحالات التالية: تغير سمك الطبقة ذات معامل الانكسار العالي و تغير العدد الكلي للحزوز وتغير عمق الحزوز وكذلك تغير طول الجزء المغطى بالمعدن.
أما الطريقة الرقمية المستخدمة في هذه الحسابات فهي مبنية على طريقة الخطوط (Method of Lines, MOL) بالإضافة إلى طريقة التجميع والمضاعفة وذلك للتقليل من الجهد الحسابي المطلوب من الحاسب الآلي. بالإضافة إلى ما سبق ذكره فإننا قمنا باستخدام تقريب عالي الدرجة لحل معادلة الموجة بطريقة رقمية مع استخدام طبقة ماصة مثالية للتخلص من الإشعاع الكهرومغناطيسي الناجم عن وجود انقطاع فجائي في موجه الموجة.

Chapter 1

Introduction

1.1 Integrated Optics

In the late 1960's the concept of Integrated Optics emerged to describe circuits in which the signals that undergo processing and transmission were optical beams rather than electrical currents [1, 2]. Integrated optics is primarily based on the fact that light beams can propagate through and can be contained by very thin layers (films) of transparent materials. By combining such layers and shaping them into appropriate configurations, integrated optics technology has realized a large variety of components which can perform a wide range of operations on optical waves. Thus, light can be guided, modulated, deflected, filtered, radiated into space, or by using laser action, it can be generated within thin-film structure. Two important technical developments gave impetus to this new technology, these are the development of the laser as a source of light that can be manipulated to carry information and the

development of the optical fiber as a viable low-loss transmission medium.

Integrated optics gave rise to a new generation of opto-electronic systems in which the familiar wires and cables are replaced by light guiding optical fibers, and conventional integrated circuits are replaced by optical integrated circuits (OIC). Some advantages of integrated optic systems are reduced weight, increased bandwidth or multiplexing capability, resistance to electromagnetic interference and low loss signal transmission. When the basic components: source, waveguide and detector are all integrated on a single substrate, we have a monolithic OIC. Compound semiconductors such as gallium arsenide ($GaAs$) and indium phosphide (InP) are the candidate substrates for this type of IC. When the components are made of different materials, we have a hybrid OIC. For example, the source and detector are made of compound semiconductors such as silicon (Si) and the waveguide is made of dielectric materials such as lithium niobate ($LiNbO_3$) or silica (SiO_2).

1.2 Optical Waveguides

An optical waveguide is a device which can confine light energy and transport it from one region of space to another with low power loss. A well-known and important example of an optical waveguide is the optical fiber which is a cylindrical waveguide. Usually, total-internal-reflection (TIR) phenomenon is utilized to design such an arrangement. Another example is the dielectric slab waveguide which has a middle layer of high refractive index surrounded by layers of lower refractive indices on both

sides. Thus, electromagnetic energy can be trapped inside the high index layer (core) by TIR phenomenon on both sides of the core and can be transported over a long distance. These waveguides could also have a multi-layer structure with more than three layers including metallic layers. The refractive index profile may be uniform (step-index) or continuously varying (graded-index) in each layer.

1.3 Waveguide Gratings

Periodic patterns (i.e. gratings) fabricated in optical waveguide structures are one of the most important elements of OIC. They can be used as passive components (e.g. couplers, deflectors, reflectors, wavelength filters, and mode converters), and they have many applications to functional devices for optical wave control. The operation of devices based on gratings depends on electromagnetic wave coupling through phase matching of different propagating modes by the grating region. Figure 1.1 shows a waveguide grating structure, with grating period T and height h. This structure is typically composed of hundreds or thousands of periods. Each discontinuity or period causes a small reflection of the field and the total reflected field is the phasor sum of individual reflections. The grating parameters T, h_g and total number of grating periods affect the power reflection and transmission spectra of the structure.

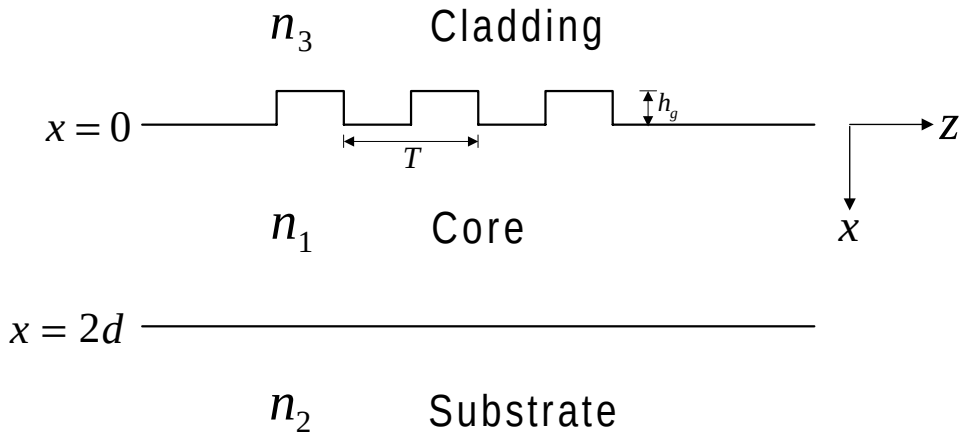

Figure 1.1: Waveguide Grating Structure

1.4 Metal-Clad Waveguide

The basic unit that connects the various components of the optical circuits such as sources, detectors, modulators, etc. is the optical waveguide. The optical waveguide performs the function of the metallic strip in electronic circuits, and a rigorous understanding of the operation of the waveguide is essential to the understanding of the operation of other optical circuit components. In addition to this, the use of metals, as well as dielectrics, in the fabrication of optical waveguides offers novel applications that depend on the way different modes and polarizations behave in the presence of metals, in particular on the influence of the metals on the absorption loss of the different modes and polarizations. Early investigations of the effect of metallic layers on the propagation losses in planar film waveguides are reported in the references [3, 4, 5, 6, 7, 8].

Metal-clad waveguides are important in integrated optics because of the variety

of applications they offer. Some of the important devices which can be potentially configured around such metal-clad waveguides are photodetectors, modulators, switches, polarization selectors and wavelength filters [9, 10, 11]. In these applications it is important to determine the absorption loss of TE and TM waves. The features of interest are the loss dependence on mode order and the differential TE-TM mode attenuation [12, 13, 14, 15, 16, 17]. A typical three-layer metal-clad waveguide is shown in figure 1.2. In this structure TM modes are more lossy than TE modes [3, 4].

In recent years there has been interest in four-layer metal-clad waveguides in which a buffer layer is introduced between the metal and core layers. A typical four-layer metal-clad waveguide with buffer is shown in figure 1.3. The extinction ratio between the TE and TM modes for either a TE-pass or a TM-pass configuration can be greatly enhanced through appropriate combination of buffer layer and metal layer thicknesses. Some experimental results concerning the role of an intermediate dielectric buffer layer between the waveguide core and its metal cladding are available in the literature. For example, introduction of a low-index buffer layer has been shown to lead to enhanced attenuation of the TM modes for a certain critical buffer layer thickness [18, 19, 20, 21]. Similarly it has been shown that a buffer layer of relatively high refractive index results in causing the TE mode to be more lossy than the TM mode [21, 22, 23].

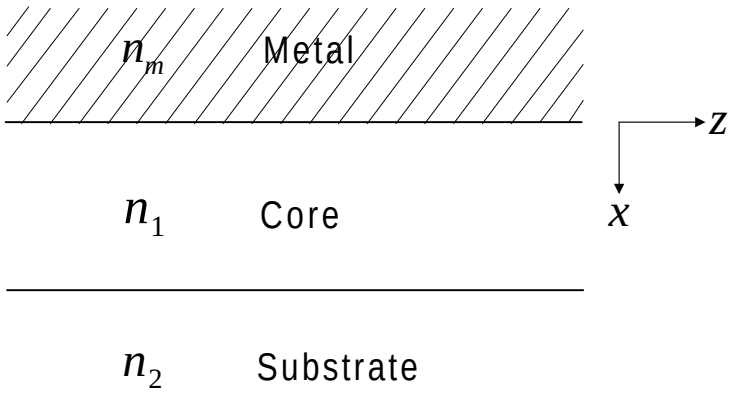

Figure 1.2: Three Layer Metal-Clad Waveguide

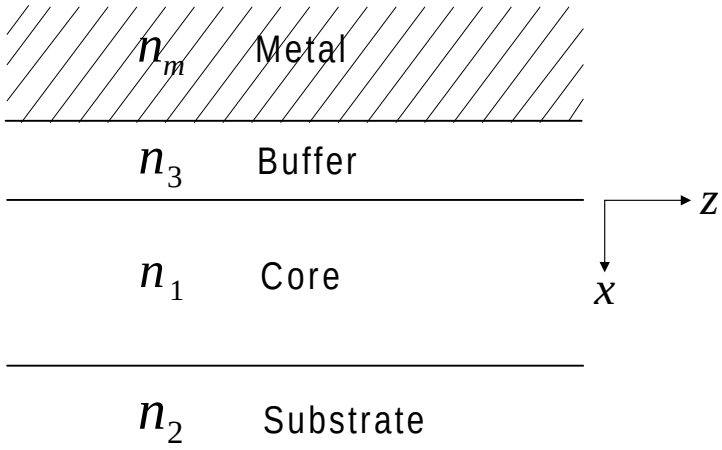

Figure 1.3: Metal-Clad Waveguide with a Buffer Layer

1.5 Method of Lines and other Numerical Methods

Optical waveguide problems that can be analytically solved are limited to simple structures and devices. For complicated devices, either analytical solutions do not exist in closed form or even if they exist, they are difficult to obtain. Several numerical methods have been developed to model longitudinally-varying waveguide structures. Among these methods are the Beam Propagation Method (BPM) [24, 25], Finite Difference Time Domain (FDTD) method [26], Collocation Method [27], Mode Matching Method (MMM) [28] and Method of Lines (MOL) [29, 30]. A good review of these and some other numerical methods is given in [31, 32].

The basic BPM can not be used to model waveguide discontinuities due to its inability to account for backward reflected waves at a longitudinal discontinuity. It is also an approximate method which requires the wave to be paraxial [28]. The FFT-BPM version is also known to be inefficient in problems having large index discontinuities in the transverse direction. Hence, it is good only for low contrast waveguides and for gradual bends in optical waveguides.

The FDTD method can be used to model longitudinal discontinuity problems but it requires the whole structure to be discretized and stored in computer memory. Hence to model long gratings, the FDTD requires excessively large memory. Also this is a time-domain method and the algorithm should be run for considerable amount of time to get steady state response and some post-processing may be

necessary. At any rate this method is gaining popularity due to both its ease of understanding and implementation.

The Collocation Method is based on the Helmholtz equation and does not require the Fresnel approximation for its implementation [33]. In this method, the field is expanded into a set of suitable orthogonal basis functions $\phi_n(x)$ in the transverse direction. The choice of basis functions depend on the problem geometry. Since these basis are not eigen-modes of the problem, we need a larger number of basis functions to achieve accurate results.

The Mode Matching Method (MMM) or Eigenmode Propagation Method (EPM) employs eigen-mode expansion of the field, in which the discrete guided modes, the continuous radiation modes and continuous evanescent modes are taken as basis [34]. The choice of these basis functions is problem dependent. The reflected and transmitted fields are solved through a mode matching procedure.

The Method of Lines (MOL) is a semi-analytical technique used to solve partial differential equations (PDE). For an n-independent variable PDE, only (n-1) variables are discretized to obtain a system of ordinary differential equations (ODE) [35, 36] in the remaining independent variable, which can be solved analytically. This results in a higher numerical accuracy due to the reduced number of discretized variables, less computational time due to the analyticity in the remaining independent variable and smaller memory requirements as we do not need to discretize in the analytical direction. Instead of approximating the field by a series expansion of basis functions (as done in the Mode Matching Method), the second-derivative

operator is approximated by a finite-difference scheme. The resulting matrix ODE is solved to find the eigenmodes of the structure. This method can account for backward reflected field due to longitudinally inhomogenous structures, which permits the analysis of planar waveguides having longitudinal discontinuities.

1.6 Statement of the Problem

The Method of Lines is chosen for the analysis of waveguide structures in this thesis, because it is a rigorous method and which can model high-contrast waveguides including metals. It can account for the reflected field at sudden longitudinal waveguide discontinuities, junctions and bends. The basic three-point central-difference approximation of the second derivative operator, which is used in the Method of Lines gives relatively poor estimate of the modal fields and effective indices of a multi-layer waveguide structure. Thus we will use higher-order approximations of the second derivative operator with appropriate interface conditions to improve the accuracy while using fewer discretization lines to sample the problem space. This helps to reduce the computational time required to obtain stationary solutions as well as the analysis of multiple discontinuity problems. Another improvement to MOL is achieved by using a non-uniform meshing scheme to reduce the number of required sampling points. When radiative fields are involved in the problem, we need to terminate the problem space by an appropriate absorbing boundary condition to model an infinite space. In this thesis, a Perfectly-Matched-Layer (PML)

[37] is used as an absorbing layer. In order to model a grating having many periods, the basic method is to match the tangential fields at each longitudinal discontinuity and to express unknown field values in each region in terms of the known incident field. This layer-by-layer procedure is very slow and requires a large memory in order to store the intermediate results. Our aim in this thesis is to implement a cascading and doubling algorithm which is a fast and memory efficient algorithm to model long periodic gratings taking advantage of the periodic nature of the grating [38]. MOL will be used to calculate the modal fields and effective indices of the metal-clad waveguide.

In this thesis, we will analyze two types of TM-pass metal-clad polarizers. The first polarizer is a TM-pass transmission mode polarizer and the second one is a reflection mode polarizer. We will study the insertion loss and extinction ratio of the first type of TM-pass polarizer. We will also study the effect of both the refractive index of the high-index buffer layer and its thickness.

For the second type of polarizer, we will use a grating in tandem with the first structure to achieve a reflection mode TM-pass polarizer. The spectral response of this device will be calculated for different high-index buffer thicknesses, different number of grating periods, different groove depths and different length of the polarizer. A conclusion will then be drawn about the performance of the second device. In this work, both TE and TM modes will be analyzed and a general purpose software will be developed.

1.7 Thesis Organization

This thesis is organized starting with a review of the basic slab waveguide theory and ending with the analysis of the metal-clad TM-pass polarizers. In this thesis, we present the analysis of two types of TM-pass metal-clad polarizers. The first polarizer is a TM-pass transmission mode polarizer (discussed in chapter 5) and the second one is a reflection mode polarizer (discussed in chapter 7). To our knowledge, the second type of polarizer is novel and it has not been studied previously.

Chapter one, being an introductory chapter, briefly enumerates the historical background of integrated optical systems. The waveguide gratings and metal-clad waveguides are also discussed.

The fundamental component of guided-wave opto-electronic devices is the optical waveguide which supports the optical field. That is why, the theory of the dielectric slab waveguides is presented in chapter two. The second chapter starts by introducing Maxwell's equations. By using Maxwell's equations, the wave equation is obtained and subsequently used to analyze the stationary modes of a slab waveguide. The same chapter also includes discussions of the mode number, mode cut-offs and weakly-guiding waveguide.

In chapter three, the numerical Method of Lines (MOL) is introduced. The necessary interface conditions are discussed for multi-layer structures. Besides the three-point central-difference approximation of the second derivative operator, the five-point and seven-point approximations with appropriate interface conditions are

discussed. Exact results are compared to the numerical results based on the MOL in order to establish the accuracy of the MOL.

In chapter 4, the implementation and importance of absorbing boundary conditions, Mur's absorber and Perfectly Matched Layer (PML) absorber, are explained. The MOL is subsequently used to model single and multiple waveguide discontinuities.

In chapter 5, the metal-clad waveguide without a buffer layer and with a buffer layer is described and analyzed using the MOL. The effective indices and the modal fields for this waveguide structure are calculated and compared with exact results. The effect of the buffer layer refractive index and thickness is explained. The calculation of modal power and modal coefficients is presented. The performance of TE-pass and TM-pass polarizers is evaluated.

In chapter 6, the Cascading and Doubling Algorithm is described to model long gratings having thousands of periods. This algorithm is started by first finding the equivalent reflection and transmission matrices of two discontinuities joined together from their individual reflection and transmission matrices. This procedure is repeated to find the total reflection and transmission matrices of a grating. As it will be seen later, the cascading and doubling algorithm allows us to model 2^n periods in n steps. This algorithm gives us improved speed and smaller memory requirement as compared to other methods.

In chapter 7, the TM-pass reflection mode polarizer which has periodic corrugations in addition to the metal-clad section, is modeled using the MOL and the

Cascading and Doubling Algorithm. To our knowledge, the reflection mode polarizer is novel and it has not been studies previously. The modal spectral reflectivity and transmissivity of the reflection mode polarizer are calculated for different high-index buffer thicknesses, different number of grating periods, different groove depths and different length of metal-clad section. At the end of the chapter, suggested parameters for obtaining a short polarizer length are recommended.

In the last chapter, this work presented is summarized along with conclusions and few possible future extensions are proposed.

Chapter 2

Dielectric Slab Optical Waveguide

2.1 Introduction

Dielectric slab waveguides are the simplest optical waveguiding structures. Because of their simple geometry, guided and radiation modes can be described by simple mathematical expressions. The study of slab waveguides is important in gaining understanding of the wave-guiding properties of more complicated dielectric waveguides. It must be noted, however, that slab waveguides are not only useful as models for more general types of optical waveguides but they are actually employed for light guidance in integrated optical circuits [39, 40, 41, 42, 43].

In this chapter, the theory of planar dielectric waveguides will be explained. Starting with Maxwell's equations, we will obtain the details of the propagation of optical modes in a slab waveguide.

2.2 Maxwell's Equations

The propagation of electromagnetic waves in dielectric media is governed by Maxwell's equations which are [40, 41]:

$$\nabla \times \mathbf{E} + \frac{\partial \mathbf{B}}{\partial t} = 0 \tag{2.1}$$

$$\nabla \times \mathbf{H} - \frac{\partial \mathbf{D}}{\partial t} = \mathbf{J} \tag{2.2}$$

$$\nabla \cdot \mathbf{B} = 0 \tag{2.3}$$

$$\nabla \cdot \mathbf{D} = \rho \tag{2.4}$$

where

$\mathbf{E}$ is the electric field strength.

$\mathbf{H}$ is the magnetic field strength.

$\mathbf{B}$ is the magnetic flux density.

$\mathbf{D}$ is the electric displacement.

$\mathbf{J}$ is the electric current density.

ρ is the electric charge density.

The basic four quantities $\mathbf{E}$, $\mathbf{B}$, $\mathbf{H}$ and $\mathbf{D}$ are vectors in the three-dimensional space. They are generally functions of both space and time.

2.3 Dielectric Slab Waveguide

Figure 2.1 shows a schematic diagram of a three-layer planar waveguide. The core region of the waveguide, which is also called the film, is assumed to have refractive

index n_1. The film is deposited on a layer called substrate which has a refractive index n_2. The cladding on the film is called superstrate and it has a refractive index n_3.

The behavior of dielectric waveguides can be explained with the aid of the three-layer model shown in figure 2.2. As can be seen, this figure is a longitudinal cross-section of the slab waveguide shown in figure 2.1. In figure 2.2, we assume that the dimension of the slab along the y-axis is considerably larger than its dimension along the x-axis and that no material or field variation exist along the y-direction. Such a waveguide supports a finite number of guided modes as well as an infinite number of unguided radiation modes. In order to achieve mode guidance, it is necessary that n_1 be greater than n_2 and n_3 that is $n_1 > n_2 \geq n_3$. If $n_2 = n_3$, the slab waveguide is said to be symmetric. For the case of figure 2.2 where n_2 is different from n_3, the slab waveguide is asymmetric. For a symmetric waveguide, the guided modes are either even or odd in their field distributions, as shown in figure 2.3. This waveguide can be considered to constitute a limiting case of an asymmetric waveguide. As will be analytically shown in the subsequent sections of this chapter, the number of guided modes that can be supported by a slab waveguide depends on the thickness $2d$, the wavelength λ and the indices of refraction, n_1, n_2 and n_3.

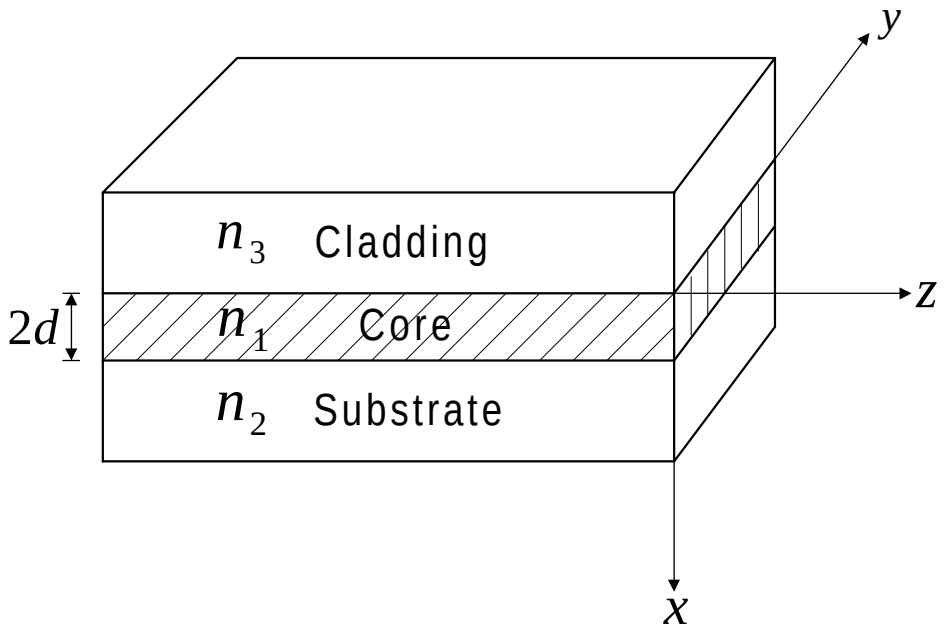

Figure 2.1: Schematic Diagram of A Dielectric Slab Waveguide

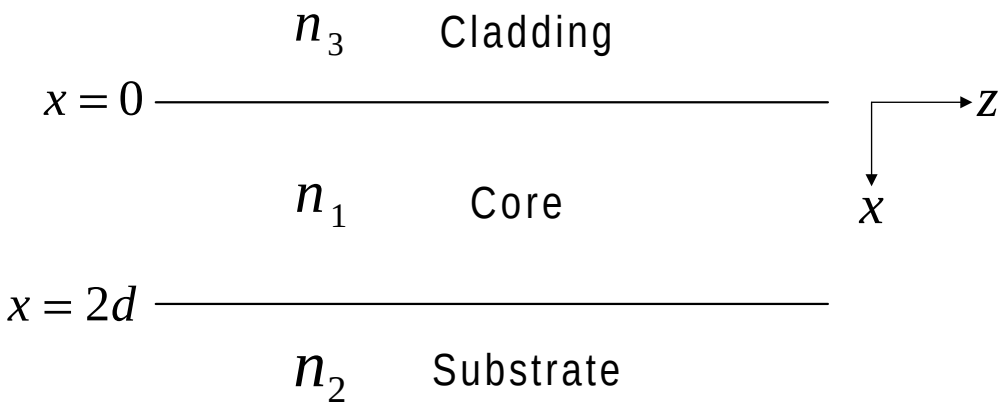

Figure 2.2: A Three-Layer Dielectric Slab Waveguide

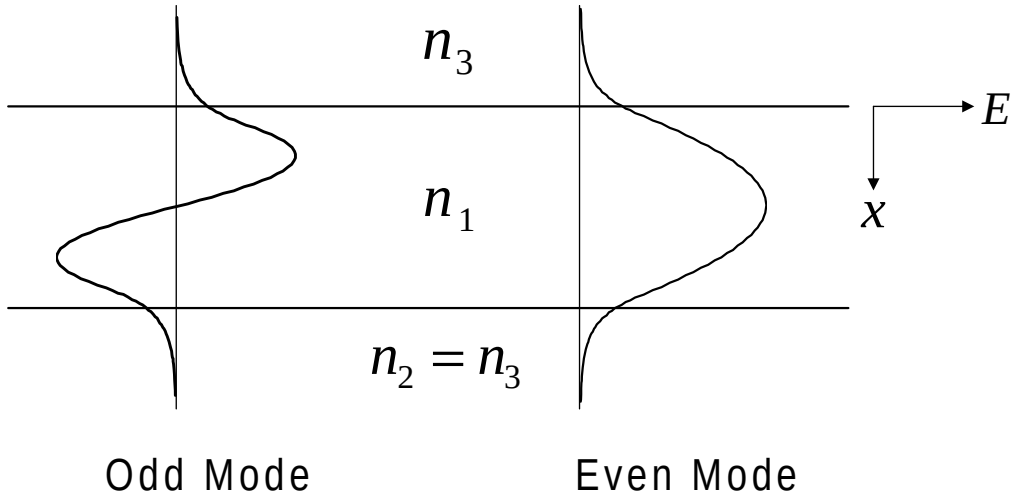

Figure 2.3: Electric Field Distribution in a Symmetric Slab Waveguide

2.4 The Wave Equation for a Slab Waveguide

Consider the asymmetric slab waveguide shown in figure 2.2. Maxwell's equations can be written in terms of the refractive index n_i $(i = 1, 2, 3)$ of the three layers and by assuming that the material of each layer is non-magnetic and isotropic, that is $\mu = \mu_0$ and ϵ is a scalar, we have [39, 40, 41]:

$$\nabla \times \mathbf{E} = -\mu_o \frac{\partial \mathbf{H}}{\partial t} \tag{2.5}$$

$$\nabla \times \mathbf{H} = n_i^2 \epsilon_o \frac{\partial \mathbf{E}}{\partial t} \tag{2.6}$$

$$\nabla \cdot \mathbf{E} = 0 \tag{2.7}$$

$$\nabla \cdot \mathbf{H} = 0 \tag{2.8}$$

To obtain the above equations, we used $\mathbf{D} = \epsilon \mathbf{E} = n^2 \epsilon_o \mathbf{E}$, $\mathbf{B} = \mu_o \mathbf{H}$, $\mathbf{J} = 0$, and

$\rho = 0$ in equations 2.1 to 2.4.

If we apply the curl operator to equation 2.5, we get:

$$\nabla \times \nabla \times \mathbf{E} = -\mu_o \nabla \times \frac{\partial \mathbf{H}}{\partial t} \tag{2.9}$$

$$= -\mu_o n_i^2 \epsilon_o \frac{\partial^2 \mathbf{E}}{\partial t^2} \tag{2.10}$$

where equation 2.6 has been used to eliminate $\mathbf{H}$. To simplify further, we use the vector identity

$$\nabla \times \nabla \times \mathbf{A} = \nabla(\nabla \cdot \mathbf{A}) - \nabla^2 \mathbf{A} \tag{2.11}$$

where $\mathbf{A}$ is an arbitrary vector field. Using equations 2.7 and 2.11, equation 2.10 can be simplified to:

$$\nabla^2 \mathbf{E} = \mu_o \epsilon_o n_i^2 \frac{\partial^2 \mathbf{E}}{\partial t^2} \tag{2.12}$$

Writing the above equation in phasor notation (assuming a time-harmonic field of the form $e^{-j\omega t}$) we obtain [39, 40]:

$$\nabla^2 \mathbf{E} + k_o^2 n_i^2 \mathbf{E} = 0 \tag{2.13}$$

which is the familiar three-dimensional vector wave equation for a uniform dielectric with refractive index n_i. Here k_o is the free-space wave number given by $k_o = \omega\sqrt{\mu_o \epsilon_o}$. The electric field vector $\mathbf{E}$ in equation 2.13 is a phasor quantity, which is complex and has both a magnitude and a phase. In addition, $\mathbf{E}$ is in general a function of space co-ordinates x, y, z and angular frequency ω. $\mathbf{E}$ is independent of time since the time dependence has been removed by the phasor transformation.

We may simplify equation 2.13 by assuming that the structure is uniform in the y-direction (see figure 2.1) and extends to infinity in the y-direction. This allows us to assume that the field $\mathbf{E}$ is also uniform in this direction. Thus $\frac{\partial}{\partial y}$ is replaced by zero. If we further assume a z-dependence of the form $e^{j\beta z}$, with β as the longitudinal propagation constant, equation 2.13 is simplified and takes the form:

$$\frac{d^2\mathbf{E}}{dx^2} + (k_o^2 n_i^2 - \beta^2)\mathbf{E} = 0 \tag{2.14}$$

The above equation is known as Helmholtz equation. In this case $\mathbf{E}$ is a function of x only and the equation is a second order ordinary differential equation. The propagation constant β can be expressed as $\beta = k_o n_{eff}$, where n_{eff} is called the effective index. The field of a slab waveguide is in general a superposition of Transverse Electric (TE) polarized field and Transverse Magnetic (TM) polarized field. The field components of the two polarizations are H_x, E_y and H_z for TE-polarized waves and E_x, H_y and E_z for TM-polarized waves.

2.5 Transverse Electric (TE) Guided Modes

By using equation 2.14, the TE scalar wave equation for the three waveguide regions takes the following form:

$$\frac{d^2E_y}{dx^2} - r^2 E_y = 0 \quad , \quad x \leq 0 \tag{2.15}$$

$$\frac{d^2E_y}{dx^2} + q^2 E_y = 0 \quad , \quad 0 \leq x \leq 2d \tag{2.16}$$

$$\frac{d^2E_y}{dx^2} - p^2 E_y = 0 \quad , \quad x \geq 2d \tag{2.17}$$

where $r^2 = \beta^2 - k_o^2 n_3^2$, $q^2 = k_o^2 n_1^2 - \beta^2$ and $p^2 = \beta^2 - k_o^2 n_2^2$. For guided modes, we require that the power to be confined largely to the central region of the guide and no power escapes from the structure. The form of equations 2.15, 2.16 and 2.17 then implies that this requirement will be satisfied for an oscillatory solution in the core region ($q^2 \geq 0$) with evanescent tails in the cladding and substrate regions ($r^2, p^2 \geq 0$) (see figure 2.4). Assuming $n_1 > n_2 \geq n_3$, it is straightforward to show that for guided modes, the possible range of β is given by $k_o n_1 \geq \beta \geq k_o n_2 \geq k_o n_3$.

From equation 2.5, the other field components of the TE modes are obtained in terms of E_y as follows:

$$H_x = -\frac{\beta}{\omega \mu_o} E_y \tag{2.18}$$

$$H_z = -\frac{j}{\omega \mu_o} \frac{\partial E_y}{\partial x} \tag{2.19}$$

Thus, for guided modes the solution of E_y in the three regions is [39, 40]:

$$E_y = \begin{cases} A e^{rx} & , x \leq 0 \\ A\cos(qx) + B\sin(qx) & , 0 \leq x \leq 2d \\ \left(A\cos(2dq) + B\sin(2dq)\right) e^{-p(x-2d)} & , x \geq 2d \end{cases} \tag{2.20}$$

where A and B are constants. By examining equation 2.20, the boundary condition on E_y is satisfied by its continuity at both $x = 0$ and $x = 2d$. The other tangential field component to the waveguide interfaces, namely H_z, must also be continuous at

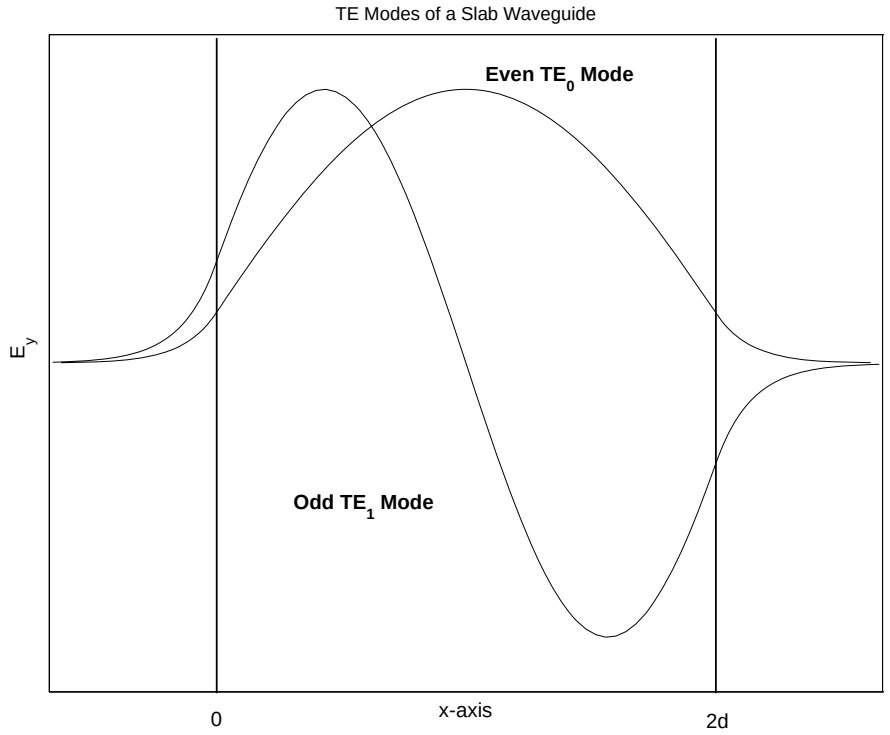

Figure 2.4: TE Mode Patterns of a Slab Waveguide

these interfaces. From equations 2.19 and 2.20, we have:

$$H_z = \frac{-j}{\omega\mu_o}\begin{cases} rAe^{rx} & ,x \leq 0 \\ q\left(-A\sin(qx) + B\cos(qx)\right) & ,0 \leq x \leq 2d \\ -p\left(A\cos(2dq) + B\sin(2dq)\right)e^{-p(x-2d)} & ,x \geq 2d \end{cases} \tag{2.21}$$

The continuity condition of H_z yields two equations. One at $x = 0$ and the second at $x = 2d$, that is:

$$rA = qB \tag{2.22}$$

and

$$q\left(-A\sin(2dq) + B\cos(2dq)\right) = -p\left(A\cos(2dq) + B\sin(2dq)\right) \tag{2.23}$$

Eliminating the ratio A/B from these equations yields [39, 40]:

$$\tan(2dq) = \frac{q(p+r)}{q^2 - pr} \tag{2.24}$$

This is the eigenvalue equation for the TE modes of the asymmetric slab waveguide. Equation 2.24 is an implicit relationship which involves the wavelength, refractive indices of the layers and core thickness as known quantities, and the propagation constant β as the only unknown quantity. It can be shown that only certain discrete values of β can satisfy the above equation, so this waveguide will only support a *discrete* set of guided modes. The allowed values of β can be found from this equation using numerical or graphical methods. After evaluating β, the previous equations are used to obtain the modal field in each layer. The symmetric waveguide ($n_2 = n_3$) can only support modes with even or odd electric field patterns. In this case it can be easily shown that the eigen-value equation 2.24 reduces to ($p = r$):

$$\tan(2dq) = \frac{2pq}{q^2 - p^2} \tag{2.25}$$

An example of the field pattern of the TE modes for a three-layer slab waveguide is given in figure 2.4.

2.6 Transverse Magnetic (TM) Guided Modes

The wave equation for this polarization is obtained in terms of the magnetic field component H_y as:

$$\frac{d^2 H_y}{dx^2} - r^2 H_y = 0 \quad , \quad x \leq 0 \tag{2.26}$$

$$\frac{d^2H_y}{dx^2} + q^2 H_y = 0 \quad , \quad 0 \leq x \leq 2d \tag{2.27}$$

$$\frac{d^2H_y}{dx^2} - p^2 H_y = 0 \quad , \quad x \geq 2d \tag{2.28}$$

From equation 2.6, the other field components of the TM modes are obtained in terms of H_y as:

$$E_x = \frac{\beta}{\omega n_i^2 \epsilon_o} H_y \tag{2.29}$$

$$E_z = \frac{j}{\omega n_i^2 \epsilon_o} \frac{\partial H_y}{\partial x} \tag{2.30}$$

Thus, the solution of H_y in the three regions for the guided modes is [39, 40]:

$$H_y = \begin{cases} Ce^{rx} & , x \leq 0 \\ C\cos(qx) + D\sin(qx) & , 0 \leq x \leq 2d \\ \left(C\cos(2dq) + D\sin(2dq)\right) e^{-p(x-2d)} & , x \geq 2d \end{cases} \tag{2.31}$$

where C and D are constants. The field component E_z is obtained from equations 2.30 and 2.31 as follows:

$$E_z = \frac{j}{\omega\epsilon_o} \begin{cases} \frac{rC}{n_3^2} e^{rx} & , x \leq 0 \\ \frac{q}{n_1^2}\left(-C\sin(qx) + D\cos(qx)\right) & , 0 \leq x \leq 2d \\ \frac{-p}{n_2^2}\left(C\cos(2dq) + D\sin(2dq)\right) e^{-p(x-2d)} & , x \geq 2d \end{cases} \tag{2.32}$$

Continuity of E_z at $x = 0$ and $x = 2d$ leads to:

$$\frac{rC}{n_3^2} = \frac{qD}{n_1^2} \tag{2.33}$$

and

$$\frac{q}{n_1^2}\left(-C\sin(2dq)+D\cos(2dq)\right)=\frac{-p}{n_2^2}\left(C\cos(2dq)+D\sin(2dq)\right) \tag{2.34}$$

Eliminating the ratio C/D from these two equations results in [39, 40]:

$$\tan(2dq)=\frac{qn_1^2\left(n_3^2p+n_2^2r\right)}{n_2^2n_3^2q^2-n_1^4pr} \tag{2.35}$$

which is the eigenvalue equation for TM modes of an asymmetric slab waveguide. An example of the TM mode patterns for a symmetric slab waveguide is given in figure 2.5. As evident from the figure, H_y is continuous across a layer interface but its derivative is discontinuous there, causing a sudden change in the slope of H_y there.

2.7 Mode Numbers and Cut-Offs

The notation TE_N (and similarly TM_N) is used to refer to a mode possessing N nodes in the distribution of E_y for TE modes and H_y for TM modes. The value of N can be obtained by taking the argument of the tangent in the eigenvalue equations 2.24 and 2.35 to be $(2dq-N\pi)$. Since $n_1>n_2>n_3$, the cut-off condition is given by [39]:

$$\beta=k_on_2 \tag{2.36}$$

This corresponds to loss of optical confinement due to loss of exponential decay away from the waveguide in the substrate. The resultant effect is a field-spreading throughout the substrate region.

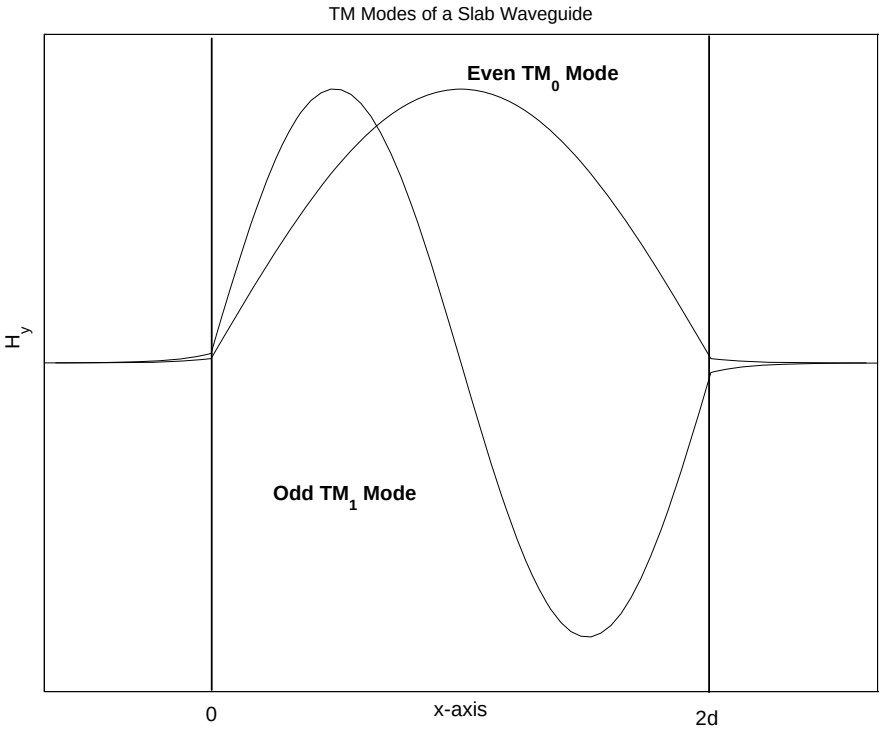

Figure 2.5: TM Mode Patterns of a Slab Waveguide

The cut-off conditions for TE_N and TM_N modes can be found by using the above definitions for the mode numbers and cut-offs. Substituting equation 2.36 into equation 2.24 along with the appropriate expressions for p, q, r at cut-off, the cut-off condition for the TE modes is stated as [39]:

$$\tan(2dk_c(n_1^2 - n_2^2)^{1/2} - N\pi) = \left(\frac{n_2^2 - n_3^2}{n_1^2 - n_2^2}\right)^{1/2} \tag{2.37}$$

where k_c corresponds to the cut-off wave number for TE_N. In terms of the normalized frequency (v), given by:

$$v = k_o d(n_1^2 - n_2^2)^{1/2} \tag{2.38}$$

the cut-off value v_c for the TE_N mode is [39]:

$$v_c = \frac{1}{2}\tan^{-1}\left[\left(\frac{n_2^2 - n_3^2}{n_1^2 - n_2^2}\right)^{1/2}\right] + \frac{N\pi}{2} \tag{2.39}$$

where $\tan^{-1}$ is restricted to the range $0 - \pi/2$. Equation 2.39 can be used to obtain M, the number of TE guided modes and is found to be [39]:

$$M = \left\{\frac{1}{\pi}\left(2v - \tan^{-1}\left[\left(\frac{n_2^2 - n_3^2}{n_1^2 - n_2^2}\right)^{1/2}\right]\right)\right\}_{int} \tag{2.40}$$

where the subscript *int* indicates the next largest integer.

The corresponding cut-off condition and number of guided TM modes are given as follows [39]:

$$v_c = \frac{1}{2}\tan^{-1}\left[\left(\frac{n_1}{n_3}\right)^2\left(\frac{n_2^2 - n_3^2}{n_1^2 - n_2^2}\right)^{1/2}\right] + \frac{N\pi}{2} \tag{2.41}$$

$$M = \left\{\frac{1}{\pi}\left(2v - \tan^{-1}\left[\left(\frac{n_1}{n_3}\right)^2\left(\frac{n_2^2 - n_3^2}{n_1^2 - n_2^2}\right)^{1/2}\right]\right)\right\}_{int} \tag{2.42}$$

Chapter 3

The Method of Lines

3.1 Introduction

Various numerical algorithms have been utilized for the analysis of waveguide structures, the Method of Lines (MOL) is one of them. The MOL has been applied to several types of planar longitudinally uniform waveguide problems. The MOL has been used to analyze single discontinuity [44, 45] and multiple discontinuities in optical waveguides [29, 36, 46, 47, 48, 49, 50]. It has also been applied to solve non-linear waveguide problems [51] as well as diffraction problem from waveguide ends [52]. This method has also been used to model 3-D problems [53, 54, 55] for both optical and microwave waveguides.

3.2 Principle of the Algorithm

When the MOL is applied to two dimensional structures, the wave equation is discretized in the transverse direction (the direction normal to the direction of propagation) and calculated analytically in the longitudinal direction [50].

Figure 3.1 shows a planar two-dimensional waveguide structure in which the interfaces of layers are parallel to the z-axis. Consequently, discretization will be applied along the the x-axis. This implies that the field will be calculated on lines that are equidistant from each other and parallel to the z-axis. The investigated structure is bounded by an electric wall where $E_y = 0$ or a magnetic wall where $H_y = 0$ as appropriate. The resulting difference equations are then decoupled and manipulated through algebraic transformation.

In some instances, it might be more advantageous to have non-equidistant discretization. An example of this is the case when the widths of the different layers of the structure exhibit extreme differences which results in increasing the number of lines and, consequently the associated computational time and memory requirements. In such cases, the distance between the lines (i-e. mesh size) is increased in regions where the field exhibits smaller variations and vice versa [56, 57].

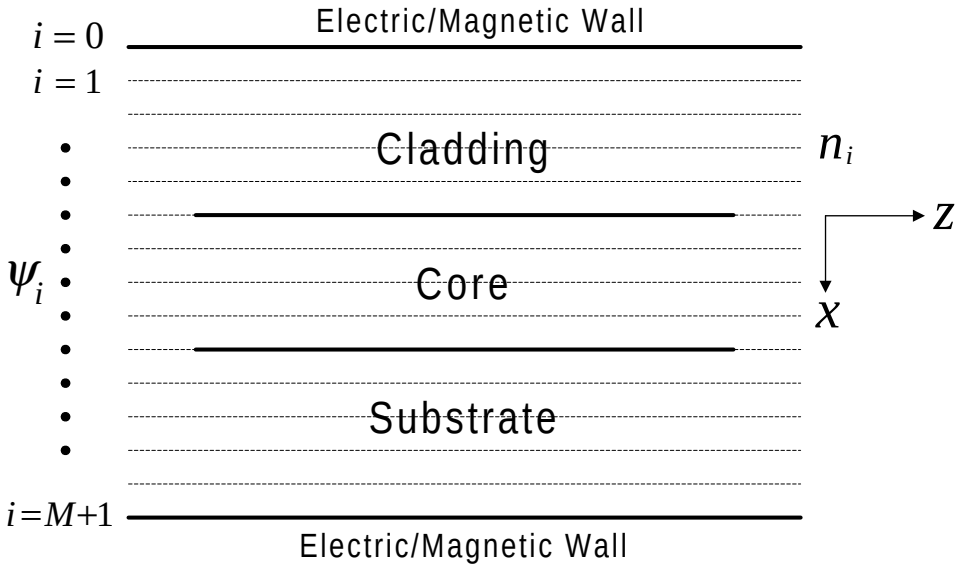

Figure 3.1: Mesh Discretization used in the MOL

3.3 Mathematical Formulation

Consider the two dimensional wave equation:

$$\frac{\partial^2\psi(x,z)}{\partial x^2} + \frac{\partial^2\psi(x,z)}{\partial z^2} + k_o^2 n^2 \psi(x,z) = 0 \tag{3.1}$$

where

ψ = Electric or Magnetic Field (E_y or H_y)

$k_o = 2\pi/\lambda_o$

λ_o = Free space wavelength

n = Refractive index of the medium

In the MOL, both the field $\psi(x,z)$ and the refractive index $n(x)$ are discretized along the x-axis and calculated on lines in the z-direction (direction of propagation). To calculate the field ψ in a discretized form, we first need to obtain its second derivative with respect to x in discrete form. This can be accomplished using the

well-known three-point central difference approximation.

3.3.1 The Three-Point Central Difference Approximation

To obtain an expression for the discretized second derivative of a certain function, we express the function in terms of a power series. We can have a good approximation of the given function in terms of a polynomial by neglecting all except the first few terms of the resulting series. One of the most convenient power series is the Taylor's Series which can be expressed as:

$$f(x) = \sum_{n=0}^{\infty} \frac{f^{(n)}(a)}{n!}(x-a)^n \tag{3.2}$$

where $f^{(n)}$ is the nth derivative of $f(x)$ with respect to x.

If Taylor's series is expanded about $x = 0$, the resulting series is often called a Maclaurin's Series expansion. Expanding $\psi(x)$ about $x = 0$ using equation 3.2:

$$\psi(x) = \psi(0) + \frac{\psi^{'}(0)}{1!}x + \frac{\psi^{''}(0)}{2!}x^2 + \frac{\psi^{'''}(0)}{3!}x^3 + \frac{\psi^{''''}(0)}{4!}x^4 + ... \tag{3.3}$$

Evaluating the above equation at $x = \pm\Delta x$ results in:

$$\psi_1 = \psi(0) + \frac{\psi^{'}(0)}{1!}\Delta x + \frac{\psi^{''}(0)}{2!}(\Delta x)^2 + \frac{\psi^{'''}(0)}{3!}(\Delta x)^3 + \frac{\psi^{''''}(0)}{4!}(\Delta x)^4 + ... \tag{3.4}$$

$$\psi_{-1} = \psi(0) - \frac{\psi^{'}(0)}{1!}\Delta x + \frac{\psi^{''}(0)}{2!}(\Delta x)^2 - \frac{\psi^{'''}(0)}{3!}(\Delta x)^3 + \frac{\psi^{''''}(0)}{4!}(\Delta x)^4 + ... \tag{3.5}$$

Adding equations 3.4 and 3.5, we have:

$$\psi_1 + \psi_{-1} = 2\psi(0) + \psi^{''}(0)(\Delta x)^2 + \frac{\psi^{''''}(0)}{12}(\Delta x)^4 + ... \tag{3.6}$$

this equation leads to:

$$\psi^{''}(0) = \frac{\psi_1 - 2\psi(0) + \psi_{-1}}{(\Delta x)^2} - \frac{\psi^{''''}(0)}{12}(\Delta x)^2 - ... \tag{3.7}$$

which can be approximated as:

$$\psi^{''}(0) \approx \frac{\psi_1 - 2\psi(0) + \psi_{-1}}{(\Delta x)^2} \tag{3.8}$$

It is apparent from equation 3.8 that the leading error resulting from the approximation is proportional to $(\Delta x)^2$.

3.3.2 Discretization of the Wave Equation

The second derivative operator ($\frac{\partial^2}{\partial x^2}$) term in equation 3.1 is replaced by the three-point central difference approximation from equation 3.8. So at the *ith* grid we get:

$$\frac{\psi_{i+1}(z) - 2\psi_i(z) + \psi_{i-1}(z)}{(\Delta x)^2} + \frac{d^2\psi_i(z)}{dz^2} + k_o^2 n_i^2 \psi_i(z) = 0 \tag{3.9}$$

If the field in the x-direction is discretized into M points, then equation 3.9 yields the following M equations:

$$i = 1: \qquad \frac{1}{(\Delta x)^2}\left[\psi_2 - 2\psi_1 + \psi_0\right] + \frac{d^2}{dz^2}\left[\psi_1\right] + k_o^2 n_1^2 \left[\psi_1\right] = 0 \tag{3.10}$$

$$i = 2: \qquad \frac{1}{(\Delta x)^2}\left[\psi_3 - 2\psi_2 + \psi_1\right] + \frac{d^2}{dz^2}\left[\psi_2\right] + k_o^2 n_2^2 \left[\psi_2\right] = 0 \tag{3.11}$$

$$i = 3: \qquad \frac{1}{(\Delta x)^2}\left[\psi_4 - 2\psi_3 + \psi_2\right] + \frac{d^2}{dz^2}\left[\psi_3\right] + k_o^2 n_3^2 \left[\psi_3\right] = 0 \tag{3.12}$$

$$\vdots$$

$$i = M: \qquad \frac{1}{(\Delta x)^2}\left[\psi_{M+1} - 2\psi_M + \psi_{M-1}\right] + \frac{d^2}{dz^2}\left[\psi_M\right] + k_o^2 n_M^2\left[\psi_M\right] = 0 \quad (3.13)$$

The above equations can be written in matrix form as:

$$\frac{1}{(\Delta x)^2}\begin{bmatrix} -2 & 1 & & & & & \\ 1 & -2 & 1 & & & \mathcal{O} & \\ & 1 & -2 & 1 & & & \\ & & \ddots & \ddots & \ddots & & \\ & \mathcal{O} & & & 1 & -2 & 1 \\ & & & & & 1 & -2 \end{bmatrix}\begin{bmatrix} \psi_1(z) \\ \psi_2(z) \\ \psi_3(z) \\ \vdots \\ \vdots \\ \psi_M(z) \end{bmatrix} + \frac{d^2}{dz^2}\begin{bmatrix} \psi_1(z) \\ \psi_2(z) \\ \psi_3(z) \\ \vdots \\ \vdots \\ \psi_M(z) \end{bmatrix}$$

$$+k_o^2\begin{bmatrix} n_1^2 & & & & & & \\ & n_2^2 & & & & \mathcal{O} & \\ & & n_3^2 & & & & \\ & & & \ddots & & & \\ & \mathcal{O} & & & \ddots & & \\ & & & & & & n_M^2 \end{bmatrix}\begin{bmatrix} \psi_1(z) \\ \psi_2(z) \\ \psi_3(z) \\ \vdots \\ \vdots \\ \psi_M(z) \end{bmatrix} = \begin{bmatrix} 0 \\ 0 \\ 0 \\ \vdots \\ \vdots \\ 0 \end{bmatrix}$$

written in compact notation, we get:

$$\frac{1}{(\Delta x)^2} C\Psi + \frac{d^2}{dz^2}\Psi + k_o^2 N\Psi = 0 \quad (3.14)$$

where C is a tri-diagonal second-order central-difference matrix , N is a diagonal matrix whose elements are $n_1^2, n_2^2, ..., n_M^2$ and $\Psi = [\psi_1(z), \psi_2(z), ..., \psi_M(z)]^t$ is the

discretized field vector of either E_y or H_y depending upon the polarization. The above equation may then be written in the form:

$$\frac{d^2}{dz^2}\Psi + Q\Psi = 0 \tag{3.15}$$

where

$$Q = \frac{1}{(\Delta x)^2}C + k_o^2 N \tag{3.16}$$

The solution of this 2nd-order ordinary matrix differential equation is formally given by [29]:

$$\Psi = e^{j\sqrt{Q}z}A + e^{-j\sqrt{Q}z}B \tag{3.17}$$

where $e^{j\sqrt{Q}z}$ represents field propagation in the $+z$ direction and $e^{-j\sqrt{Q}z}$ represents field propagation in $-z$ direction. The matrices $e^{j\sqrt{Q}z}$ and $e^{-j\sqrt{Q}z}$ are calculated by diagonalizing matrix Q to find the eigenvalues and eigenvectors. Matrix Q may be written in the form:

$$Q = UVU^{-1} \tag{3.18}$$

where U is the eigenvector matrix and V is a diagonal matrix containing the eigenvalues of Q. The matrix exponent is then calculated using the following well known relation of linear algebra:

$$e^{j\sqrt{Q}z} = Ue^{j\sqrt{V}z}U^{-1} \tag{3.19}$$

3.4 Convergence of the MOL

The convergence behavior of the results of a numerical method serves as a good indicator of the accuracy of the chosen parameters. One important parameter in the MOL is the mesh size (h) that is the number of discretization lines (M). The accuracy of the results should improve as the mesh size decreases. However, as mesh size decreases, the number of discretization lines increases. This leads to longer computational time and larger memory requirement.

3.5 Interface Conditions

In order to correctly model the electric and magnetic fields behavior at an interface, the interface conditions (I.Cs.) should be appropriately accounted for in the Method of Lines formulation. In this thesis, we are mainly concerned with multi-layer structures in which the material properties are constant within each layer and change abruptly from one layer to the next (see figure 2.2). The tangential electric field E_y and its first derivative are continuous across an interface. The tangential magnetic field H_y is continuous but its first derivative is discontinuous at an interface. All the higher order derivatives of both E_y and H_y are discontinuous at an interface. We can derive these relations using Maxwell equations. For TE polarization, applying equation 2.19

$$H_z = -\frac{j}{\omega \mu_o} \frac{\partial E_y}{\partial x} \tag{3.20}$$

at an interface along with the fact that H_z is continuous at an interface, that is $H_z^{0^+} = H_z^{0^-}$, equation 3.20 gives:

$$-\frac{j}{\omega\mu_o}\frac{\partial E_y^{0^+}}{\partial x} = -\frac{j}{\omega\mu_o}\frac{\partial E_y^{0^-}}{\partial x} \tag{3.21}$$

that is

$$\frac{\partial E_y^{0^+}}{\partial x} = \frac{\partial E_y^{0^-}}{\partial x} \tag{3.22}$$

which is the statement of the continuity of $\frac{\partial E_y}{\partial x}$ at a horizontal interface. Similarly for TM polarization, using equation 2.30

$$E_z = \frac{j}{\omega n_j^2 \epsilon_o}\frac{\partial H_y}{\partial x} \tag{3.23}$$

at an interface along with the fact that E_z is continuous, that is $E_z^{0^+} = E_z^{0^-}$, we obtain:

$$\frac{j}{\omega n_2^2 \epsilon_o}\frac{\partial H_y^{0^+}}{\partial x} = \frac{j}{\omega n_1^2 \epsilon_o}\frac{\partial H_y^{0^-}}{\partial x} \tag{3.24}$$

that is:

$$\frac{1}{n_2^2}\frac{\partial H_y^{0^+}}{\partial x} = \frac{1}{n_1^2}\frac{\partial H_y^{0^-}}{\partial x} \tag{3.25}$$

which means that $\frac{\partial H_y}{\partial x}$ is discontinuous at a horizontal interface.

Depending upon the polarization of the field, ψ may represent either E_y for the TE polarization or H_y for the TM polarization. At an index discontinuity in the transverse direction x, ψ is continuous. However, all its higher order derivatives with respect to x are in general discontinuous there. With reference to Figure 3.2,

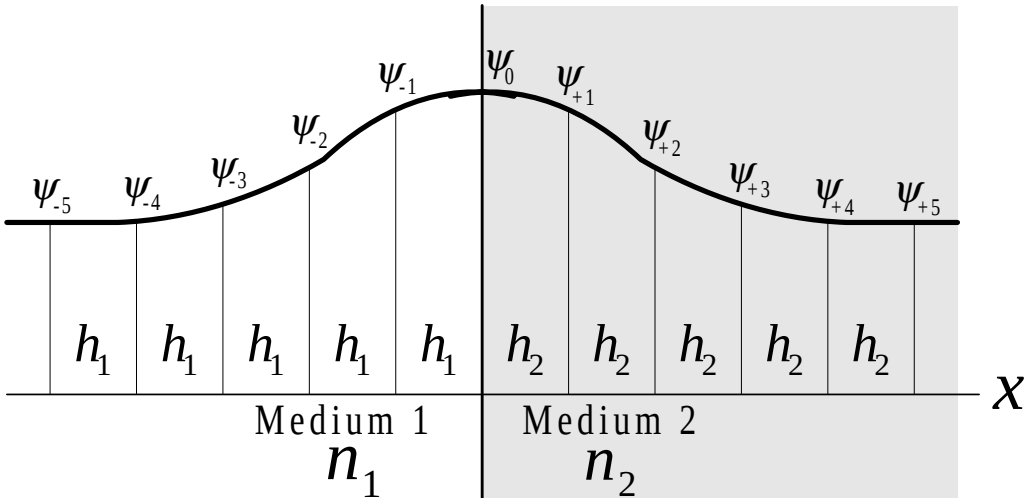

Figure 3.2: Discretized Field in the Transverse Direction

where an index discontinuity is assumed to exist at $x = 0$, the discontinuities in the higher-order derivatives of ψ can easily be deduced from the wave equation, and are summarized below [58]:

$$\psi_{0+} = \psi_{0-} = \psi_0 \tag{3.26}$$

$$\psi'_{0+} = \rho_{21}\psi'_{0-} \tag{3.27}$$

$$\psi''_{0+} = \psi''_{0-} + \zeta_{12}\psi_0 \tag{3.28}$$

$$\psi'''_{0+} = \rho_{21}\left(\psi'''_{0-} + \zeta_{12}\psi'_{0-}\right) \tag{3.29}$$

$$\psi''''_{0+} = \psi''''_{0-} + 2\zeta_{12}\psi''_{0-} + \zeta_{12}^2\psi_0 \tag{3.30}$$

$$\psi'''''_{0+} = \rho_{21}\left(\psi'''''_{0-} + 2\zeta_{12}\psi'''_{0-} + \zeta_{12}^2\psi'_{0-}\right) \tag{3.31}$$

$$\psi''''''_{0+} = \psi''''''_{0-} + 3\zeta_{12}\psi''''_{0-} + 3\zeta_{12}^2\psi''_{0-} + \zeta_{12}^3\psi_0 \tag{3.32}$$

where $\zeta_{12} = k_o^2(n_1^2 - n_2^2)$, $\rho_{21} = n_2^2/n_1^2$ for the TM case and $\rho_{21} = 1$ for the TE case.

The subscripts 0^+ and 0^- represent the field immediately to the right and to the left of the interface, respectively.

3.6 Improved Three-Point Formulation with Interface Conditions

The field is sampled or discretized so that there is always a sample point at an interface. Within a certain layer i, the refractive index n_i and mesh size h_i are uniform. From one layer to the next, either the refractive index n_i or the mesh size h_i or both may abruptly change. The refractive index chosen at the interface sampling point is either the refractive index of left layer or the refractive index of right layer. This choice should be consistent throughout the whole structure. In this manner, we can correctly model the layer thickness and abrupt refractive index discontinuity. With reference to figure 3.2, the field on either side of the interface is expanded in terms of the field at the interface using Taylor's series expansion, that is:

$$\psi_{-1} = \psi_{0^-} - h_1\psi'_{0^-} + \frac{h_1^2}{2!}\psi''_{0^-} + ... \tag{3.33}$$

$$\psi_{+1} = \psi_{0^+} + h_2\psi'_{0^+} + \frac{h_2^2}{2!}\psi''_{0^+} + ... \tag{3.34}$$

Here ψ_{0^+} and ψ_{0^-} represent the field at $x = 0^+$ and $x = 0^-$ respectively. Using the interface conditions 3.26, 3.27 and 3.28 and expressing all ψ_{0^+} in terms of ψ_{0^-}

in equation 3.34, we obtain:

$$\psi_{+1} = \left(1 + 0.5h_2^2\zeta_{12}\right)\psi_o + h_2\rho_{21}\psi_{0-}^{'} + 0.5h_2^2\psi_{0-}^{''} + ... \tag{3.35}$$

Eliminating $\psi_{0-}^{'}$ from equations 3.35 and 3.33, we get [36, 58]:

$$\psi_{0-}^{''} = \frac{\psi_{+1} - (\tau_{21}\rho_{21} + 1 + 0.5h_2^2\zeta_{12})\,\psi_0 + \tau_{21}\rho_{21}\psi_{-1}}{0.5h_2(h_1\rho_{21} + h_2)} \tag{3.36}$$

where $\tau_{21} = \frac{h_2}{h_1}$. The above relation can be used to approximate the $\frac{\partial^2}{\partial x^2}$ operator at any sampling point i in terms of the field values at $i+1$, i and $i-1$ sampling points. So this represents an improved three-point finite-difference approximation of $\frac{\partial^2}{\partial x^2}$ operator because it accounts for the interface boundary conditions. In the case of uniform refractive index and uniform mesh size i.e. $n_1 = n_2$ and $h_1 = h_2$, equation 3.36 reduces to the familiar three-point central-difference approximation, that is:

$$\psi_{0-}^{''} \approx \frac{\psi_{+1} - 2\psi_0 + \psi_{-1}}{h^2} \tag{3.37}$$

3.7 Higher-Order Finite Difference Approximation

The improved formula 3.36 for the second derivative approximation has an accuracy of $O(h^2)$ at regions of uniform index and mesh size. Its accuracy decreases at a mesh or index discontinuity. In integrated optical waveguide modeling, the required accuracy in estimating the effective index is fairly high. So we need to use a relatively

large number of discretization lines to reduce numerical errors. This leads to larger matrices and longer computational time.

The higher-order approximation scheme of the second-derivative operator $\frac{\partial^2}{\partial x^2}$ presented in references [36, 58] gives sufficiently high accuracy and accurate estimation of the modal field profile and the effective indices. The necessary interface conditions for the electric and magnetic fields are appropriately included in the scheme. This scheme results in a much reduced matrix size, faster computational speed and lower memory usage. This high-order approximation scheme is discussed in appendix A and it is used in this thesis.

3.8 Results

The previously developed formulae for the three-point, five-point and seven-point approximation of the second derivative operator ($\frac{\partial^2}{\partial x^2}$) are used to model a high-contrast waveguide and a metal-dielectric single interface. The effective index n_{eff} and modal field of the fundamental TE and TM modes are calculated using the MOL. These MOL results are compared with exact results and their convergence behavior is studied by decreasing the mesh size (that is increasing the number of discretization points) in the problem space. It is observed that the 7-point formula gives a better estimate of n_{eff} and modal field with relatively few sample points as compared to the 5-point and the 3-point formulas. The basic 3-point formula without interface conditions can not distinguish between the TE and TM polarizations.

3.8.1 High-Contrast Waveguide

A high-contrast waveguide structure (shown in the inset of figure 3.3) is modeled using the MOL. In this simulation, a uniform mesh is used and the mesh size is varied. During simulation the outermost layers thickness is kept sufficiently large so that the modal field decays to a sufficiently small value (approximately 10^{-5}) as compared to its value at the $Air/GaAs$ interface. The phase parameter, defined as $B = (n_{eff}^2 - 1^2)/(3.6^2 - 1^2)$, is used to assess the accuracy of the computed results. The exact values of the TE_0 and TM_0 modes are calculated by STF1 program (see Appendix B). For the TE_0 mode, we have $n_{eff} = 3.543961609340564$ and $B_0 = 0.9665270809765686$, and for the TM_0 mode, $n_{eff} = 3.529434420038923$ and $B_0 = 0.9579353950966126$. The relative error in phase parameter which is defined as $\frac{B_{MOL} - B_0}{B_0}$ is plotted against the mesh size (h) (see figures 3.3 and 3.4). The results show that for relatively large values of the mesh size, the error due to higher order formulation exceeds the corresponding error for lower order formulation. However, as the mesh size decreases, the error due to higher order formulation becomes much lower than that due to the lower order formulation [58]. This shows the superiority of the 5-point and the 7-point formulation to find n_{eff} and modal field for both the TE and TM polarization as compared to the 3-point formulation.

The 7-point formulation takes approximately 0.10 seconds per mesh size to calculate the relative error in the phase parameter for TE_0 mode and the 3-point and 5-point formulation take 0.02 and 0.08 seconds per mesh size respectively (using an

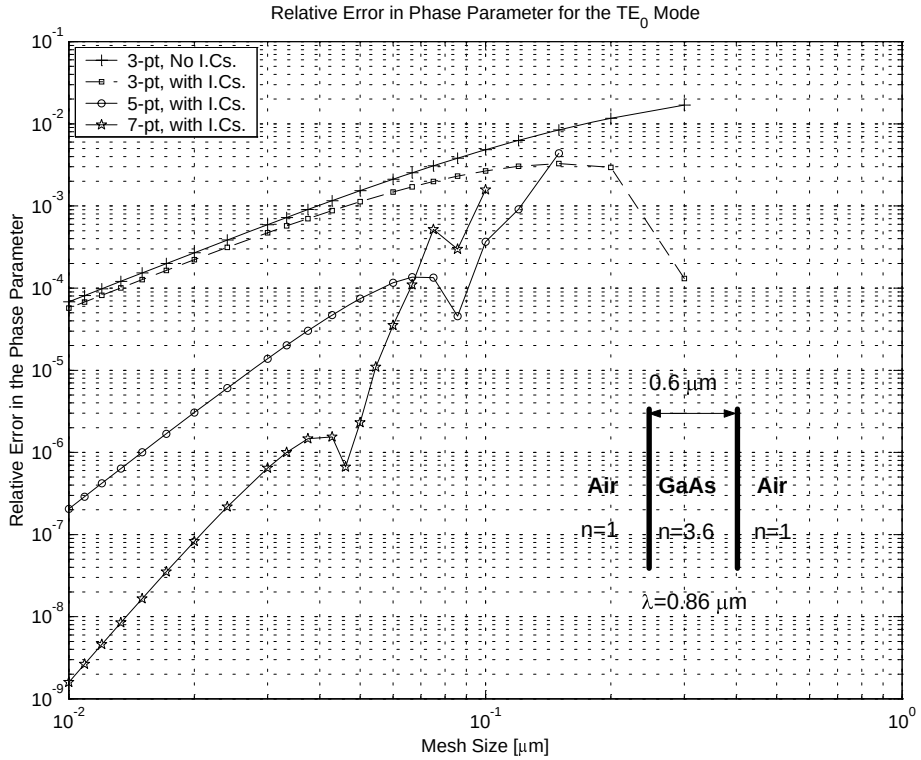

Figure 3.3: Relative Error in Phase Parameter for the TE_0 Mode

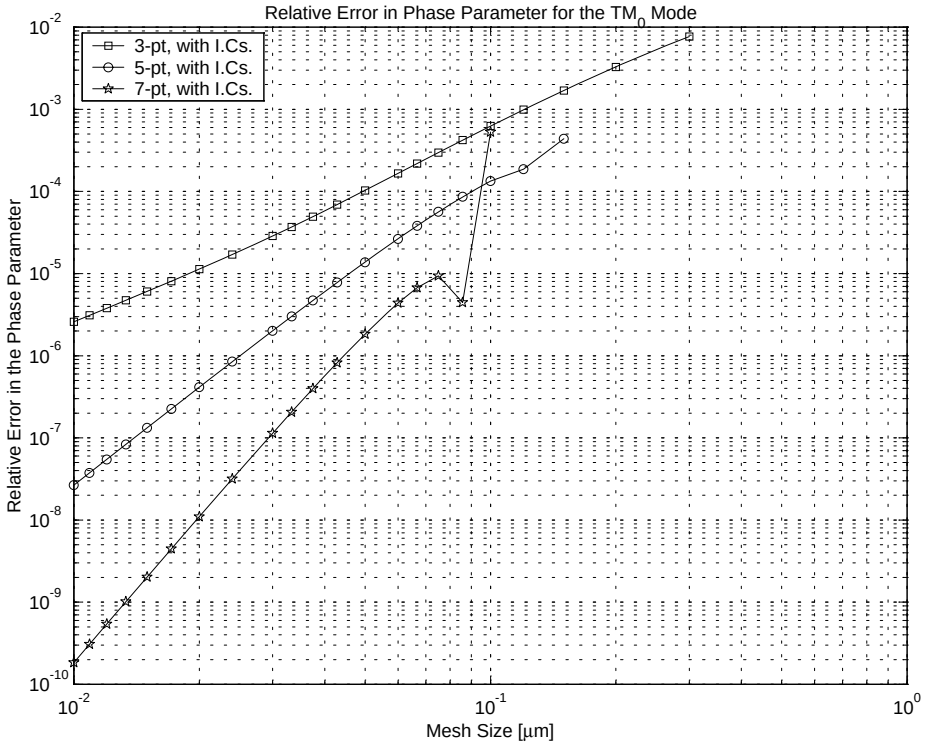

Figure 3.4: Relative Error in Phase Parameter for the TM_0 Mode

IBM Pentium-III machine with 128 MB RAM running MATLAB 5.2 under Windows 98). This indicates that the 5-point and 7-point formulation are slow as compared to the 3-point formulation.

3.8.2 Metal-Dielectric Single Interface

The single interface between a metal and a dielectric supports a surface plasmon mode. This mode is TM polarized and is characterized by a field (called evanescent field) that decays exponentially on both sides of the interface. This field decays in the metal much faster than it does in air. A Surface plasmon mode is known to be lossy with a complex propagation constant [39, 59]. It can only exist as surface wave at a metal/dielectric interface when the complex dielectric constant (i-e. n^2) of the metal has a negative real part. The following analytic expression is used to calculate the effective index (n_{eff}) of the surface plasmon mode [58].

$$n_{eff} = \frac{n_1 n_2}{\sqrt{n_1^2 + n_2^2}} \tag{3.38}$$

where n_1 and n_2 are the refractive indices of the metal and dielectric respectively.

A metal/air single interface structure (see figure 3.5) is modeled at the operating wavelength, $\lambda = 0.6328\mu m$. The problem space is divided into many artificial layers and a non-uniform discretization scheme is used to sample the waveguide efficiently. A fine mesh is used in regions of fast field decay and a coarse mesh is employed in regions of slow field decay. This decreases the total number of sampling points considerably as compared to a uniform sampling scheme. The effective index is

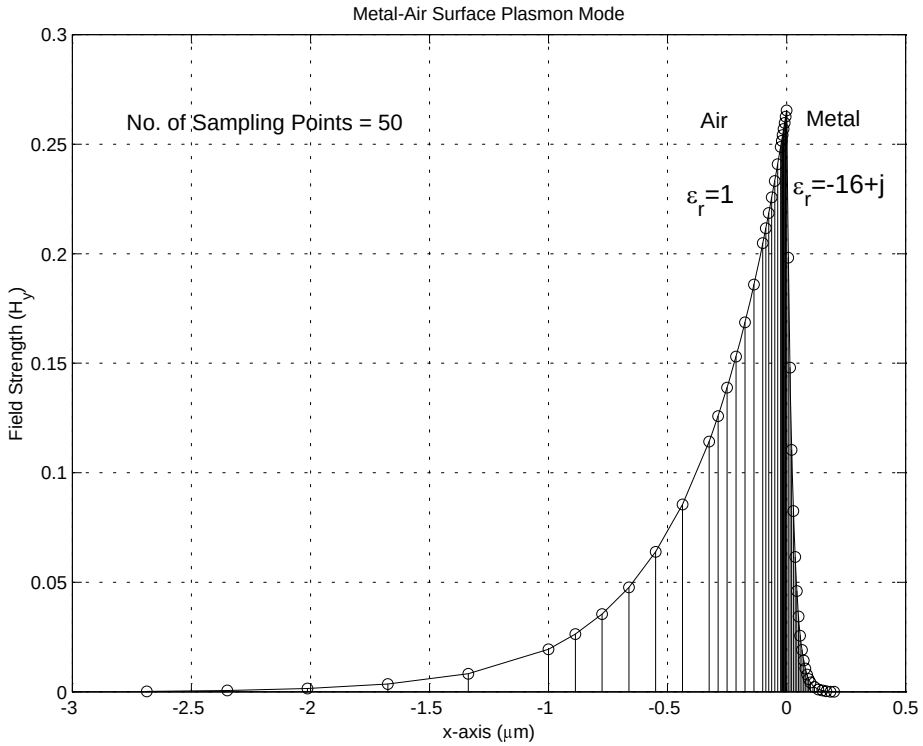

Figure 3.5: Magnetic Field Pattern of A Surface Plasmon Mode at a Metal-Air Interface

calculated and compared against analytical values for the 3-point, the 5-point and the 7-point formulations. The results are given in table 3.1. It is found that the 7-point formulation gives more accurate results than the 5-point or the 3-point schemes for a fixed total number of mesh points [58]. The basic 3-point formulation without interface conditions can not be used to model this problem. The results obtained are in close agreement with those given in reference [36].

3-Point	5-Point	7-Point
-5.046e-4+j7.733e-6	7.652e-6-j8.145e-7	1.147e-8+j3.261e-8

Table 3.1: Error in n_{eff} for the Surface Plasmon Mode. (Analytical value of $n_{eff} = 1.032654962422412 + j0.002142428459687181$, total number of sampling points = 50)

Chapter 4

Absorbing Boundary Conditions and Waveguide Discontinuities

4.1 Absorbing Boundary Conditions

To analyze planar waveguide structures numerically, they must be enclosed by walls to limit the area of discretization. The use of electrical or magnetic walls produces errors, since the corresponding tangential field components, E_y and H_y, are set to zero. This electric/magnetic wall reflects back the radiated waves into the problem space producing errors in the computed results. To overcome this difficulty, free space can be simulated at an arbitrarily fixed position by using a numerical absorbing boundary conditions (ABC) [60].

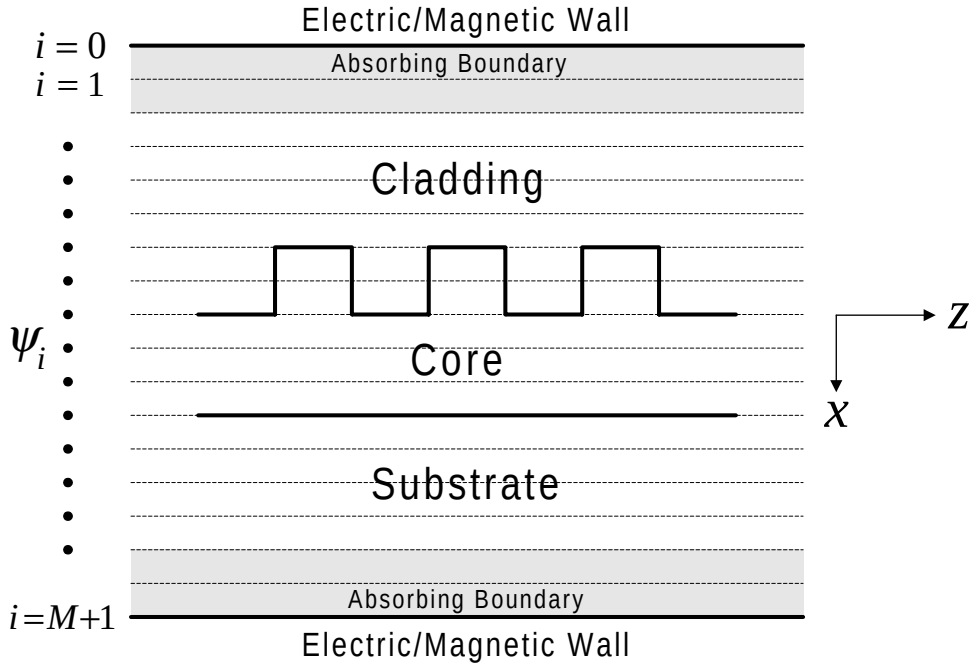

Figure 4.1: Mesh Discretization in the MOL with Absorbing Boundary

4.2 Perfectly Matched Layer

The perfectly matched layer (PML) as a material absorbing boundary condition is introduced for electromagnetic waves by Berenger [61]. This material absorbing boundary condition is based on a non-Maxwellian approach and has been applied to a variety of time-domain problems. A PML absorbing scheme based on complex distance approach was first incorporated into the MOL by Al-Bader and Al-Jamid [37]. This approach was shown to be equivalent to Berenger's method. This type of PML which provides reflectionless absorption at a wide range of incident angles and frequencies [37] independent of polarization, makes it particularly suited for truncating the computational window in the MOL calculations. The absorption of the radiative wave is done by changing the distance x from real to complex. This

introduces an numerical attenuation factor in the radiative field and hence causes decay of the radiative field in the PML region. The last mesh point is terminated by an electric/magnetic wall boundary condition. In this approach the real distance is transformed to a complex one according to:

$$x \rightarrow x(1 + j\sigma) \tag{4.1}$$

where σ is the decay factor constant. The wave radiative e^{+jkx} propagating in $+x$ direction in the real space will be converted to

$$e^{+jkx(1+j\sigma)} = e^{+jkx}e^{-k\sigma x} \tag{4.2}$$

in the complex space. The factor $e^{-k\sigma x}$ causes the decay of the field in the $+x$ direction. The value of σ is set arbitrarily and the number of samples in the PML absorber is chosen to cause a significant decay in the field so that it becomes negligible at the electric/magnetic wall. The choice of the decay factor σ is discussed in reference [62]. If the PML region is made sufficiently wide, only negligible reflections at the extreme edges of the computational window may occur. However, significant numerical reflection may occur at the inner wall of the PML [63]. The choice of σ and the number of sample points in the PML are chosen appropriately in order to minimize reflection from the inner wall of the PML. This PML absorbing scheme is incorporated into the MOL and used throughout this thesis.

Gaussian Field Propagation in Air:

The performance of PML is analyzed by modeling free-space surrounded by PML layers on both sides. A Gaussian field is launched in air and its propagation along the z direction is observed (see figures 4.3-4.10). An analytical expression based

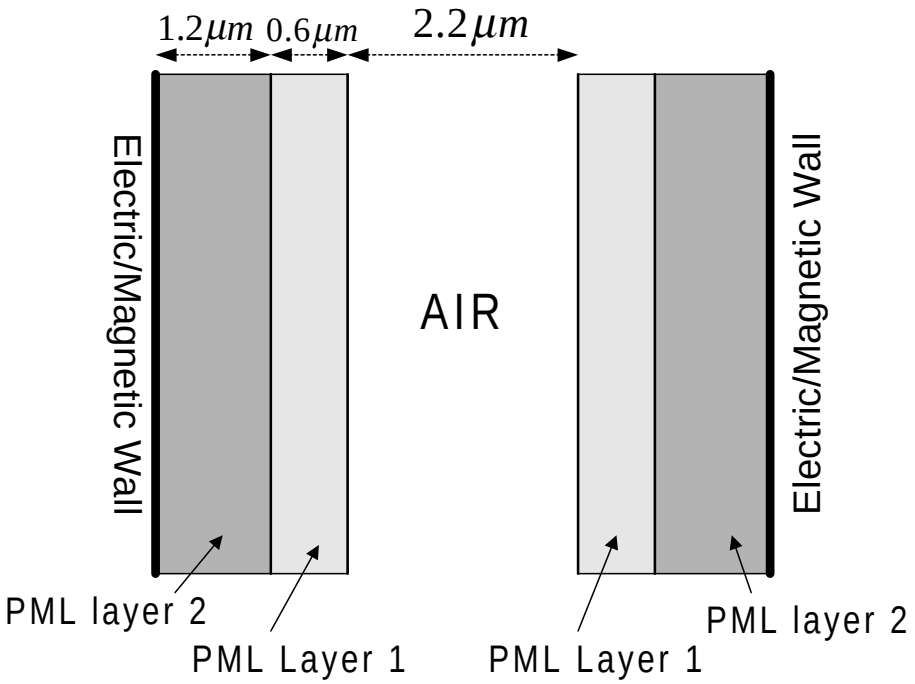

Figure 4.2: A Perfectly Matched Layer (PML) Scheme

on scalar diffraction theory is used to calculate the spread of Gaussian field [59] as it propagates in a medium. The MOL propagated field is compared against the analytically propagated field over a large distance. Each PML layer has 5 sample points with $\sigma = 1$. A non-uniform double layer scheme is used to model a relatively thicker PML. Thus, the field magnitude at the last mesh point drops considerably

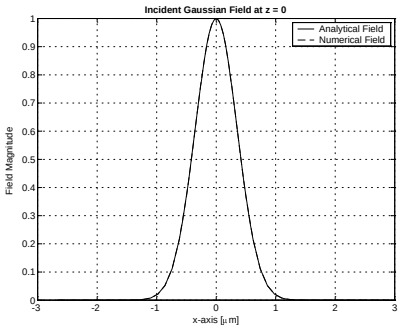

Figure 4.3: Incident Gaussian Field

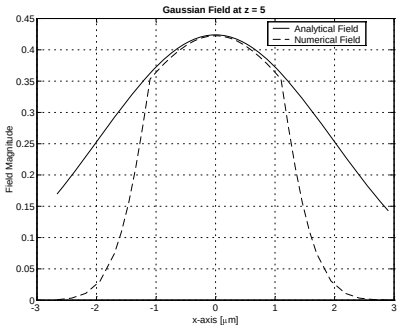

Figure 4.4: Field at $z = 5\mu m$

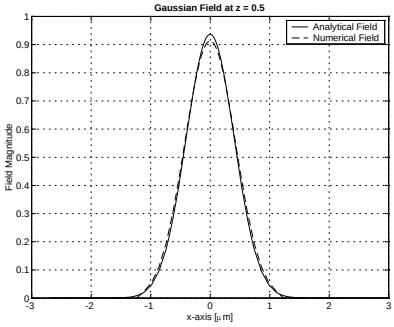

Figure 4.5: Field at $z = 0.5\mu m$

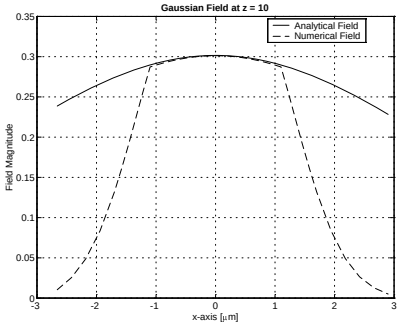

Figure 4.6: Field at $z = 10\mu m$

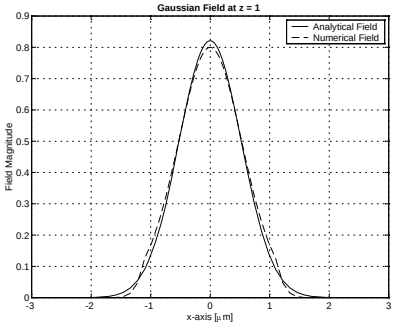

Figure 4.7: Field at $z = 1\mu m$

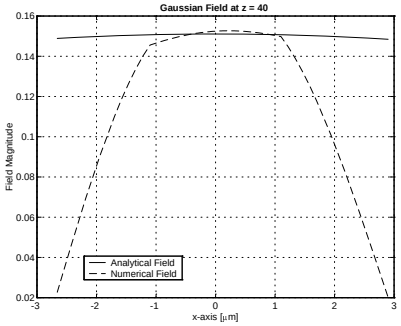

Figure 4.8: Field at $z = 40\mu m$

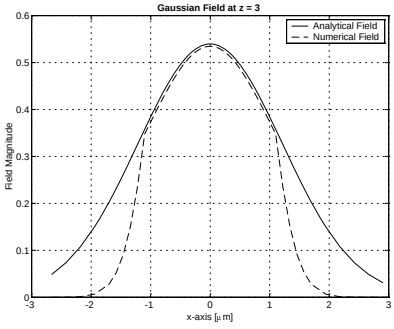

Figure 4.9: Field at $z = 3\mu m$

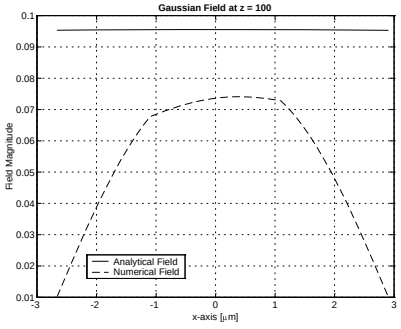

Figure 4.10: Field at $z = 100\mu m$

due to the $e^{-k\sigma x}$ factor appearing in equation 4.2. The problem space is finally terminated by an electric/magnetic wall. The visual comparison of the analytical field and the MOL computed field shows that the two fields are almost identical over a long propagation distance. This shows the PML absorbs radiative fields and correctly models open-space.

4.3 Waveguide Discontinuities

Discontinuity problems are important in the investigation of optical devices, such as laser facets, gratings, waveguide ends, and connections of different waveguide sections. The classic problem to model scattering from a single and multiple discontinuities has been solved by many workers using different analytical and numerical methods such as the Mode Matching Method [28], the Method of Lines [44, 46, 47, 64] and the Equivalent Transmission-Line Network Method [65]. A good reference to these methods is given in references [28] and [66]. The MOL has been applied to solve a variety of scattering problems, including non-linear scattering problem from a single discontinuity [67] and surface-plasmon mode scattering [68, 69].

4.4 Single Discontinuity

Consider a waveguide having a single discontinuity as shown in figure 4.11. The problem space is divided into two regions, region 0 and region 1. The field is incident

from region 0 resulting in a reflected field in region 0 and a transmitted field in region 1. The total field in each region is the sum of the forward traveling field, e^{+jSz}, and the backward traveling field, e^{-jSz}.

The total field (Ψ_0) in region 0 is the sum of the incident and reflected fields:

$$\Psi_0 = e^{+jS_0z}A_0 + e^{-jS_0z}B_0 \tag{4.3}$$

The total field (Ψ_1) in region 1 is only the transmitted field:

$$\Psi_1 = e^{+jS_1z}A_1 \tag{4.4}$$

where Ψ is a column vector containing the sampled fields. A_0, B_0 and A_1 are constant vectors, $S = \sqrt{Q}$ and Q is defined in chapter 3. For TM polarization, Ψ is continuous at the interface at $z = 0$, that is $\Psi_0|_{z=0} = \Psi_1|_{z=0}$. From equations 4.3 and 4.4, we have:

$$A_0 + B_0 = A_1 \tag{4.5}$$

From the interface condition equation 3.27, the field on either side of the discontinuity at $z = 0$ is related by:

$$\Psi_0^{'} = \frac{N_0}{N_1}\Psi_1^{'} \tag{4.6}$$

$$(N_0)^{-1}\Psi_0^{'} = (N_1)^{-1}\Psi_1^{'} \tag{4.7}$$

where the matrix N is a diagonal matrix of refractive index squared n_i^2 at each sample point. Differentiating equation 4.3 with respect to z and evaluating the result at the interface $z = 0$, we have:

$$\Psi_0^{'} = jS_0e^{jS_0z}A_0 - jS_0e^{-jS_0z}B_0 \tag{4.8}$$

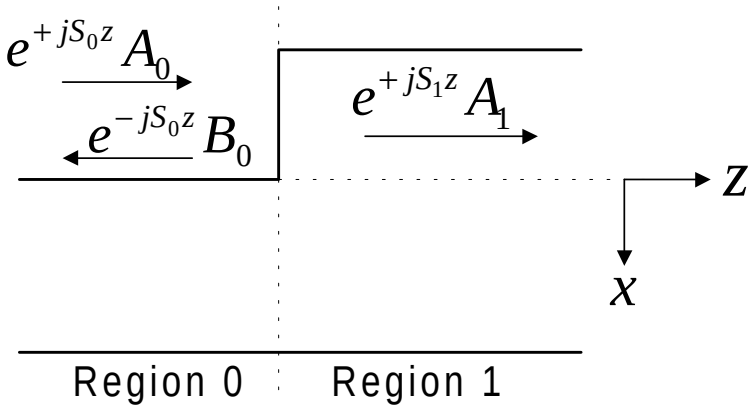

Figure 4.11: A Single Waveguide Discontinuity

$$\Psi_0^{'}|_{z=0} = jS_0(A_0 - B_0) \tag{4.9}$$

Similarly from equation 4.4, we have:

$$\Psi_1^{'} = jS_1 e^{jS_1 z} A_1 \tag{4.10}$$

$$\Psi_1^{'}|_{z=0} = jS_1 A_1 \tag{4.11}$$

Substituting equations 4.9 and 4.11 into equation 4.7 and simplifying we have:

$$(N_0)^{-1} S_0 (A_0 - B_0) = (N_1)^{-1} S_1 A_1 \tag{4.12}$$

$$(A_0 - B_0) = S_0^{-1}(N_0)(N_1)^{-1} S_1 A_1 \tag{4.13}$$

Eliminating B_0 from equations 4.5 and 4.13, we get the transmitted field, A_1:

$$A_1 = 2(I + S_0^{-1} N_0 N_1^{-1} S_1)^{-1} A_0 \tag{4.14}$$

$$A_1 = TA_0 \tag{4.15}$$

where T is the transmission matrix. Similarly eliminating A_0, we get the reflected field, B_0:

$$B_0 = (I - S_0^{-1} N_0 N_1^{-1} S_1)(I + S_0^{-1} N_0 N_1^{-1} S_1)^{-1} A_0 \tag{4.16}$$

$$B_0 = RA_0 \tag{4.17}$$

where R is the reflection matrix.

For the TE polarization, both field and its z derivatives are continuous across the interface. We follow the same procedure to derive the transmission (T) and reflection (R) matrices for the TE case.

$$A_1 = 2(I + S_0^{-1}S_1)^{-1}A_0 = TA_0 \tag{4.18}$$

$$B_0 = (I - S_0^{-1}S_1)(I + S_0^{-1}S_1)^{-1}A_0 = RA_0 \tag{4.19}$$

The transmission matrix T and the reflection matrix R are related by:

$$A_1 = B_0 + A_0 \tag{4.20}$$

$$= RA_0 + A_0 \tag{4.21}$$

$$= (R + I)A_0 = TA_0 \tag{4.22}$$

4.4.1 Results

A single waveguide discontinuity is modeled as shown in figure 4.12 at $\lambda = 0.86\,\mu m$. The TM_0 mode of the narrow waveguide is incident from the left on the waveguide. The reflected and transmitted fields are calculated and propagated backward and forward in the respective waveguides. The problem space is terminated with a single layer PML on both sides. The results are shown in figures 4.13 and 4.14. The reflected field consists of the TM_0 mode of the narrow waveguide after propagating backward a long distance as the radiative part of the field leaks out and absorbed by the PML layers. This shows that the PML absorbs the radiative fields effectively.

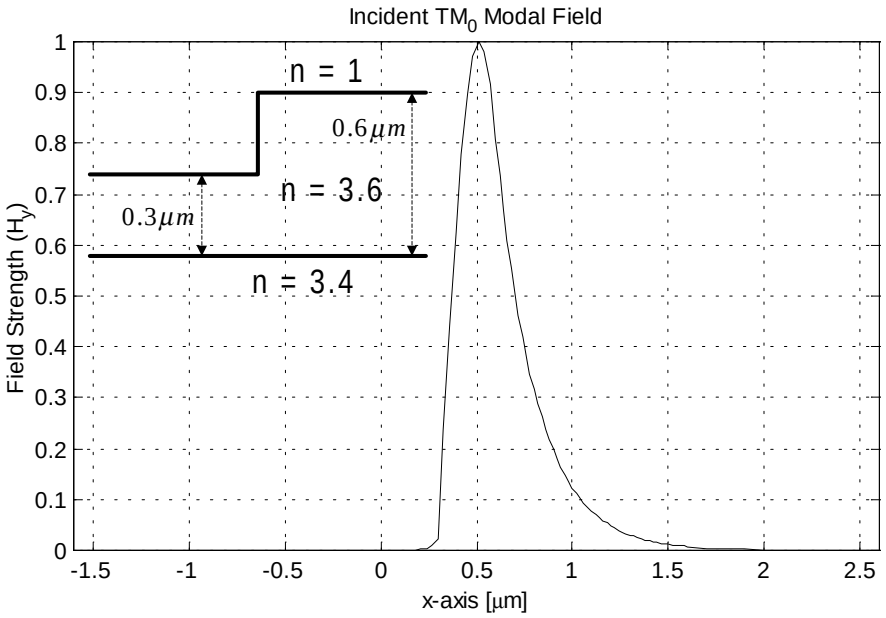

Figure 4.12: Incident TM_0 Modal Field at the Discontinuity

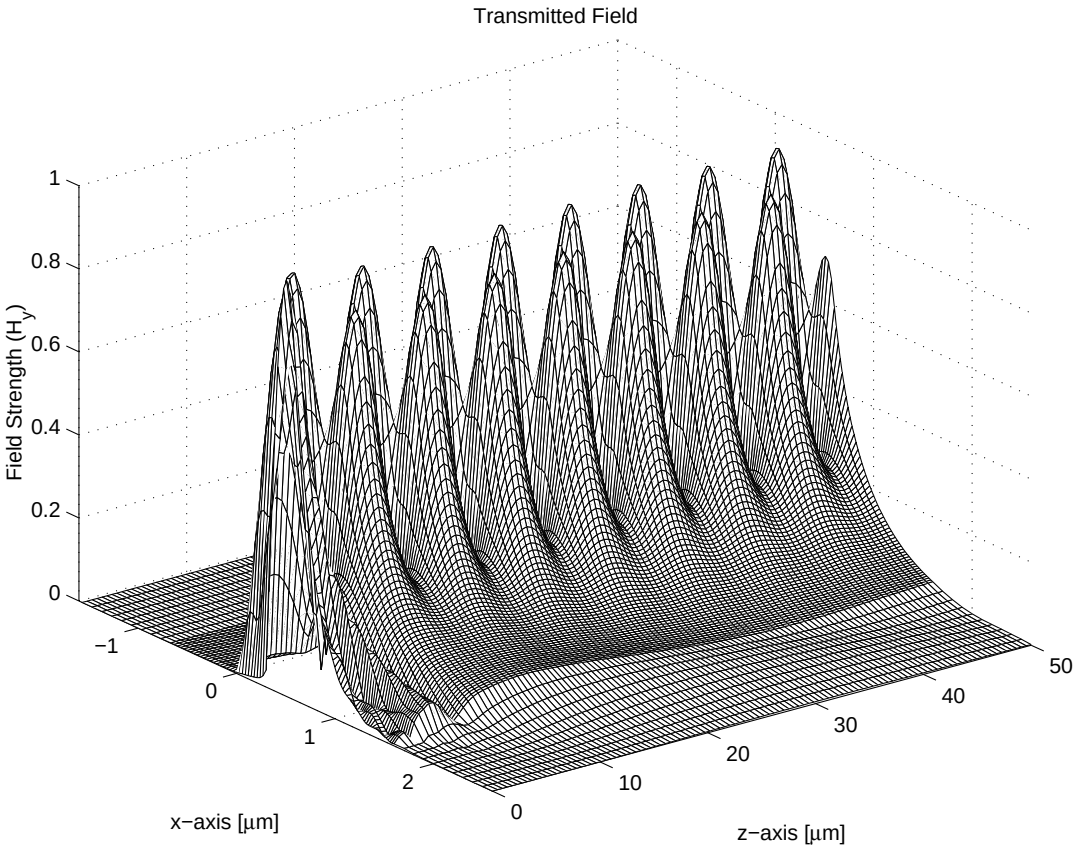

Figure 4.13: Transmitted Field

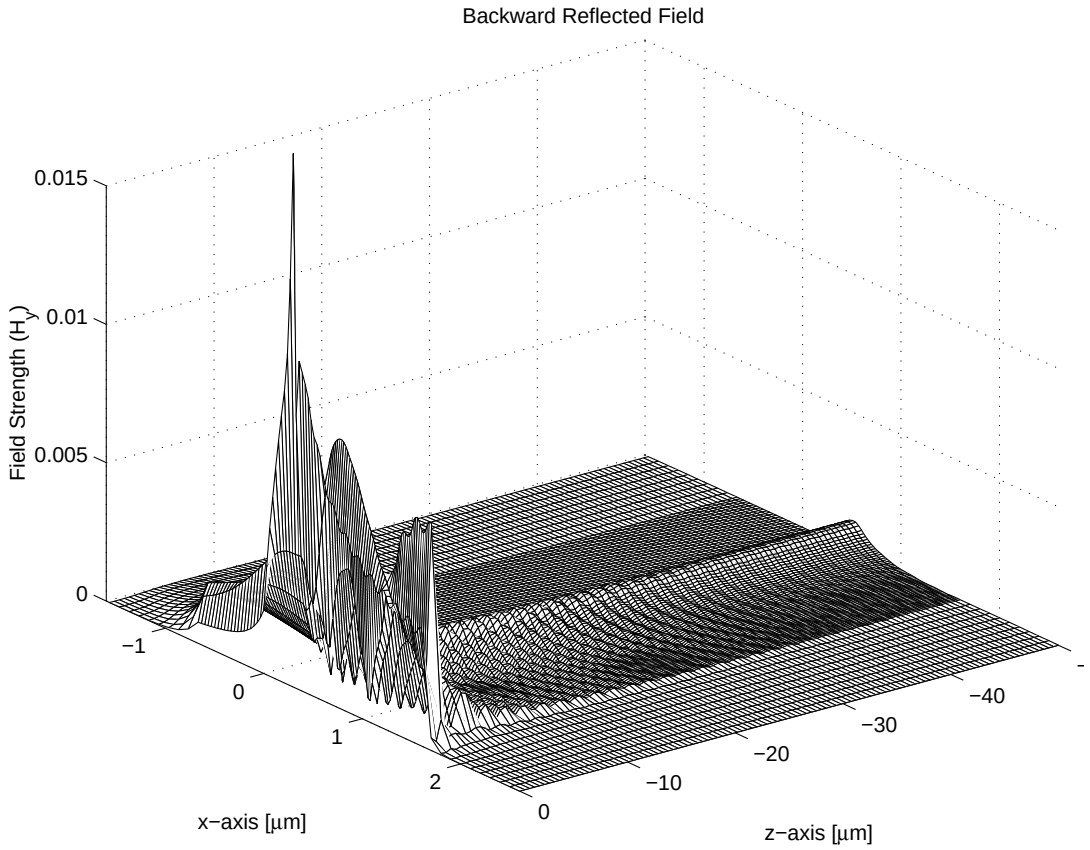

Figure 4.14: Backward Reflected Field

4.5 Double Discontinuity

Consider a waveguide having a double discontinuity as shown in figure 4.15. The problem space is divided into three regions, region 0, region 1 and region 2. The total field in each region is the sum of the forward traveling field, e^{+jSz}, and the backward traveling field, e^{-jSz}.

The field is incident from region 0. After reflection from the first discontinuity at $z = 0$, there is a reflected field in region 0 and a transmitted field in region 1. The transmitted field in region 1 is the incident at the second discontinuity $z = d$,

thus there is a reflected field in region 1 and a transmitted field in region 2.

Thus the total field in all three regions is given by:

$$\Psi_0 = e^{+jS_0z}A_0 + e^{-jS_0z}B_0 \quad (4.23)$$

$$\Psi_1 = e^{+jS_1z}A_1 + e^{-jS_1(z-d)}B_1 \quad (4.24)$$

$$\Psi_2 = e^{+jS_2(z-d)}A_2 \quad (4.25)$$

For the TE polarization, the field vector Ψ and its derivative $\Psi^{'}$ with respect to z are continuous at a discontinuity. Applying the interface condition $\Psi_0|_{z=0} = \Psi_1|_{z=0}$, we get:

$$A_0 + B_0 = A_1 + e^{+jS_1d}B_1 \quad (4.26)$$

Similarly applying the interface condition $\Psi_0^{'}|_{z=0} = \Psi_1^{'}|_{z=0}$, we get:

$$S_0A_0 - S_0B_0 = S_1A_1 - S_1e^{+jS_1d}B_1 \quad (4.27)$$

$$T_1(A_0 - B_0) = A_1 - e^{+jS_1d}B_1 \quad (4.28)$$

where $T_1 = S_1^{-1}S_0$. Similarly applying the interface conditions at $z = d$ and simplifying, we get:

$$e^{+jS_1d}A_1 + B_1 = A_2 \quad (4.29)$$

$$T_2(e^{+jS_1d}A_1 - B_1) = A_2 \quad (4.30)$$

where $T_2 = S_2^{-1}S_1$. By eliminating A_1 and B_1 from equations 4.26, 4.28, 4.29 and 4.30, we get the total transmitted and reflected fields [36]:

$$A_2 = (I + T_2)^{-1}T_2e^{+jS_1d}K_4A_0 \quad (4.31)$$

$$B_0 = K_3A_0 \quad (4.32)$$

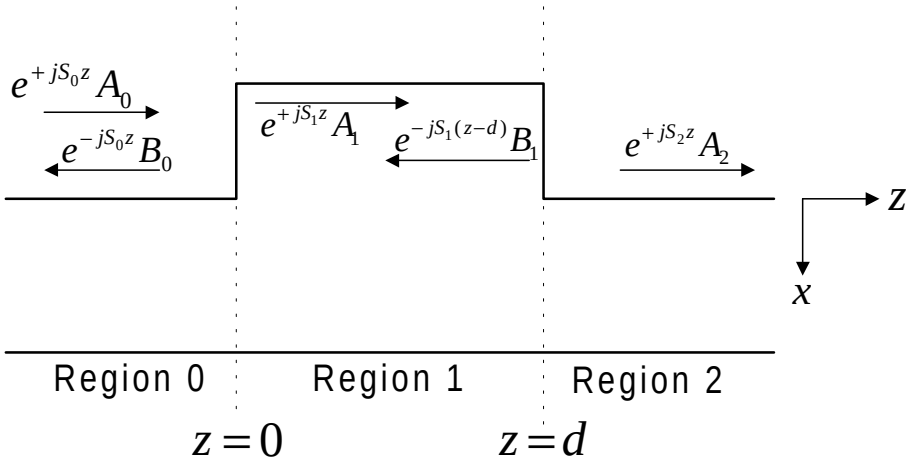

Figure 4.15: A Double Waveguide Discontinuity

where

$$K_4 = (I + T_1) + (I - T_1)K_3 \tag{4.33}$$

and

$$K_3 = (S_1 + S_2)^{-1}(S_2 - S_1) \tag{4.34}$$

For the TM polarization, the results are similar but with $T_1 = S_1^{-1}N_1N_0^{-1}S_0$ and $T_2 = S_2^{-1}N_2N_1^{-1}S_1$.

4.5.1 Results

A double waveguide discontinuity (see figure 4.16) is modeled at $\lambda = 0.86\,\mu m$. The TM_0 mode of the narrow waveguide is incident from the left on the junction. The reflected and transmitted fields are calculated and propagated backward and forward in the respective waveguides. The results are shown in figures 4.17 and

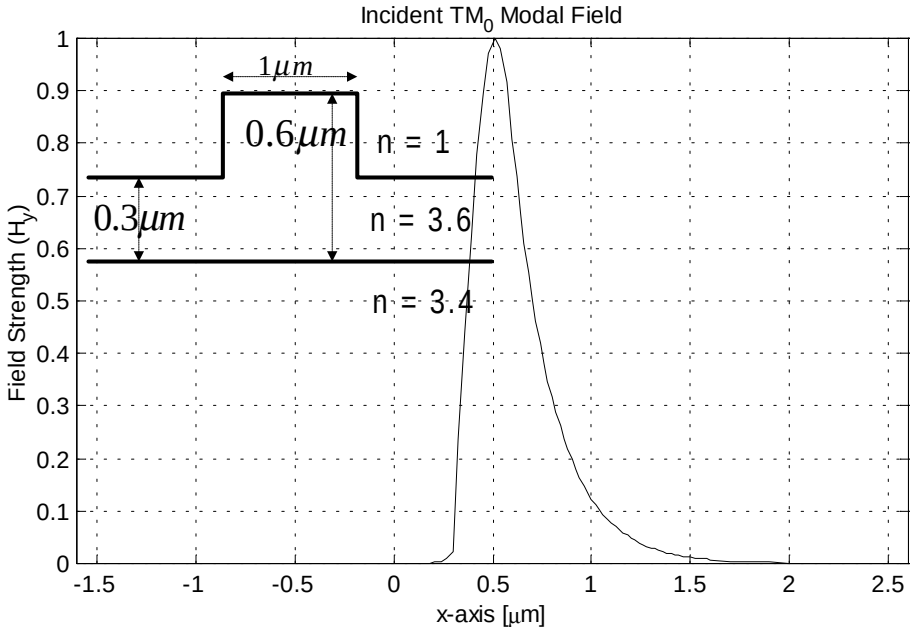

Figure 4.16: Incident TM_0 Modal Field at the First Discontinuity

4.18. The reflected field develops to the TM_0 mode of the narrow waveguide after propagating backward a long distance as the radiative energy leaks out. Similarly, the transmitted field gradually develops into the TM_0 mode of the narrow output waveguide.

4.6 Multiple Discontinuities

Consider the multi-layer structure shown in figure 4.19 [49]. The total field is composed of forward traveling field and backward traveling field. Thus, the total field in each layer is expressed as:

$$\Psi_0 = e^{+jS_0z}A_0 + e^{-jS_0z}B_0 \tag{4.35}$$

$$\Psi_1 = e^{+jS_1z}A_1 + e^{-jS_1(z-d_1)}B_1 \tag{4.36}$$

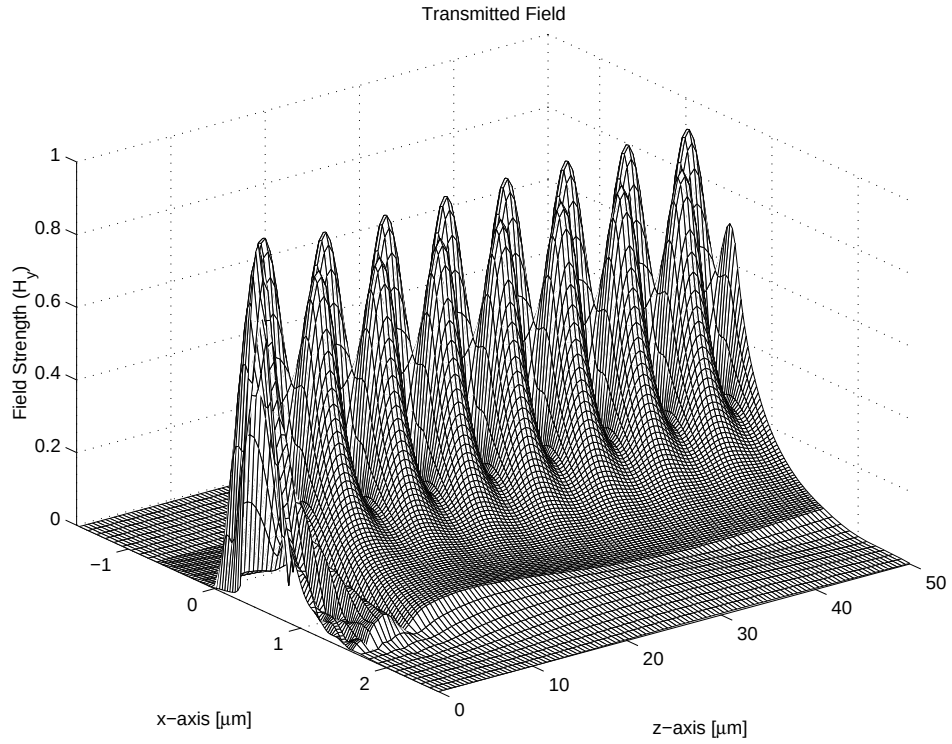

Figure 4.17: Transmitted Field after the Second Discontinuity

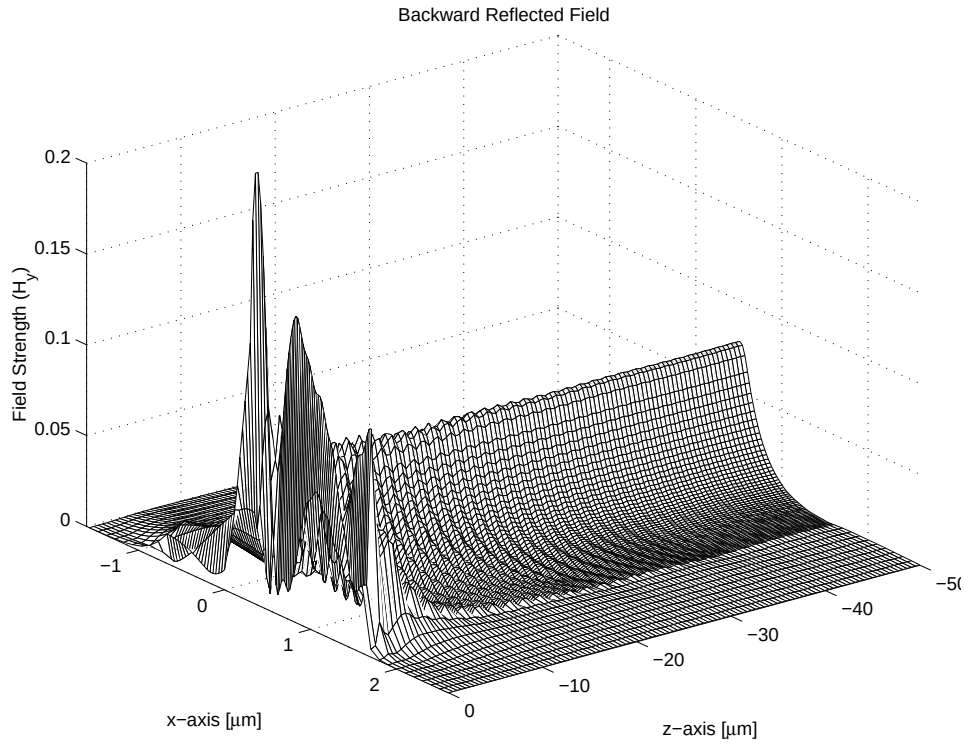

Figure 4.18: Backward Reflected Field from the First Discontinuity

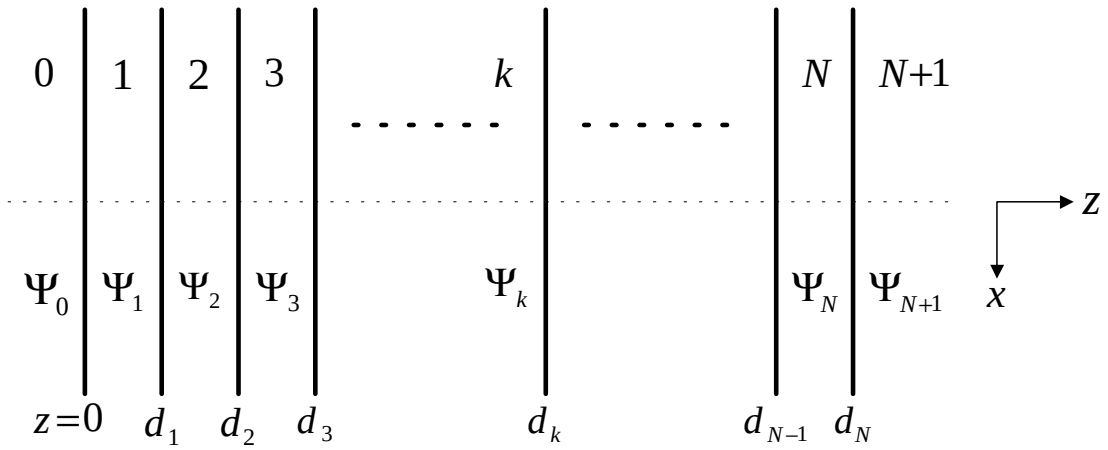

Figure 4.19: Multiple Waveguide Discontinuities

$$\vdots$$

$$\Psi_k = e^{+jS_k(z-d_{k-1})}A_k + e^{-jS_k(z-d_k)}B_k \tag{4.37}$$

$$\vdots$$

$$\Psi_{N+1} = e^{+jS_{N+1}(z-d_N)}A_{N+1} \tag{4.38}$$

The subscript k in Ψ_k and S_k denotes that the column vector Ψ_k and the matrix S_k in the k region. In figure 4.19, the wave is incident on the interface $z = 0$ from the left. In region $N + 1$, the wave is assumed to propagate without reflection in the $+z$ direction. At each discontinuity, the boundary condition requires the continuity of the tangential fields, E_y and H_x. In other words, the continuity of Ψ and $\frac{d\Psi}{dz}$ must be satisfied at the interfaces. Application of these conditions results in the following relationships [49]:

$$e^{jS_k(d_k-d_{k-1})}A_k = \frac{1}{2}(I + S_k^{-1}S_{k+1})A_{k+1} + \frac{1}{2}(I - S_k^{-1}S_{k+1})e^{jS_{k+1}(d_{k+1}-d_k)}B_{k+1} \tag{4.39}$$

$$B_k = \frac{1}{2}(I - S_k^{-1}S_{k+1})A_{k+1} + \frac{1}{2}(I + S_k^{-1}S_{k+1})e^{jS_{k+1}(d_{k+1}-d_k)}B_{k+1} \quad (4.40)$$

where $k = 0, 1, 2, ..., N$, For $k = 0$, $d_0 = d_{-1} = 0$ and for $k = N$, $B_{N+1} = 0$. This is a recursive relationship which expresses the field in layer k in terms of the field in layer $k + 1$. We start from the last layer, in which there is only a forward propagating wave, and work backward layer by layer, until we reach the first layer. Thus the field in last layer is expressed in terms of the field in first layer. From this, we can find the reflection and transmission matrices and hence the reflected and transmitted fields. The field in the intermediate layers can also be calculated if required.

Chapter 5

Analysis of Metal-Clad Waveguide

5.1 Introduction

Metal-clad slab waveguides are of interest in the technology of integrated optics. Metallic layers have been made necessary by a number of applications such as connecting the optical components to other circuits, protecting the optical devices against stray light, and heat sinking. Because of their discrimination against TM modes, metal-clad waveguides have also found application in mode and polarization filtering. The characteristics of the waveguides are strongly influenced by the properties of the metals.

Polarization filters are important elements of integrated optical circuits with applications in the processing of signals from optical fiber sensors and in fiber optic gyroscopes. TE mode transmission has been based on the discriminatory absorption of TE and TM modes such as in metal-clad waveguides, [4, 6]. Experimental work

related to TE-pass polarizers has been reported in references [18], [70] and [71]. TM-pass waveguide polarizers have also been reported. These are based on the discriminatory radiation of the TE and TM modes [72, 73].

The basic three layer metal-clad waveguides are characterized by TM waves with much higher absorption loss than TE waves. The use of a low-index buffer layer of suitable thickness between the core and the metallic layer can further enhance the attenuation of TM waves with respect to TE waves [6]. To reverse this effect and realize a TM-pass polarizer a groove adjacent to a channel waveguide has been made with a low-index buffer layer and a metallic layer deposited on the vertical wall of the groove [71]. This approach can be used to fabricate TM-Pass polarizers on already existing waveguides, but it is somewhat elaborate and would require specialized techniques. The method of reference [72] relies on the fact that by coating a waveguide which is just above cut off with a very thin metallic layer, the TE_0 mode becomes cut off while the TM_0 mode remains guided. This approach cannot be implemented in single mode waveguides in which the TE_0 mode is well guided.

TM_o mode transmission can also be obtained in planar metal-clad waveguides when a high-index buffer layer of suitable thickness is introduced between the core and the metallic layer [22]. The waveguide geometry is shown in Figure 1.3.

5.2 Analysis of Metal-Clad Waveguide by MOL

In this section, the Method of Lines (MOL) is applied to analyze the three-layer metal-clad waveguide without a buffer layer (see figure 5.1) and the four-layer metal-clad waveguide with a high-index buffer layer (see figure 5.2) taken from reference [22], the results are compared with published as well as exact results. A close agreement is found between the MOL calculation of the effective indices (real and imaginary parts) and the modal fields with those available in the literature. Gold is used as a cladding to the waveguides. The operating wavelength is chosen to be $1.55\mu m$. Gold has refractive index of $n = 0.1804 + j10.2$ at $\lambda = 1.55\mu m$. The real part of refractive index square ($n^2 = -104 + j3.68$) is negative. A non-uniform mesh scheme is used in the MOL to model the device effectively. There is no need for the absorbing boundary condition (i-e. PML layer) on the metal-clad side of the waveguide, because the metallic cladding absorbs the field.

The calculations are done using the 7-point formulation to efficiently analyze the metal-clad waveguide using the MOL. The number of sample points used in the middle layer (core) is 40 with a total number of 135 sample points used in the entire problem space. For the metal and the buffer layers very fine mesh size (approximately 0.02 micron) is used. The resulting error in n_{eff} (MOL vs. Exact) is 5.72e-8-j3.63e-9. The time required to calculate n_{eff} and the modal field is around 5 seconds (using an IBM Pentium-III machine at 500 MHz with 128 MB RAM running MATLAB 5.2 under Windows 98).

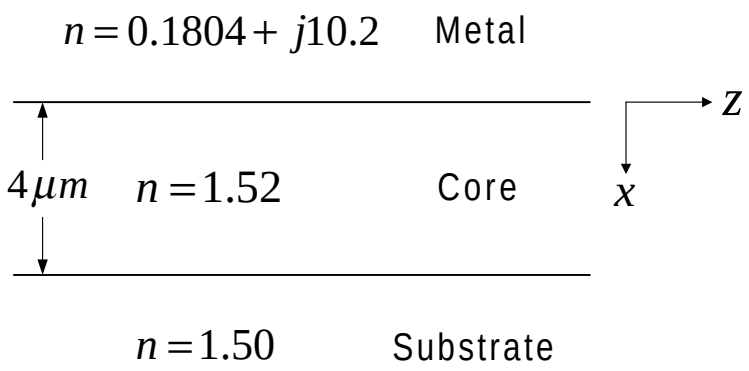

Figure 5.1: Metal-Clad Waveguide without a Buffer Layer

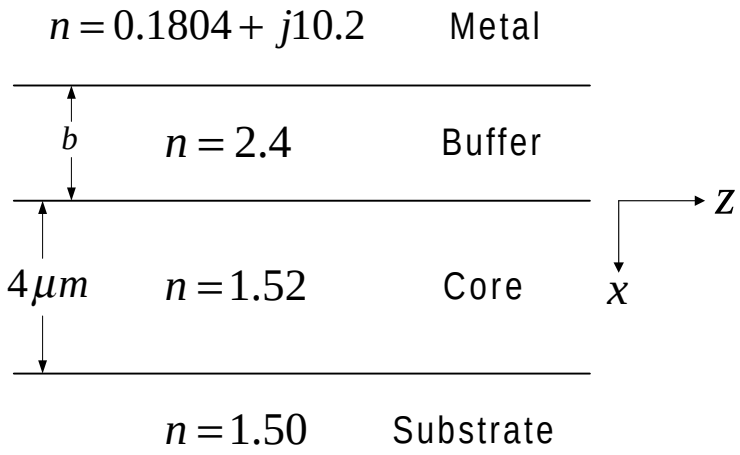

Figure 5.2: Metal-Clad Waveguide with a High-Index Buffer Layer

5.3 Effect of the High-Index Buffer Layer

The metal-clad waveguides shown in figures 5.1 and 5.2 are analyzed by the MOL. The waveguide modes are lossy and therefore have complex effective indices ($n_{eff} = {n_{eff}}' + j{n_{eff}}''$), where ${n_{eff}}'$ is the real part of effective index and ${n_{eff}}''$ is the imaginary part. For guided modes, the real part of the effective index, ${n_{eff}}'$, lies between that of the substrate layer refractive index and the core layer refractive index, that is $1.50 < {n_{eff}}' < 1.52$. The imaginary part of the effective index, ${n_{eff}}''$, is converted into power loss per unit distance, that is in terms of dB/cm. The field patterns of the supported TE and TM modes for both types of waveguides without and with a buffer layer are shown in figures 5.3 and 5.4 respectively. The real and imaginary parts of the effective index and power loss are shown in tables 5.1, 5.2, 5.3 and 5.4.

Without a buffer layer, the TM_0 mode is seen to have higher attenuation (i-e. higher power loss) than the TE_0 mode, while the TE_1 mode is cut-off. This makes the three-layer metal-clad waveguide a TE-pass polarizer.

Mode	${n_{eff}}'$	${n_{eff}}''$	Power Loss (dB/cm)
TE_0	1.51241	2.37701e-6	0.837
TM_0	1.50818	144.93140e-6	51.030

Table 5.1: ${n_{eff}}'$, ${n_{eff}}''$ and Power Loss of the supported TE and TM modes for a Metal-Clad Waveguide without a Buffer Layer at $\lambda = 1.55\mu$m

However, the introduction of a high-index buffer layer of suitable thickness between the core and the metallic cladding enhances the attenuation of all TE modes

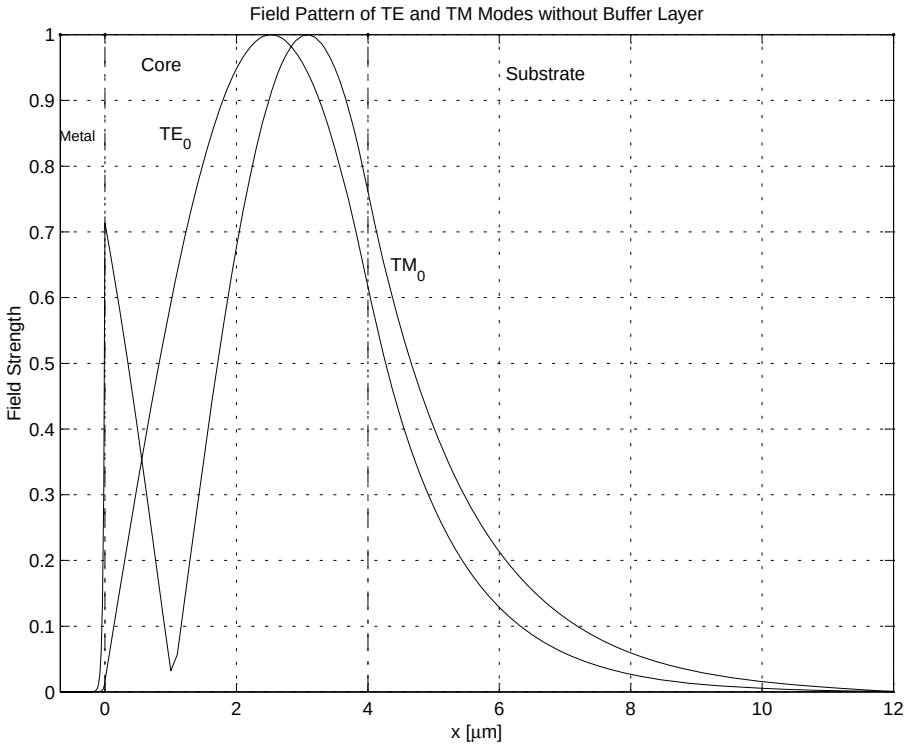

Figure 5.3: Field Pattern for TE and TM modes without a Buffer Layer

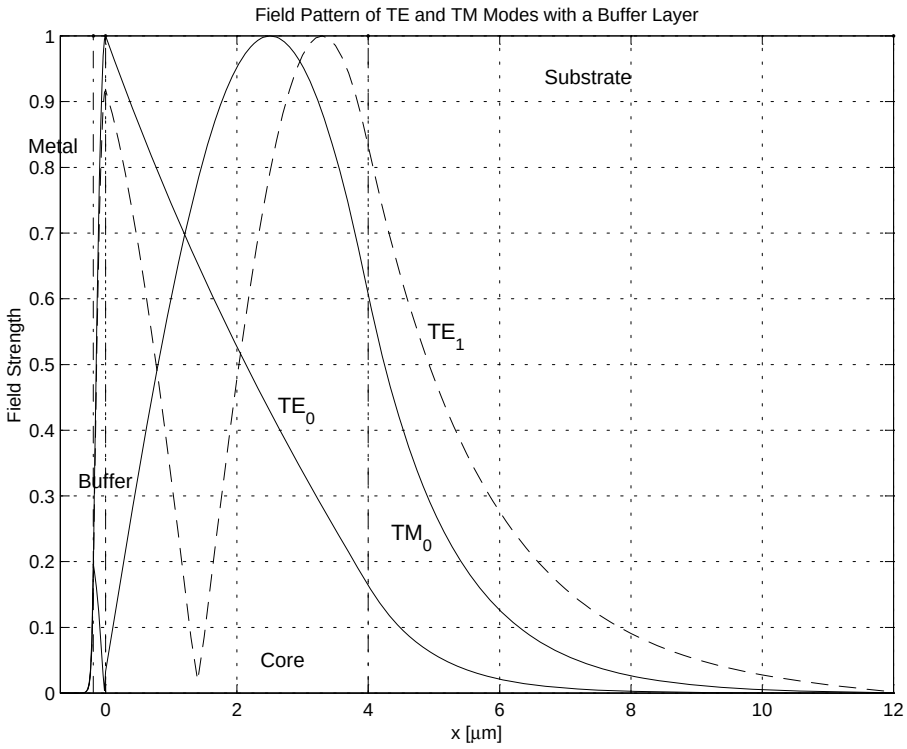

Figure 5.4: Field Pattern for TE and TM modes with a Buffer Layer ($b = 0.190\mu$m)

and reduces the attenuation of the TM_0 mode. This makes the metal-clad waveguide with a high-index buffer layer of suitable thickness effectively a single-mode waveguide and a TM-pass polarizer. Both TE_0 and TE_1 modes decay significantly within a short propagation distance due to their high attenuation constant.

Mode	$n_{eff}{}'$	$n_{eff}{}''$	Power Loss (dB/cm)
TE_0	1.51642	104.28290e-6	36.718
TE_1	1.50261	126.96875e-6	44.705
TM_0	1.51235	4.86571e-6	1.713

Table 5.2: $n_{eff}{}'$, $n_{eff}{}''$ and Power Loss of the supported TE and TM modes for a Metal-Clad Waveguide with a Buffer Layer ($b = 0.180\mu$m) at $\lambda = 1.55\mu$m

Mode	$n_{eff}{}'$	$n_{eff}{}''$	Power Loss (dB/cm)
TE_0	1.51812	177.21914e-6	62.398
TE_1	1.50433	147.99852e-6	52.110
TM_0	1.51239	4.86065e-6	1.711

Table 5.3: $n_{eff}{}'$, $n_{eff}{}''$ and Power Loss of the supported TE and TM modes for a Metal-Clad Waveguide with a Buffer Layer ($b = 0.185\mu$m) at $\lambda = 1.55\mu$m

Mode	$n_{eff}{}'$	$n_{eff}{}''$	Power Loss (dB/cm)
TE_0	1.52102	295.74970e-6	104.133
TE_1	1.50616	141.13064e-6	49.692
TM_0	1.51243	4.88117e-6	1.719

Table 5.4: $n_{eff}{}'$, $n_{eff}{}''$ and Power Loss of the supported TE and TM modes for a Metal-Clad Waveguide with a Buffer Layer ($b = 0.190\mu$m) at $\lambda = 1.55\mu$m

In this case, it is apparent that the introduction of a suitable high-index buffer layer between the core and the metallic cladding converts this waveguide from a TE-pass to a TM-pass polarizer.

5.4 Effect of Varying the Buffer Layer Thickness

We are interested in finding a suitable buffer layer thickness which maximize the power loss of the TE modes and that minimizes the power loss of the TM_0 mode. The mode index or effective index, n_{eff}, is given by $\beta = k_o n_{eff}$. Due to the complex nature of the dielectric constant of the metallic layer all effective indices become complex and are written as $\beta = \beta' + j\beta'' = k_o(n_{eff}{}' + jn_{eff}{}'')$, where $\beta'' = k_o n_{eff}{}''$ is the mode attenuation constant which accounts for the absorption loss due to the presence of the metal.

In figure 5.5 the TE/TM modal loss versus buffer layer thickness (b) is shown. For b=0 the TM_0 mode is seen to have higher attenuation than the TE_0 mode. However, as b increases, the TM_0 mode attenuation begins to decrease while the TE_0 mode attenuation starts to increase and the TE_1 mode becomes guided beyond some higher value of b (b=0.167 μm). For higher values of b, the TE_0 mode attenuation increases while the TE_1 mode attenuation decreases. Buffer layer thickness in the range b=0.17 μm to b=0.20 μm is favorable so that this waveguide functions as a TM-pass polarizer.

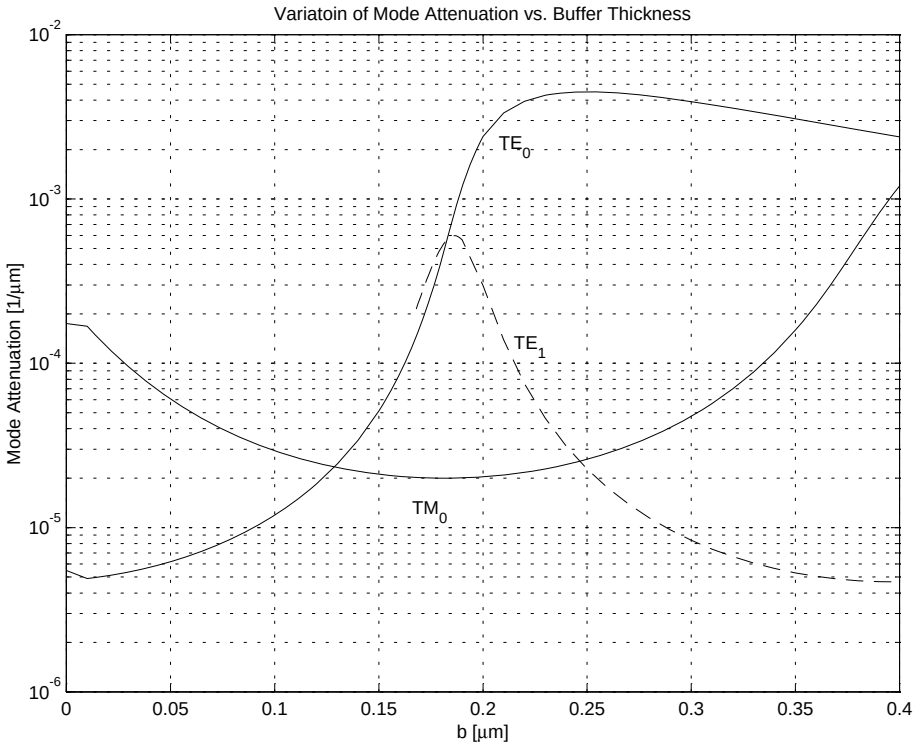

Figure 5.5: Variation of Mode Attenuation (β'') vs. Buffer Layer Thickness (b)

5.5 Comparison of the Exact and the MOL Results

The structure of the TM-pass transmission mode polarizer is shown in figure 5.6. The metal used is Gold which has a refractive index of $n = 0.1804 + j10.2$ at the operating wavelength $\lambda = 1.55\mu m$. A non-uniform mesh scheme is used in the MOL. The PML layer is used as an absorbing boundary condition to absorb the radiation from the two discontinuities at the input and output of the polarizer. A single layer PML is used on top of the computational window and a double layer PML is used at the bottom of the computational window. The first PML layer at the substrate

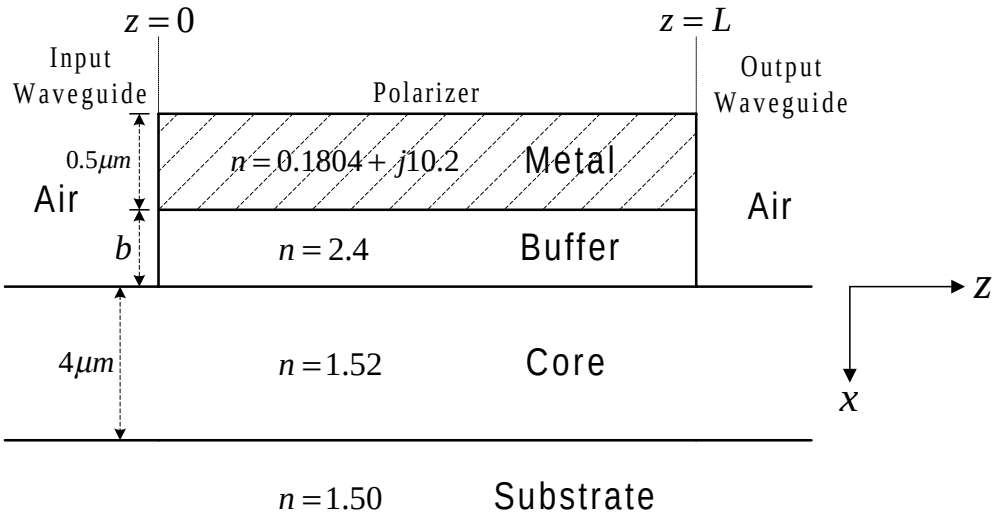

Figure 5.6: TM-Pass Transmission Mode Polarizer

has lower decay factor constant (σ) than the second layer to effectively absorb the radiation at the input and output interfaces of the waveguide. The number of sample points used in each PML layer is 7. The calculations are done using the 7-point formulation. The number of sample points used in the middle layer is 40.

The field patterns of all supported TE and TM modes of the input (and output) waveguide is shown in figure 5.7. The corresponding field pattern of the metal-clad polarizer section is shown in figure 5.8.

To verify the accuracy of the MOL results, the TE_0 and TM_0 mode power loss of the TM-Pass polarizer is plotted against the polarizer length (L) and the results are compared with the exact values obtained by the one-dimensional stationary mode solver program, STF1.

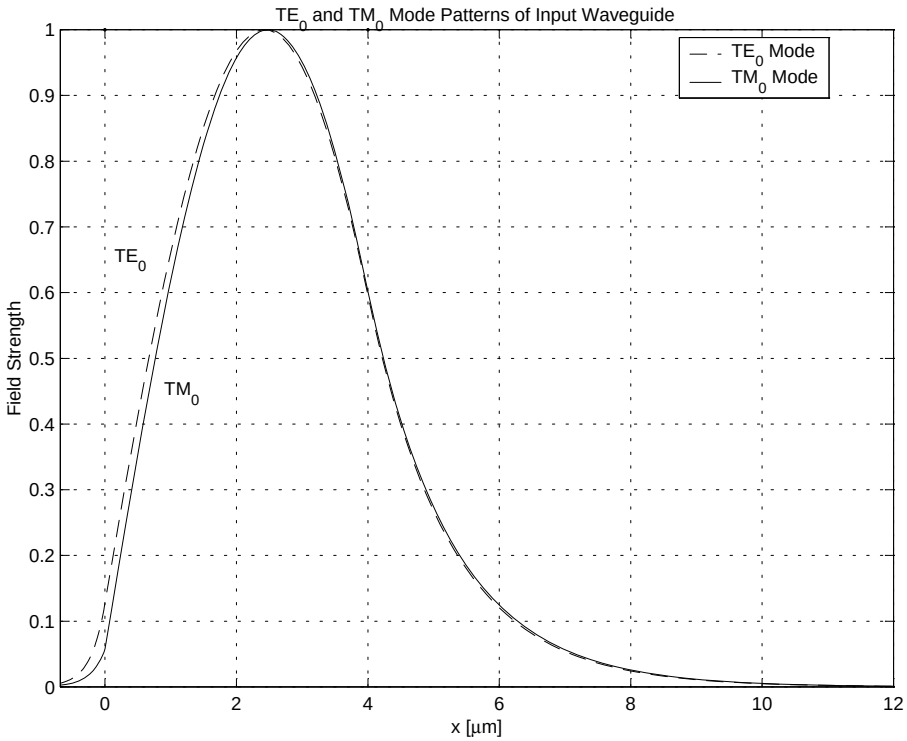

Figure 5.7: TE_0 and TM_0 Mode Patterns of the Input (and Output) Waveguide

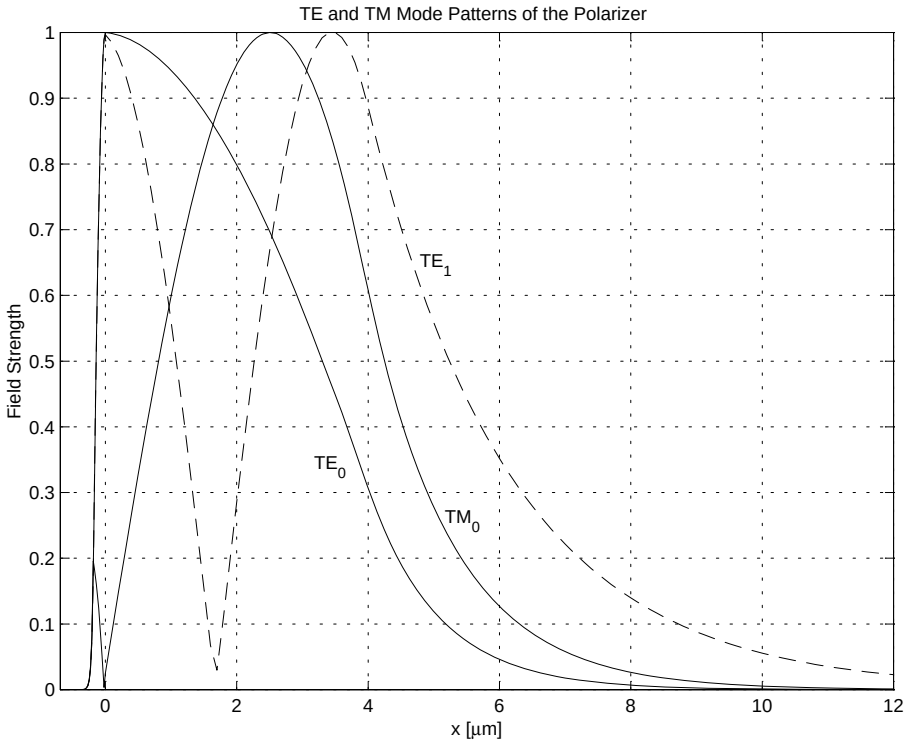

Figure 5.8: TE and TM Mode Patterns of the Polarizer

5.5.1 Calculation of Power Loss by STF1

The STF1 program is written by Al-Jamid. The program listing is shown in Appendix B. This program computes the eigenvalues of guided TE and TM modes of a slab waveguide with an arbitrary number of layers. A zero finding program based on Muller's method [74] is used in conjunction with STF1. The STF1 program gives the exact value of the modal effective index (both real and imaginary parts) and modal field pattern. The imaginary part of the effective index obtained by STF1 is then converted into power loss (dB), using the relation:

$$Power\ Loss = 20\, k_o\, n_{eff}{}''\, L\ log_{10}e \tag{5.1}$$

where L is the length of polarizer.

5.5.2 Calculation of Modal Power and Modal Coefficients in an Arbitrary Field

Any general two-dimensional field $\psi(x,z)$ can be represented as a linear combination of a complete set of orthonormal modes, that is [35]:

$$\begin{aligned}\psi(x,z) &= \alpha_0 f_0(x)e^{j\beta_0 z} + \alpha_1 f_1(x)e^{j\beta_1 z} + \alpha_2 f_2(x)e^{j\beta_2 z} + \cdots + \alpha_m f_m(x)e^{j\beta_m z} + \cdots \\ &\quad + \alpha_M f_M(x)e^{j\beta_M z} + \int_v \alpha_v f_v(x)e^{j\beta_v z}dv \end{aligned} \tag{5.2}$$

where α_m = mth-mode expansion coefficient, β_m = mth-mode propagation constant and $\int_v \alpha_v f_v(x)e^{j\beta_v z}dv$ represents an integration over the continuum of all radiation

modes. The integer M represents the highest possible order of the guided modes. The modal transverse profiles $\{f_m(x)\}$ describe a set of orthonormal functions over the transverse coordinate. For a single-mode waveguide ($M = 0$):

$$\psi(x,z) \;=\; \alpha_0 f_0(x) e^{j\beta_0 z} + \int_v \alpha_v f_v(x) e^{j\beta_v z} dv \tag{5.3}$$

At the input end of the polarizer ($z = 0$) the field ψ becomes:

$$\psi(x,0) \;=\; \alpha_0 f_0(x) + \int_v \alpha_v f_v(x) dv \tag{5.4}$$

By using the orthogonality relation between the modal fields, which is expressed as [75]:

$$\int_{-\infty}^{+\infty} \frac{f_m(x)}{K} f_n(x) dx = \begin{cases} 0 & for\ m \neq n \\ \int_{-\infty}^{+\infty} \frac{f_m^2(x)}{K} dx & for\ m = n \end{cases} \tag{5.5}$$

where K is defined as:

$$K = \begin{cases} n^2(x) & for\ TM\ modes \\ 1 & for\ TE\ modes \end{cases} \tag{5.6}$$

and $n(x)$ represents the refractive index distribution.

The modal coefficient α_m is given by [35]:

$$\alpha_m = \frac{\int_{-\infty}^{+\infty} \psi(x,0) \frac{f_m(x)}{K} dx}{\int_{-\infty}^{+\infty} \frac{f_m^*(x) f_m(x)}{K} dx} \tag{5.7}$$

Hence the coefficient of the fundamental mode α_0 is given by:

$$\alpha_0 = \frac{\int_{-\infty}^{+\infty} \psi(x,0) \frac{f_0(x)}{K} dx}{\int_{-\infty}^{+\infty} \frac{f_0^2(x)}{K} dx} \tag{5.8}$$

The power flowing in the z direction per unit length of the y direction is given by [59]:

$$P_z = \frac{1}{2} \int_{-\infty}^{+\infty} Re(\mathbf{E} \times \mathbf{H}^*)_z dx \tag{5.9}$$

5.5.3 Calculation of Power Loss and Modal Coefficients in the MOL

The field obtained at the output of the polarizer by the MOL is not composed purely of the fundamental mode. This field is a superposition of the fundamental and radiation modes of the output waveguide. Radiation modes decay along the direction of propagation in the waveguide. It is found that these radiation modes are attenuated completely after a propagation distance of $1500\mu m$. Since the input and output waveguides are single-mode the remaining field in the output waveguide after a sufficiently long distance becomes purely composed of the fundamental mode. The fundamental mode power loss can easily be found by squaring the amplitude of the modal field.

In an another method, the overlap integral given by equation 5.8 is used to calculate α_0. In this case we apply equation 5.8 at the input plane of the output waveguide, immediately after the polarizer output.

For TM modes, the incident magnetic field is:

$$H_y = e^{+jS_0 z} A_0 \tag{5.10}$$

where the $M \times 1$ column matrix, A_0, represents the incident field at $z = 0$ and the $M \times M$ matrix $S_0 = \sqrt{Q_0}$ where Q_0 is defined in chapter 3. Using Maxwell's equations, the x component of the incident electric field for TM modes is given by:

$$E_x = \frac{j}{\omega \epsilon_o n_i^2} \frac{\partial H_y}{\partial z} \tag{5.11}$$

where n_i is the sampled refractive index on the ith discretization line. Substituting equation 5.10 into equation 5.11, we have:

$$E_x = \frac{j}{\omega \epsilon_o N} \frac{\partial}{\partial z} (e^{+jS_0 z} A_0) \tag{5.12}$$

$$= -\frac{1}{\omega \epsilon_o N} S_0 e^{+jS_0 z} A_0 \tag{5.13}$$

where the matrix N is defined in chapter 3. Hence, the incident electric and the incident magnetic fields component, E_x and H_y, at $z = 0$ are given by:

$$E_x|_{z=0} = -\frac{1}{\omega \epsilon_o N} S_0 A_0 \tag{5.14}$$

$$H_y|_{z=0} = A_0 \tag{5.15}$$

The average power flow (per unit length in the y-direction) in the z direction is given by:

$$P_z = \frac{1}{2} Re \int_{-\infty}^{\infty} E_x H_y^* dx \tag{5.16}$$

For discrete samples, integration is replaced by summation over the index of the array.

$$P_z = \frac{1}{2} Re \left[\sum_{m=1}^{M} E_{xm} H_{ym}^* \Delta x \right] \tag{5.17}$$

For non-uniform mesh size the Δx can be replaced by $(\Delta x)_m$. Substituting E_x and H_y from equations 5.14 and 5.15 into equation 5.17, we have:

$$P_z = \frac{1}{2\omega\epsilon_o} Re\left[N^{-1} S_0 A_0 A_0^*\right] \Delta x \tag{5.18}$$

Using the modal coefficient formula 5.7, we can calculate the modal expansion coefficient α_m, that is:

$$\alpha_m = \frac{A^t N^{-1} F_m}{F_m^t N^{-1} F_m} \tag{5.19}$$

where the $M \times 1$ vector F_m represents the discretized modal field distribution of the mth mode, A is the discretized general field and the superscript t represents transpose of a vector. The above formula can be used for the TE modes by replacing matrix N with the identity matrix I.

5.5.4 Results

The fundamental mode power loss using the method of lines (MOL) is found by the overlap integral (refer to equation 5.19) and by calculating the fundamental mode amplitude which is obtained after a propagation of sufficiently long distance in the output waveguide. Both methods produce almost identical results and hence, equation 5.19 will be used to find the fundamental amplitude and subsequently the mode power loss throughout in this thesis.

The results by the MOL and STF1 are shown in figures 5.9 and 5.10 for TM_0 and TE_0 modes respectively. For TM_0 mode, the MOL results are in close agreement

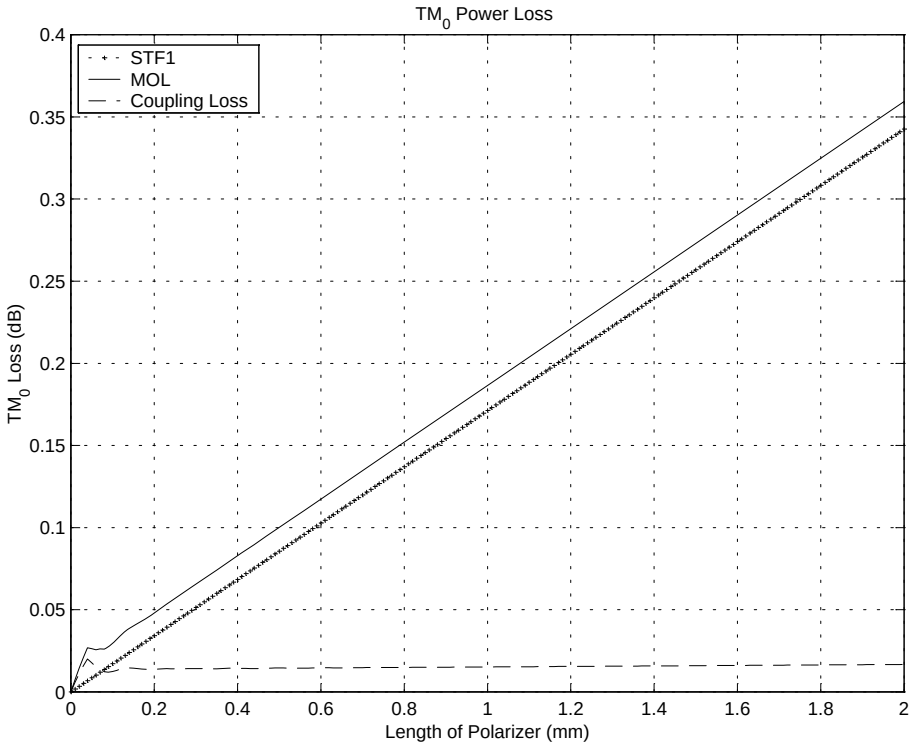

Figure 5.9: TM_0 Mode Power Loss vs. Polarizer Length

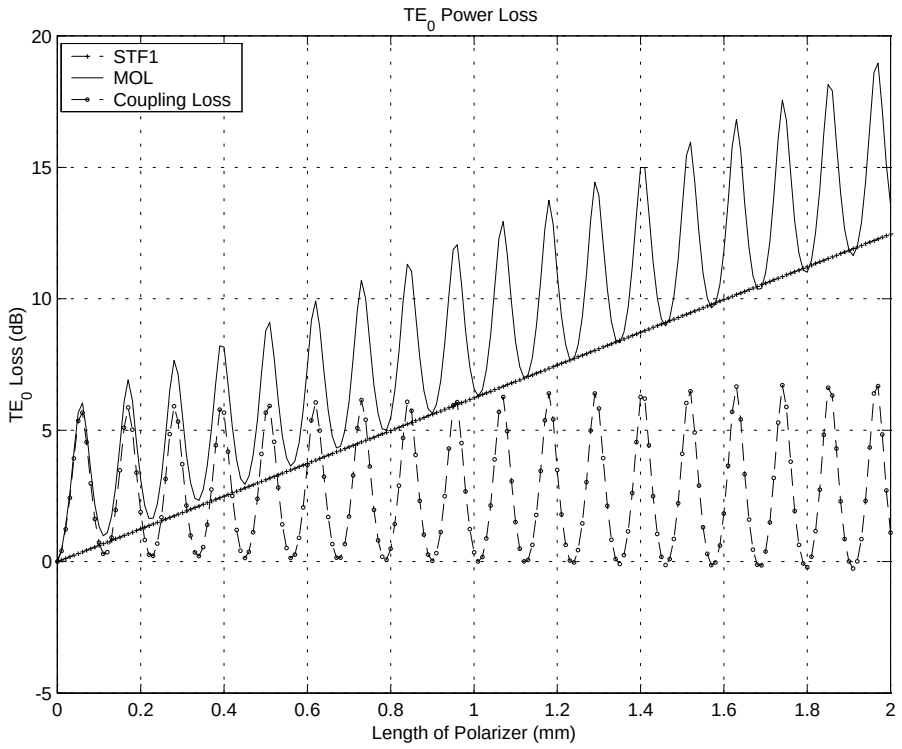

Figure 5.10: TE_0 Mode Power Loss vs. Polarizer Length

with those obtained from the STF1 program. The higher loss of the TM_0 mode as calculated by the MOL is due to the fact that the MOL account for the coupling loss, while STF1 does not. For the TE case, the MOL results are different from the STF1 program. This is due to the interference effect of the TE_0 and TE_1 modes within the polarizer which results in the observed ripples. The absence of these ripples in the STF1 results are due to the fact that STF1 accounts for the fundamental TE mode only and does not account for the interference between the TE_0 and the TE_1 modes.

5.6 Metal-Clad TE-Pass Polarizer

The metal-clad TE-pass polarizer is shown in figure 5.11. The polarizer performance is evaluated using standard methods. The most commonly used performance parameters are the extinction ratio and the insertion loss.

The extinction ratio is defined as the ratio of the power in the desired polarization to that in the orthogonal polarization [71] and insertion loss is defined as the power loss in the desired polarization.

For TE-pass polarizer, the polarization extinction ratio (PER) is given by:

$$PER = 10\ log_{10}\ \left(\frac{Power\ Remaining\ in\ TE_0\ mode}{Power\ Remaining\ in\ TM_0\ mode}\right) \tag{5.20}$$

OR

$$PER = TE_0\ dB\ Loss - TM_0\ dB\ Loss \tag{5.21}$$

where

$$TE_0\ dB\ Loss \;=\; 10\ log_{10}\ (Power\ Remaining\ in\ TE_0\ mode\ at\ the\ output)$$

$$TM_0\ dB\ Loss \;=\; 10\ log_{10}\ (Power\ Remaining\ in\ TM_0\ mode\ at\ the\ output)$$

and polarization insertion loss (PIL) is defined as:

$$PIL = 10\ log_{10}\ (Power\ Remaining\ in\ TE_0\ mode) = TE_0\ dB\ Loss \qquad (5.22)$$

It is assumed that the incident field has unit amplitude and unit power (i-e. 1 Watt), hence the power remaining in a mode is actually the fundamental mode power (i-e. the square of the fundamental amplitude) at the output.

The TE-pass polarizer extinction ratio and insertion loss increase with polarizer length as shown in figures 5.12 and 5.13. The ripples at the beginning of figure 5.12 is due to the interference of the TM_0 and TM_{-1} (surface plasmon) modes. The calculations are done using the MOL with seven-point formulation.

5.7 Metal-Clad TM-Pass Polarizer

The metal-clad TM-pass polarizer (see figure 5.6) performance mainly depends on the buffer layer thickness and polarizer length. The TE_0 loss increases with the polarizer length causing high extinction ratio which is favorable but polarizer insertion loss also increases significantly.

For a TM-pass polarizer, the polarization extinction ratio (PER) is given by:

$$PER = 10\ log_{10}\ \left(\frac{Power\ Remaining\ in\ TM_0\ mode}{Power\ Remaining\ in\ TE_0\ mode}\right) \qquad (5.23)$$

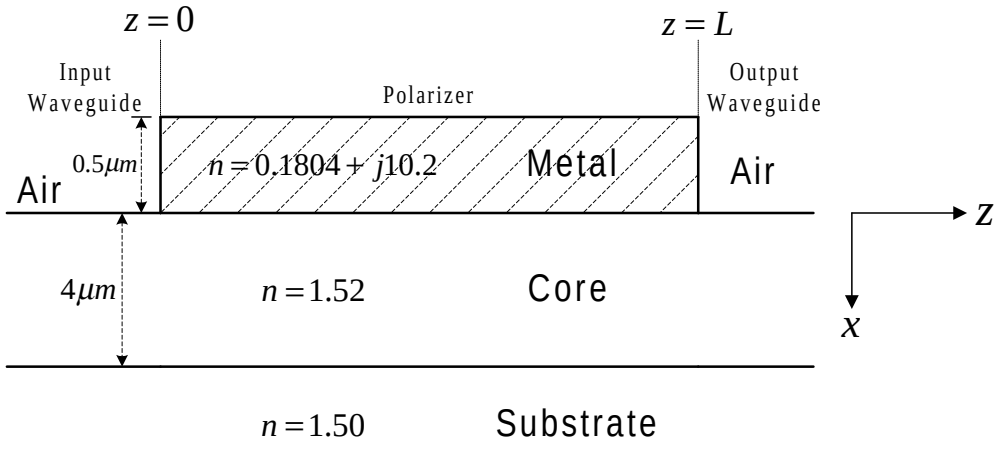

Figure 5.11: Metal-Clad TE-Pass Polarizer

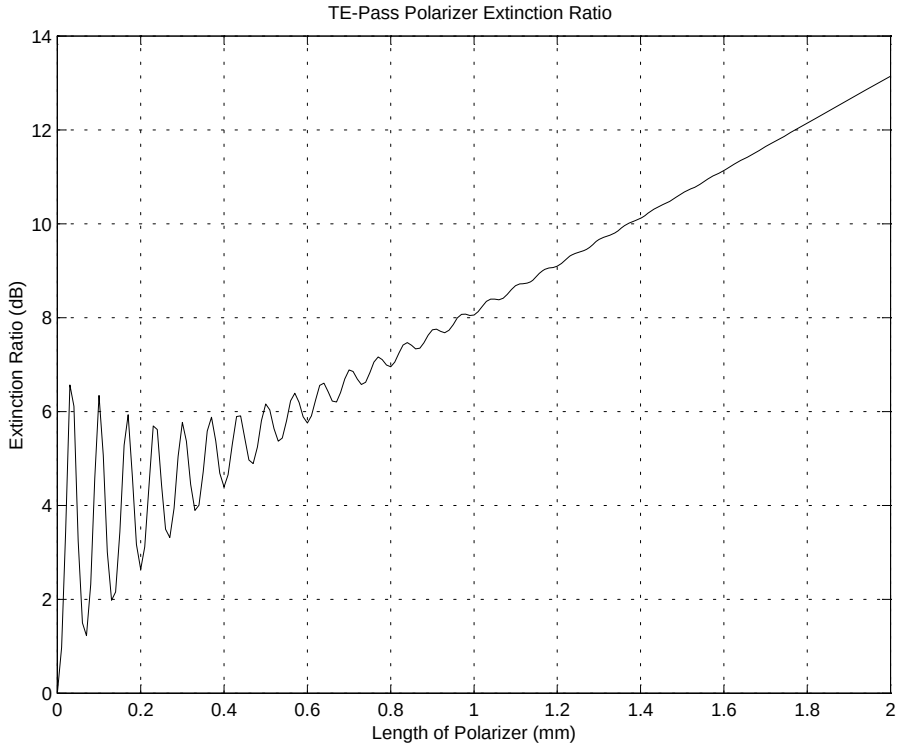

Figure 5.12: TE-Pass Polarizer Extinction Ratio

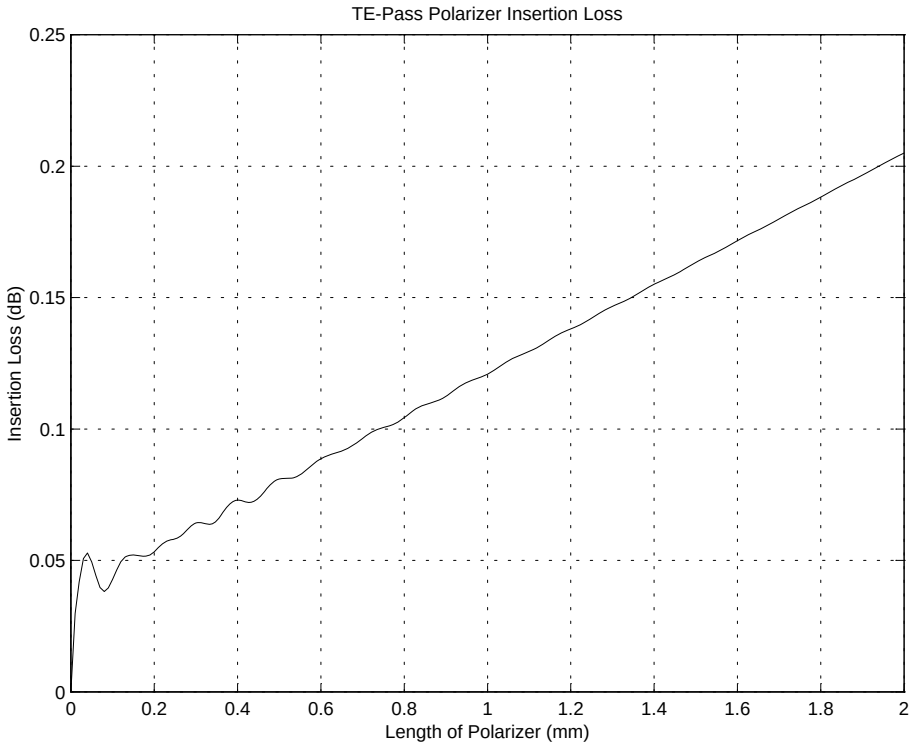

Figure 5.13: TE-Pass Polarizer Insertion Loss

OR

$$PER = TM_0\ dB\ Loss - TE_0\ dB\ Loss \tag{5.24}$$

and polarization insertion loss (PIL) is defined as:

$$PIL = 10\ log_{10}\ (Power\ Remaining\ in\ TM_0\ mode) = TM_0\ dB\ Loss \tag{5.25}$$

The results of the extinction ratio, the insertion loss and the figure of merit for different buffer layer thicknesses are obtained using the MOL with seven-point formulation. It is concluded that the insertion loss has nearly a constant rate of increase for a wide range of buffer layer thicknesses (b=0.175 μm to 0.20 μm) as shown in figure 5.14 while the extinction ratio and the figure of merit are very sensitive to the polarizer length. From figures 5.15 and 5.16, it is obvious that the

extinction ratio is very high for a certain short polarizer length, optimum polarizer length. The extinction ratio at the optimum polarizer lengths for different buffer layer thicknesses is summarized in table 5.5. For simplicity and improved understanding, the extinction ratio with buffer layer thicknesses 0.190 μm and 0.192 μm is shown in separate figures. With buffer layer thickness 0.192 μm and polarizer length 0.05 mm, the extinction ratio is very high as shown in figure 5.16. The short length polarizer offers very low loss in the TM_0 mode case.

Buffer Thickness b (μm)	Optimum Polarizer Length L (mm)	Polarizer Extinction Ratio PER (dB)
0.185	1.97	18.5
0.186	1.95	22.1
0.187	1.93	27.8
0.188	1.47	33.5
0.188	1.58	35.8
0.189	0.91	31.3
0.189	1.23	36.5
0.190	0.47	27.7
0.190	0.68	26.8
0.191	0.15	20.8
0.191	0.56	23.8
0.192	0.05	34.7
0.192	0.15	24.5
0.193	0.05	22.0

Table 5.5: TM-Pass Transmission Mode Polarizer Optimum Lengths for Different Buffer Layer Thicknesses

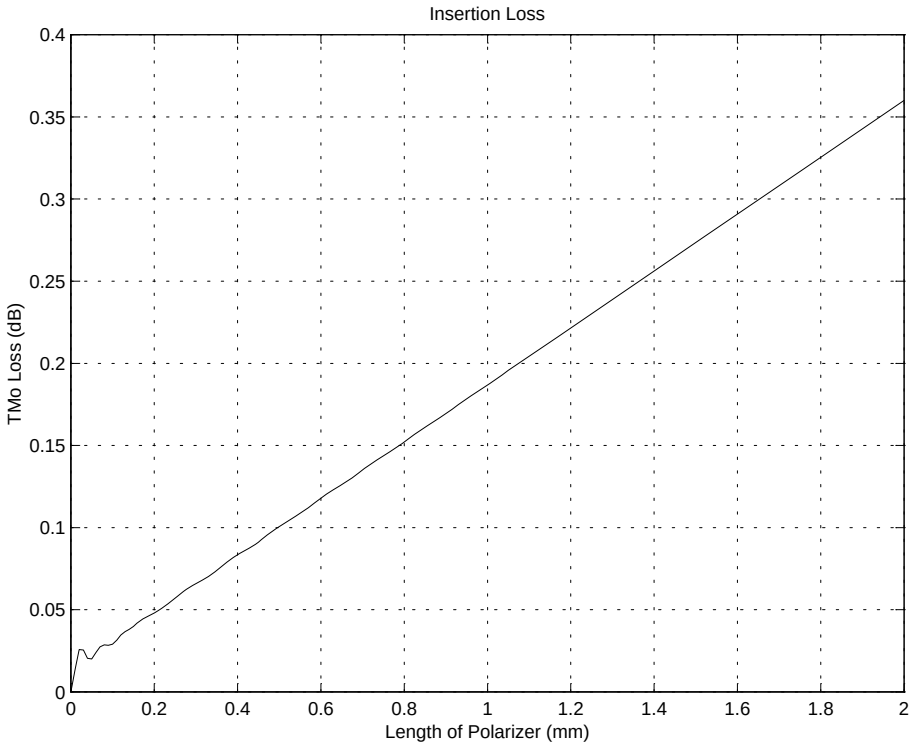

Figure 5.14: TM-Pass Polarizer Insertion Loss

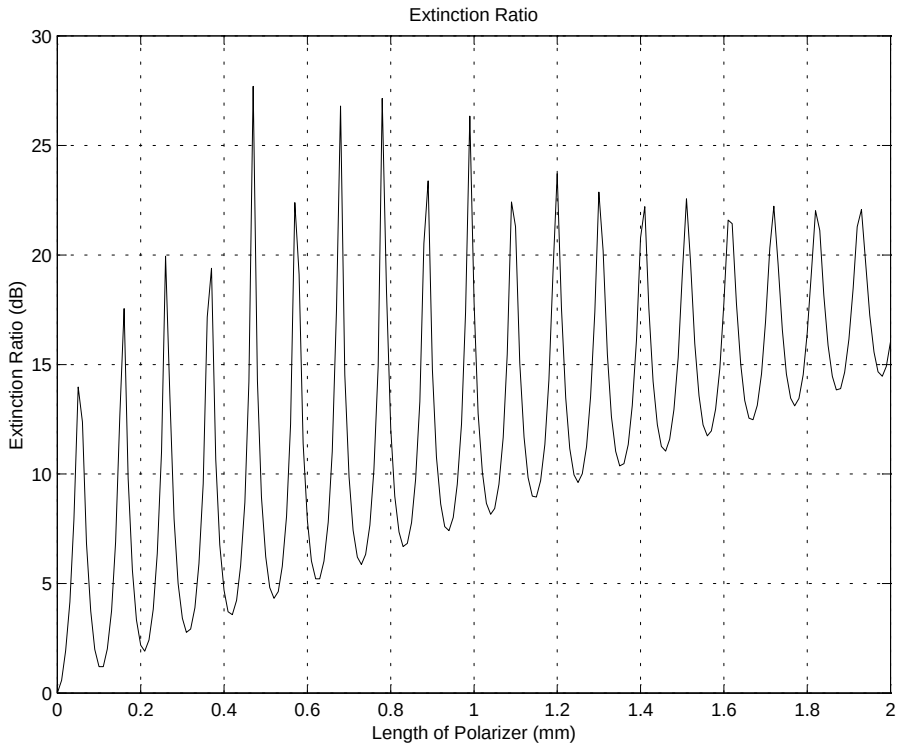

Figure 5.15: TM-Pass Polarizer Extinction Ratio for b=0.190 μm

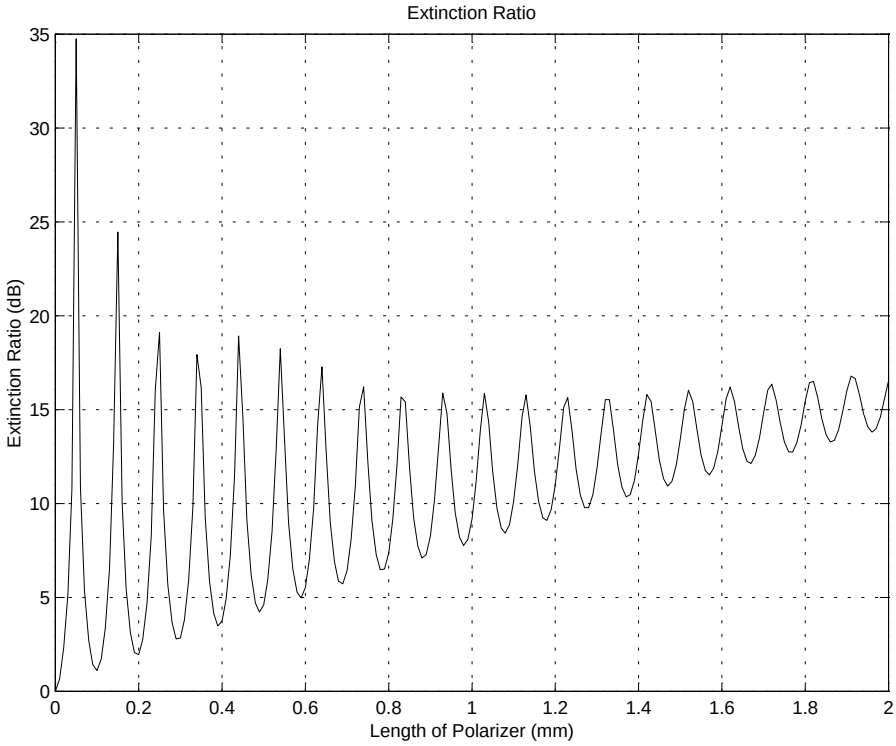

Figure 5.16: TM-Pass Polarizer Extinction Ratio for b=0.192 μm

Chapter 6

The Cascading and Doubling Algorithm: Application to Periodic Waveguide Gratings

6.1 Gratings

Although periodically stratified media have been a subject of study and discussion since 1887 [76], the interest in corrugated dielectric waveguides initially started with the possibility of guiding light by dielectric layers. Corrugated waveguides, also called gratings, have since been playing important roles in the design and operation of many devices in integrated optics. Figure 6.1 shows a typical example of a waveguide with rectangular corrugations. There are a variety of applications of

gratings in integrated optics. The most common of these applications is in wavelength filtering. In addition, gratings are used in coupling the electromagnetic field into and out of integrated optical waveguides and devices [77, 78]. This application relies on electromagnetic coupling through phase matching of the different fields by the corrugated region.

6.2 Classification of Gratings

Gratings are widely used as components for realizing wavelength dispersion, conversion, modulation and control of guided wavefronts in optical integrated circuits [79]. Gratings have dimensions, structures and fabrication processes that are suitable for integration. Gratings are also applied as both active and passive device components. Distributed Feedback (DFB) [80] and Distributed Bragg Reflector (DBR) lasers [81, 82] are examples of corrugation-based active devices. In reference [83], some examples of passive grating components are presented which includes grating couplers, deflectors, reflectors, mode converters, wavelength filters and wavelength lenses.

6.3 Analysis of Gratings

A number of theoretical methods have been reported for the analysis of waveguides with periodic corrugations. Marcuse [43] used coupled-mode theory to analyze a

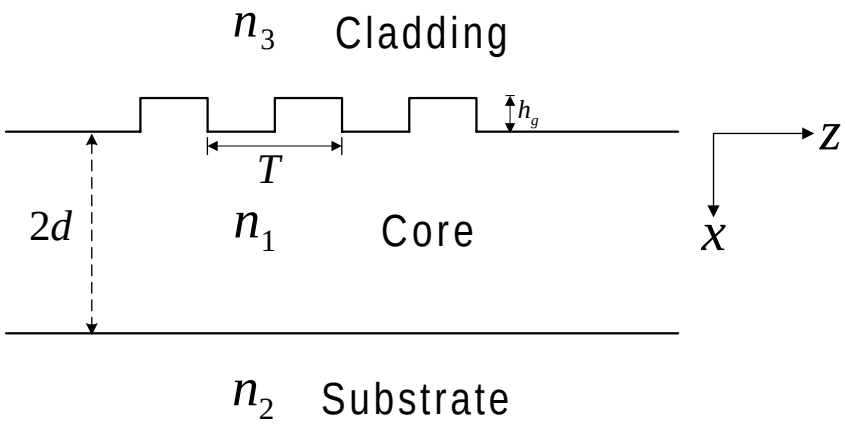

Figure 6.1: Corrugated Waveguide

slab waveguide with sinusoidal deformation on one of its interfaces. The spectral response of a grating filter using coupled-mode theory was calculated and compared with experimental work in [84]. In reference [85], the Effective-Index method was used to model a waveguide grating and the results were compared with coupled-mode theory. A major limitation of the coupled-mode theory is that it can only model small waveguide perturbations which is due to its approximate formulation. The Method of Lines is suited to model such problems, where waveguide perturbations can be large, as it does not have any approximation except for the approximation of the second-derivative operator using central-difference formula. In order to model a long grating with deep corrugations, a fast and stable algorithm within the Method of Lines framework has been developed. This method, named Cascading and Doubling Algorithm [38] can model gratings with thousands of periods much more efficiently than the layer-by-layer algorithm given in chapter 4. In the current chapter, the derivation of this algorithm is explained and comparisons are made with published

results.

6.4 The Cascading and Doubling Algorithm

With reference to figure 6.2, two distributed discontinuities 'A' and 'B' are brought together and are separated by a uniform region of width d. The quantities R_{A1}, T_{A2} (R_{A2}, T_{A1}) are respectively the reflection and transmission matrices of discontinuity 'A' when the field is incident from left(right) of the discontinuity. The individual reflection and transmission matrices of both discontinuities are assumed to be known. We will next develop a scheme to find the reflection and transmission matrices of the combined structure. R_A and T_A are reflection and transmission matrices of the isolated structure 'A'. For an asymmterical discontinuity $R_{A1} \neq R_{A2}$ and $T_{A1} \neq T_{A2}$. The same comments apply to discontinuity 'B'. If the two discontinuities are not identical then $R_A \neq R_B$ and $T_A \neq T_B$. The reflection and transmission matrices of the combined structure are denoted by R_0 and T_0 respectively. These matrices are obtained by adding the successive reflections and transmissions of the incident field as the two structures interact with each other. The field propagation in the uniform waveguide section of length 'd' is described by $e^{\pm jSz}$. The field vector a_0 is assumed to be incident from the left on the first discontinuity (see figure 6.3). We can express the net reflected field in terms of the summation of forward and backwards traveling waves after multiple reflections from the two discontinuities, which gives:

$$R_{01}a_0 = R_{A1}a_0 + T_{A1}e^{jSd}R_{B1}e^{jSd}T_{A2}a_0 + T_{A1}\left(e^{jSd}R_{B1}e^{jSd}R_{A2}\right)e^{jSd}R_{B1}e^{jSd}T_{A2}a_0 +$$

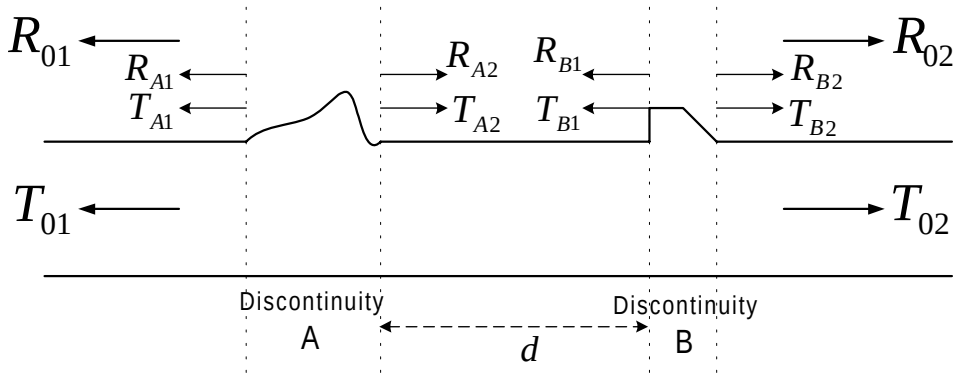

Figure 6.2: Two Waveguide Structures Cascaded Together

$$T_{A1}\left(e^{jSd}R_{B1}e^{jSd}R_{A2}\right)^2 e^{jSd}R_{B1}e^{jSd}T_{A2}a_0 +$$

$$T_{A1}(e^{jSd}R_{B1}e^{jSd}R_{A2})^3 e^{jSd}R_{B1}e^{jSd}T_{A2}a_0 + ... \tag{6.1}$$

$$R_{01}a_0 = R_{A1}a_0 + T_{A1}\left[\sum_{n=0}^{\infty}\left(e^{jSd}R_{B1}e^{jSd}R_{A2}\right)^n\right]e^{jSd}R_{B1}e^{jSd}T_{A2}a_0 \tag{6.2}$$

$$R_{01} = R_{A1} + T_{A1}\left[\sum_{n=0}^{\infty}\left(e^{jSd}R_{B1}e^{jSd}R_{A2}\right)^n\right]e^{jSd}R_{B1}e^{jSd}T_{A2} \tag{6.3}$$

$$R_{01} = R_{A1} + T_{A1}\left(I - e^{jSd}R_{B1}e^{jSd}R_{A2}\right)^{-1} e^{jSd}R_{B1}e^{jSd}T_{A2} \tag{6.4}$$

where the infinite geometric series in 6.3 is assumed to be convergent and is replaced by an equivalent quotient term. The transmission matrix T_0 of the combined structure is obtained in a similar fashion.

$$T_{02}a_0 = T_{B2}e^{jSd}T_{A2}a_0 + T_{B2}\left(e^{jSd}R_{A2}e^{jSd}R_{B1}\right)a_0 +$$

$$T_{B2}\left(e^{jSd}R_{A2}e^{jSd}R_{B1}\right)^2 e^{jSd}T_{A2}a_0 + ... \tag{6.5}$$

$$T_{02}a_0 = T_{B2}\left[\sum_{n=0}^{\infty}\left(e^{jSd}R_{A2}e^{jSd}R_{B1}\right)^n\right]e^{jSd}T_{A2}a_0 \tag{6.6}$$

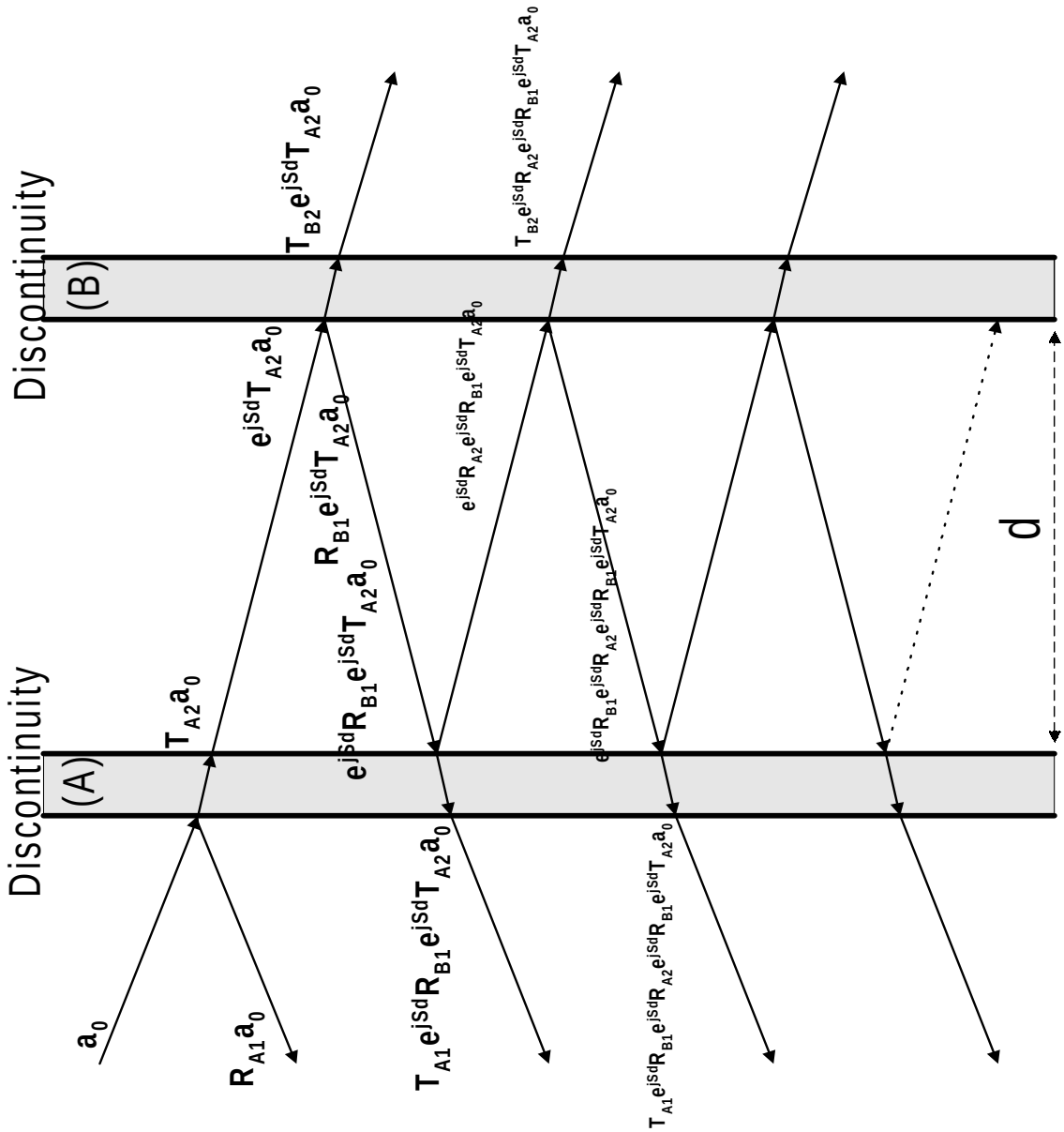

Figure 6.3: Multiple Reflections from two Cascaded Discontinuities

$$T_{02} = T_{B2}\left[\sum_{n=0}^{\infty}\left(e^{jSd}R_{A1}e^{jSd}R_{B1}\right)^{n}\right]e^{jSd}T_{A2} \quad (6.7)$$

$$T_{02} = T_{B2}\left(I - e^{jSd}R_{A2}e^{jSd}R_{B1}\right)^{-1}e^{jSd}T_{A2} \quad (6.8)$$

The quotients appearing in equations 6.4 and 6.8 are different. In order to make the computation of R_{01} and T_{02} more efficient, equation 6.1 is modified such that these quotient terms become identical. That is:

$$R_{01}a_0 = R_{A1}a_0 + T_{A1}e^{jSd}R_{B1}e^{jSd}T_{A2}a_0 + T_{A1}e^{jSd}R_{B1}\left(e^{jSd}R_{A2}e^{jSd}R_{B1}\right)e^{jSd}T_{A2}a_0 +$$

$$T_{A1}e^{jSd}R_{B1}(e^{jSd}R_{A2}e^{jSd}R_{B1}e^{jSd}R_{A2}e^{jSd}R_{B1})e^{jSd}T_{A2}a_0 + ... \quad (6.9)$$

$$R_{01} = R_{A1} + T_{A1}e^{jSd}R_{B1}\left[\sum_{n=0}^{\infty}\left(e^{jSd}R_{A2}e^{jSd}R_{B1}\right)^{n}\right]e^{jSd}T_{A2}a_0 \quad (6.10)$$

$$R_{01} = R_{A1} + T_{A1}e^{jSd}R_{B1}\left(I - e^{jSd}R_{A2}e^{jSd}R_{B1}\right)^{-1}e^{jSd}T_{A2} \quad (6.11)$$

Thus equations 6.8 and 6.11 are very similar to each other with a common quotient factor $\left(I - e^{jSd}R_{A2}e^{jSd}R_{B1}\right)^{-1}e^{jSd}T_{A2}$. This is the Cascading Algorithm which gives net reflection and transmission matrices of a cascaded structure composed of two sub-structures in terms of their individual reflection and transmission matrices.

6.4.1 Symmetrical and Periodic Structures

For symmetric discontinuities, A and B, $R_1 = R_2 = R$ and $T_1 = T_2 = T$. Thus equations 6.8 and 6.11 reduce to :

$$R_{01} = R_A + T_Ae^{jSd}R_B\left(I - e^{jSd}R_Ae^{jSd}R_B\right)^{-1}e^{jSd}T_A \quad (6.12)$$

$$T_{02} = T_B\left(I - e^{jSd}R_Ae^{jSd}R_B\right)^{-1}e^{jSd}T_A \quad (6.13)$$

If structures 'A' and 'B' are identical and symmetric, then $R_A = R_B$ and $T_A = T_B$. So the relations are further simplified to:

$$R_{01} = R + Te^{jSd}R\left(I - e^{jSd}Re^{jSd}R\right)^{-1}e^{jSd}T \tag{6.14}$$

$$T_{02} = T\left(I - e^{jSd}Re^{jSd}R\right)^{-1}e^{jSd}T \tag{6.15}$$

In addition, if the two identical and symmetric structures are connected to each other directly, such that $d = 0$, then:

$$R_{01} = R + TR\left(I - R^2\right)^{-1}T \tag{6.16}$$

$$T_{02} = T\left(I - R^2\right)^{-1}T \tag{6.17}$$

It is important to note that R_{01} and T_{02} are reflection and transmission matrices as seen from the left-hand side of the waveguide. The relations for R_{02} and T_{01} as seen from the right-hand side are easily obtained from 6.8 and 6.11 by interchanging $A \rightleftharpoons B$ and $1 \rightleftharpoons 2$. That is:

$$R_{02} = R_{B2} + T_{B2}e^{jSd}R_{A2}\left(I - e^{jSd}R_{B1}e^{jSd}R_{A2}\right)^{-1}e^{jSd}T_{B1} \tag{6.18}$$

$$T_{01} = T_{A1}\left(I - e^{jSd}R_{B1}e^{jSd}R_{A2}\right)^{-1}e^{jSd}T_{B1} \tag{6.19}$$

6.4.2 Rectangular Gratings

The rectangular grating is a classic example of a symmetrical periodic structure. With reference to figure 6.4, this problem can be solved by first considering the

discontinuity shown in figure 6.5. The reflection matrix for the TM polarized field in this case is given by:

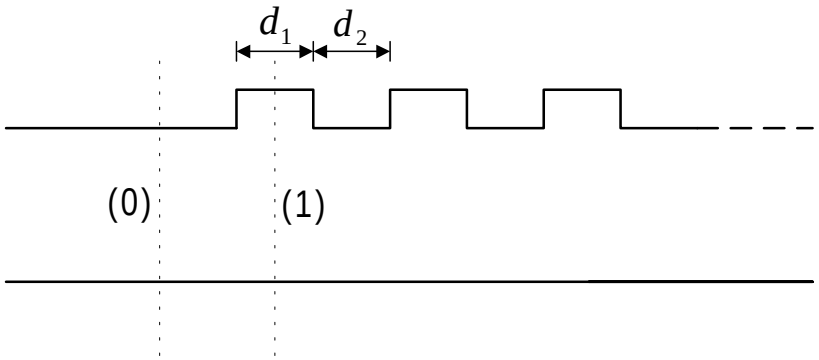

Figure 6.4: A Rectangular Waveguide Grating

$$R_{A1} = \left[I - S_0^{-1}N_0N_1^{-1}S_1\right]\left[I + S_0^{-1}N_0N_1^{-1}S_1\right]^{-1} \tag{6.20}$$

$$= \left[\left(S_0^{-1}N_0N_1^{-1}S_1\right)^{-1} - I\right] S_0^{-1}N_0N_1^{-1}S_1 \cdot \cdot \left[\left(\left(S_0^{-1}N_0N_1^{-1}S_1\right)^{-1} + I\right) S_0^{-1}N_0N_1^{-1}S_1\right]^{-1} \tag{6.21}$$

$$= \left[\left(S_0^{-1}N_0N_1^{-1}S_1\right)^{-1} - I\right] S_0^{-1}N_0N_1^{-1}S_1 \cdot \cdot \left(S_0^{-1}N_0N_1^{-1}S_1\right)^{-1}\left[\left(S_0^{-1}N_0N_1^{-1}S_1\right)^{-1} + I\right]^{-1} \tag{6.22}$$

$$= \left[\left(S_0^{-1}N_0N_1^{-1}S_1\right)^{-1} - I\right]\left[\left(S_0^{-1}N_0N_1^{-1}S_1\right)^{-1} + I\right]^{-1} \tag{6.23}$$

$$= -\left[I - \left(S_0^{-1}N_0N_1^{-1}S_1\right)^{-1}\right]\left[I + \left(S_0^{-1}N_0N_1^{-1}S_1\right)^{-1}\right]^{-1} \tag{6.24}$$

$$= -\left[I - S_1^{-1}N_1N_0^{-1}S_0\right]\left[I + S_1^{-1}N_1N_0^{-1}S_0\right]^{-1} \tag{6.25}$$

$$= -R_{A2} \tag{6.26}$$

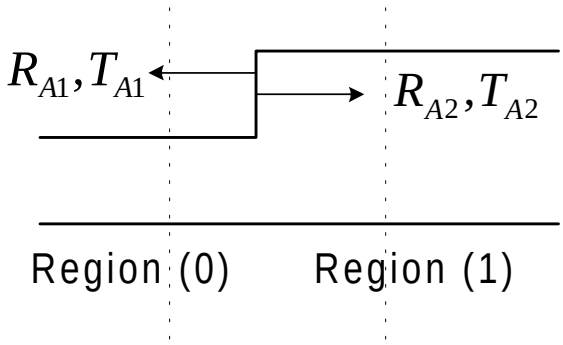

Figure 6.5: A Single Step Discontinuity

Thus for the above case $R_{A1} = -R_{A2}$, $T_{A2} = I + R_{A1}$ and $T_{A1} = I + R_{A2}$. Although these results were derived for the TM case, they also apply for the TE case as well. The next step is to treat the double discontinuity shown in figure 6.6. All Rs and Ts appearing in figure 6.6 can be expressed in terms of R_{A1}.

$$R_{A2} = -R_{A1} \tag{6.27}$$

$$T_{A1} = I + R_{A2} = I - R_{A1} \tag{6.28}$$

$$T_{A2} = I + R_{A1} \tag{6.29}$$

$$R_{B1} = R_{A2} = -R_{A1} \tag{6.30}$$

$$R_{B2} = R_{A1} \tag{6.31}$$

$$T_{B1} = T_{A2} = I + R_{A1} \tag{6.32}$$

$$T_{B2} = T_{A1} = I - R_{A1} \tag{6.33}$$

Since the structure of figure 6.6 is symmetric, we need only to define R and T

for the structure. Using equations 6.8 and 6.11 we obtain:

$$R = R_{A1} + (I - R_{A1})\, e^{jS_1 d_1}\, (-R_{A1}) \left[I - \left(e^{jS_1 d_1} R_{A1} \right)^2 \right]^{-1} \cdot e^{jS_1 d_1}\, (I + R_{A1}) \tag{6.34}$$

$$T = (I - R_{A1}) \left[I - \left(e^{jS_1 d_1} R_{A1} \right)^2 \right]^{-1} e^{jS_1 d_1}\, (I + R_{A1}) \tag{6.35}$$

The final step is to model the whole periodic structure iteratively. We start by combining the two symmetric identical structures as shown in figure 6.7. Using equations 6.14 and 6.15, the new reflection and transmission matrices for the combined structure is expressed in terms of the old reflection and transmission matrices of the individual structure, using the iterative relation:

$${R_{new}}' \leftarrow {R_{old}}' + {T_{old}}' e^{jS_0 d_0} {R_{old}}' \left[I - \left(e^{jS_0 d_0} {R_{old}}' \right)^2 \right]^{-1} e^{jS_0 d_0} {T_{old}}' \tag{6.36}$$

$${T_{new}}' \leftarrow {T_{old}}' \left[I - \left(e^{jS_0 d_0} {R_{old}}' \right)^2 \right]^{-1} e^{jS_0 d_0} {T_{old}}' \tag{6.37}$$

From figure 6.8, the above equations can be further modified and leads to the following relations:

$$R_{new} \leftarrow R_{old} + T_{old} R_{old} \left[I - R_{old}^2 \right]^{-1} T_{old} \tag{6.38}$$

$$T_{new} \leftarrow T_{old} \left[I - R_{old}^2 \right]^{-1} T_{old} \tag{6.39}$$

Equation 6.38 and 6.39 can be obtained by multiplying equations 6.36 and 6.37

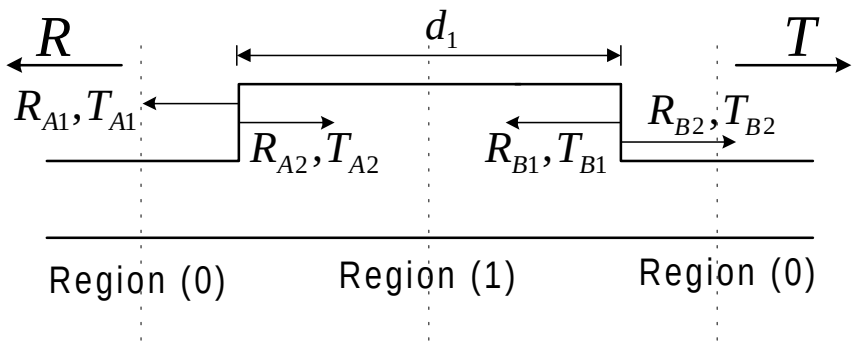

Figure 6.6: A Double Waveguide Discontinuity

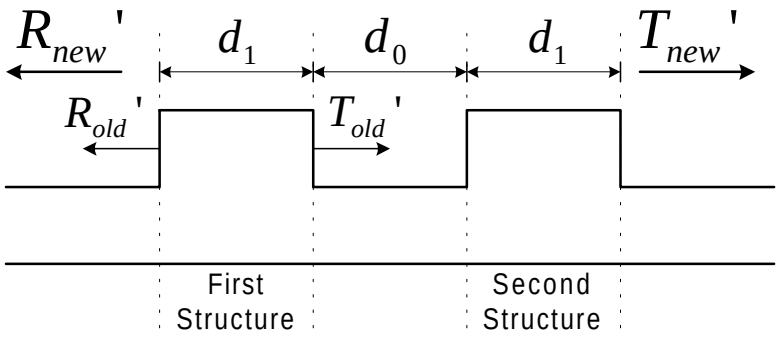

Figure 6.7: Two Identical Structures Cascaded with Separation d_0

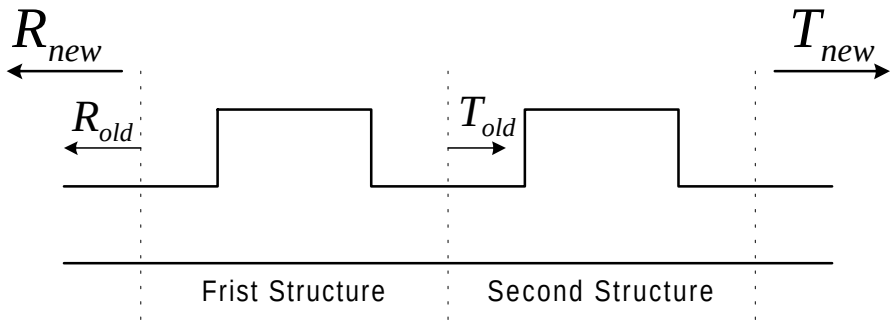

Figure 6.8: Two Identical Structures Cascaded Together

from the left by $e^{jS_0d_0}$ and defining the new quantities:

$$R_{old} = e^{jS_0d_0}R_{old}' \tag{6.40}$$

$$T_{old} = e^{jS_0d_0}T_{old}' \tag{6.41}$$

$$R_{new} = e^{jS_0d_0}R_{new}' \tag{6.42}$$

$$T_{new} = e^{jS_0d_0}T_{new}' \tag{6.43}$$

Equations 6.38 and 6.39 are the basis of the so called Doubling Algorithm. The factor $[I - R^2]^{-1}T$ is common in both equations which makes the algorithm very fast. At each iteration, the number of grating periods accounted for is doubled. That is after each iteration of equations 6.38 and 6.39 the number of periods accounted for is 2, 4, 8, 16, 32 and so on. This works in power of 2 only but we can model any number of periods by attaching the appropriate number of sections each having periods in power of 2. For example we can model 10 periods by attaching 8 and 2 periods. Note that the reflection and transmission matrices for 2 periods is already computed in the process of computing the reflection and transmission matrices of 8

periods. So these matrices are stored in a temporary location and later used in the attaching algorithm. For N discretization lines, this algorithm works on an $N \times N$ matrix for storage and eigen-value calculation. Some other algorithms [47, 64], based on raising a matrix to a certain power to model a certain number of periods, operate upon $2N \times 2N$ matrices. It becomes computationally expensive to find eigen-values and eigen-vectors of a $2N \times 2N$ matrix if the number of discretization lines N in a given problem space is large. So our algorithm has this extra advantage of modeling waveguides with wide (and hence large number N) cross-sections efficiently.

6.5 Results

In this section, the algorithm developed above is applied to calculate the spectral response of various waveguide gratings. As it will be seen later, the results obtained are in close agreement with published results, thus establishing the validity of this algorithm.

6.5.1 Air/GaAs/Air Waveguide Grating

A shallow waveguide grating having 256 periods as shown in the inset of figure 6.9 is modeled using a uniform mesh scheme. The TE_0 mode is launched in the waveguide and the reflected and transmitted fields are calculated. The fundamental-mode coefficient α_0 from the reflected field is calculated using an overlap integral (refer

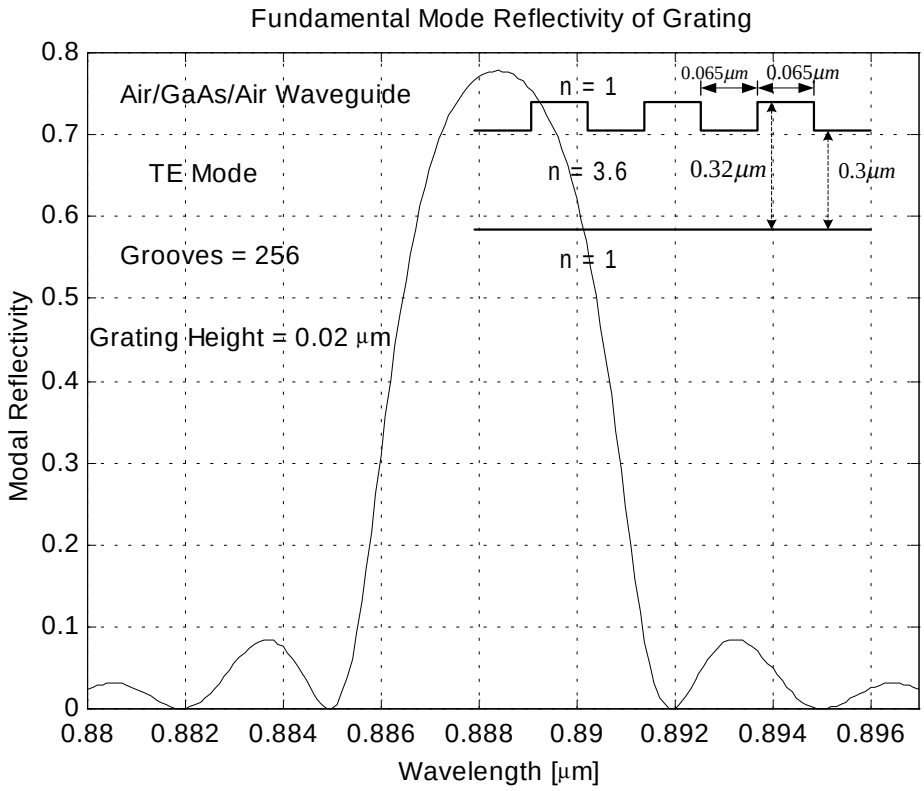

Figure 6.9: Modal Reflectivity of a Grating

to equation 5.19) and the modal reflectivity is plotted against the wavelength. As seen in figure 6.9, the modal reflectivity has a central main lobe and several side lobes. The calculation are done using a 5-point formulation. The number of sample points in the waveguide core layer is 15 and the width of cladding layers is chosen large enough (0.3 μm) to give a substantial evanescent field decay at the inner PML walls. A single layer PML is used with 7 sample points on each side of the computational window. The resulting absolute error in n_{eff} (Mol vs. Analytical) is 3.085e-5. The time required to simulate 256 periods at one wavelength is around 1.85 seconds (using an IBM Pentium III machine at 500 MHz with 128 MB RAM running MATLAB 5.2 under Windows 98).

6.5.2 Comparison with Published Results

An asymmetric waveguide with periodic deep grating (see figure 6.10) obtained from reference [86] is modeled using the Cascading and Doubling Algorithm introduced earlier. The modal spectral reflectivity is calculated for different number of periods. A non-uniform mesh with a single layer PML is used to model the device. The 5-point second-derivative approximation is used with appropriate interface conditions in the MOL . A total of 77 sample points are used in the problem space. As shown in figure 6.11, our results are in close agreement with those from [86], establishing the accuracy of our algorithm. As the number of periods is increased, the spectral reflectivity curve becomes asymmetric and the side lobes become more densely packed. Results for a grating with 262114 grooves (effectively semi-infinite) is given in figure 6.15 showing that the algorithm is stable for long gratings having several thousands of periods. It took approximately 5.5 seconds per wavelength to calculate the reflectivity and transmissivity of this semi-infinite case. The relative ease of the Doubling Algorithm to model long gratings is also evident due to the fact that, the number of periods modeled is doubled. The results for the TM polarization are also shown in figures 6.16 and 6.17 for 8192 and 16384 grating periods respectively. These results are quite different from the TE results in terms of the main lobe width and peak reflectivity. The peak reflectivity in the TM case has increased as compared to the TE case and the width of the main lobe has almost doubled.

In another simulation of the same device, the groove depth is reduced consider-

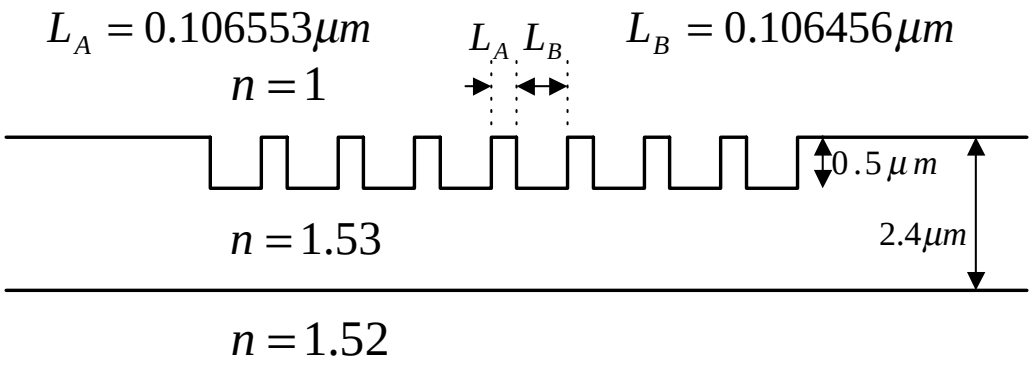

Figure 6.10: A Deep Waveguide Grating Structure

ably and the spectral response recalculated. In figure 6.18, the groove depth used is 0.42% with 65536 periods. The result shows that the main lobe width and side lobe level depend on the groove depth. For shallow gratings, the main lobe width is small and the side lobes are low, while for deep grating, the main lobe is wide and asymmetric with higher side lobe levels. The peak reflectivity becomes lower for the shallow grating. In this case, we need to use a larger number of grating periods to obtain a higher reflectivity at the resonance wavelength.

6.5.3 Effect of Changing the Groove Depth

A waveguide grating with 256 periods as shown in the inset of figure 6.21 is modeled. The spectral reflectivity of the TE_0 mode is calculated for different groove depths. The spectral responses for 10%, 20% and 30% grating depths are calculated and plotted in figures 6.21, 6.19 and 6.20 respectively. As the grating depth is increased,

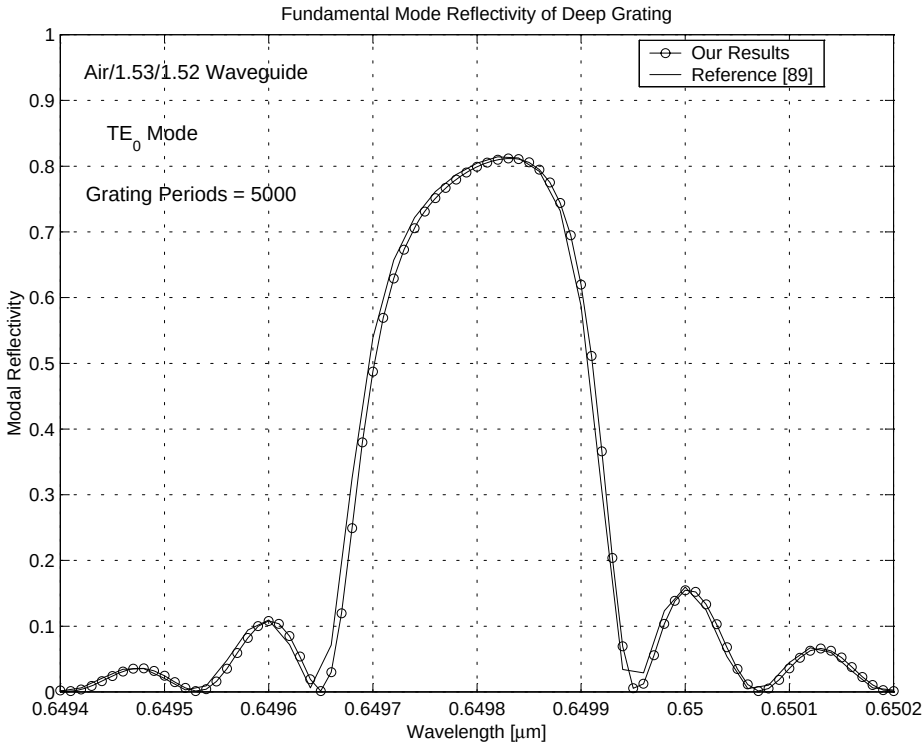

Figure 6.11: Deep Grating Modal Reflectivity

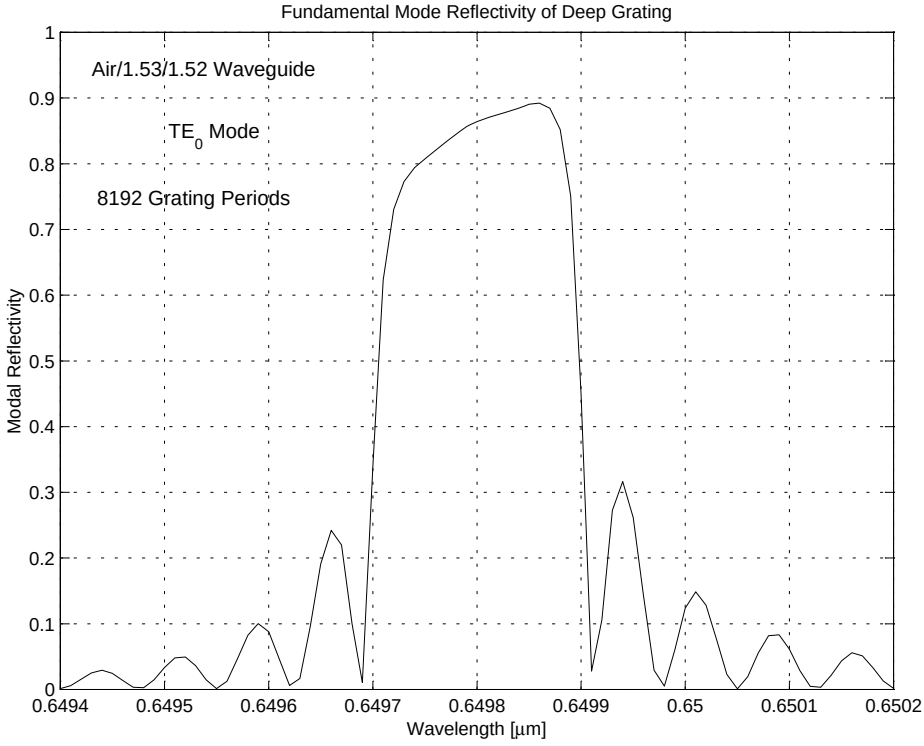

Figure 6.12: Deep Grating Modal Reflectivity, 8192 Periods

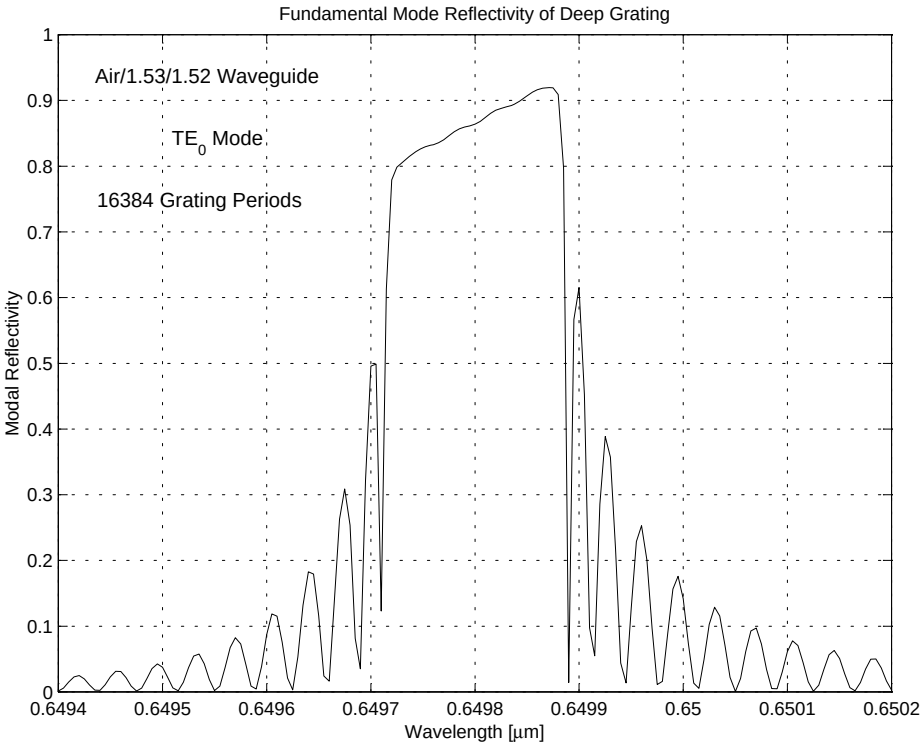

Figure 6.13: Deep Grating Modal Reflectivity, 16384 Periods

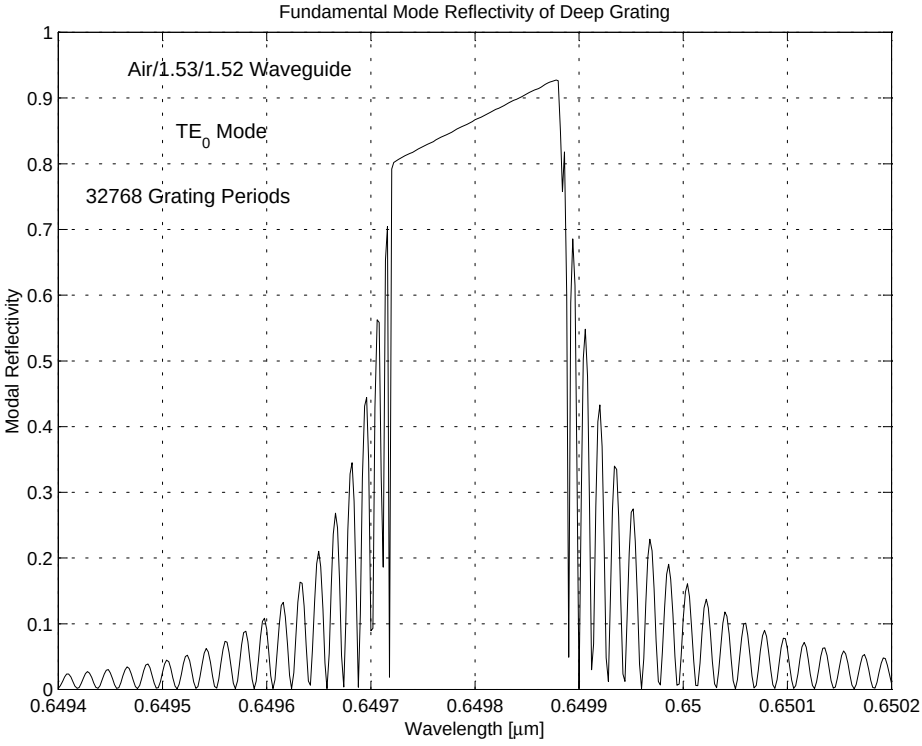

Figure 6.14: Deep Grating Modal Reflectivity, 32768 periods

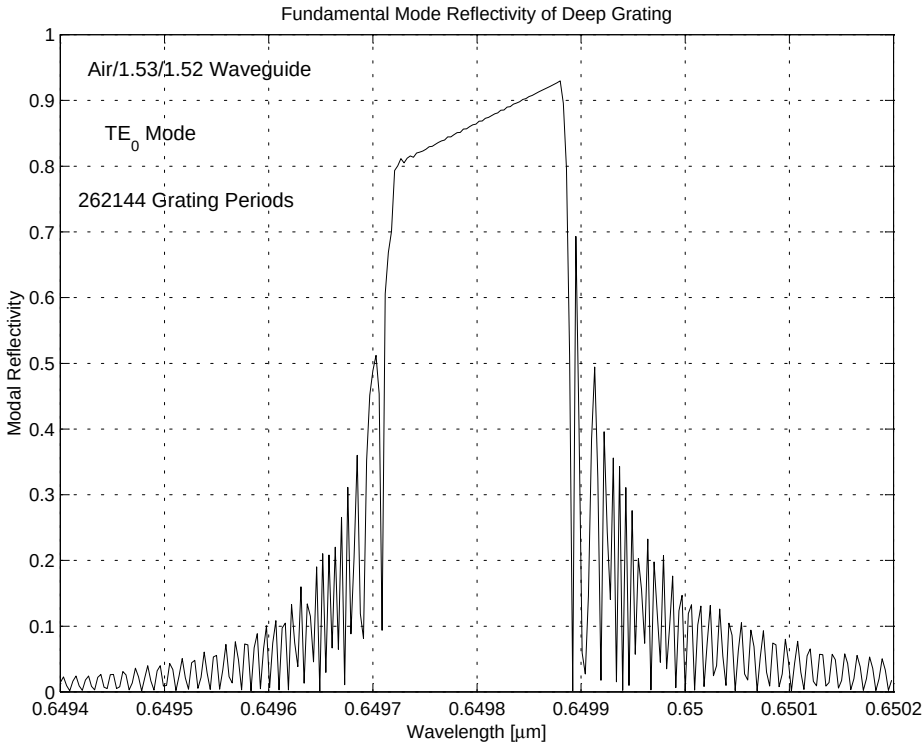

Figure 6.15: Deep Grating Modal Reflectivity, Semi-Infinite

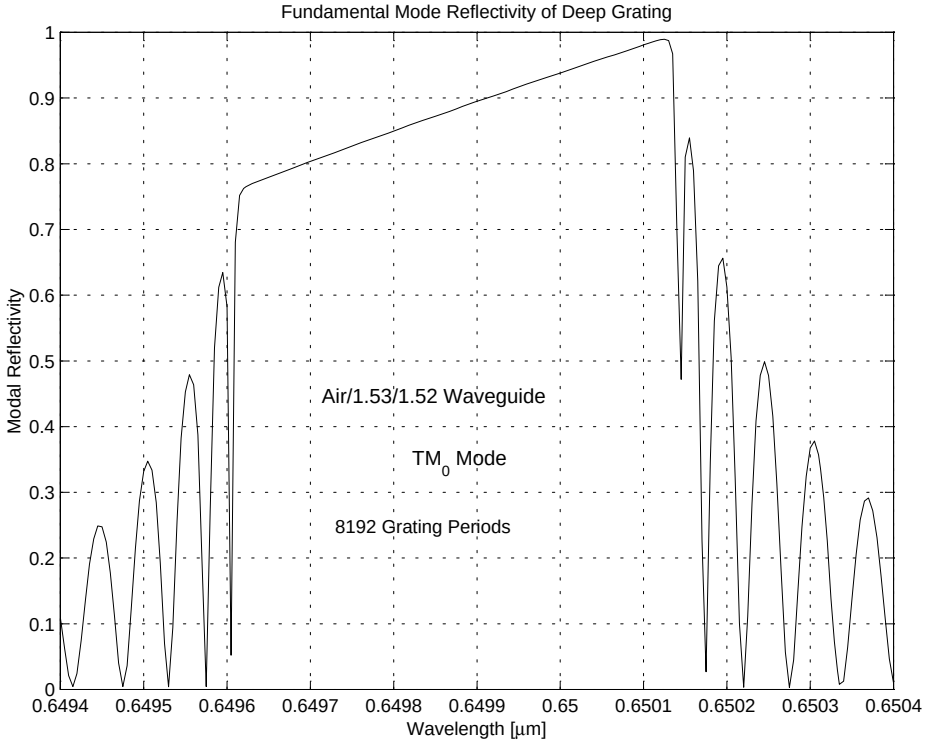

Figure 6.16: Deep Grating TM Modal Reflectivity, 8192 Periods

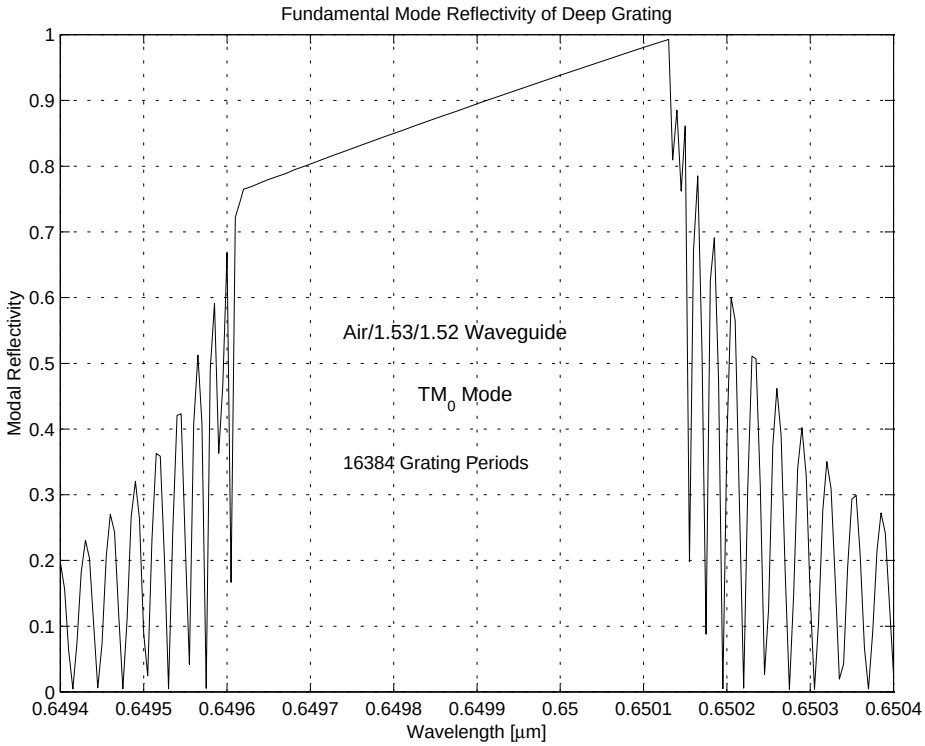

Figure 6.17: Deep Grating TM Modal Reflectivity, 16384 Periods

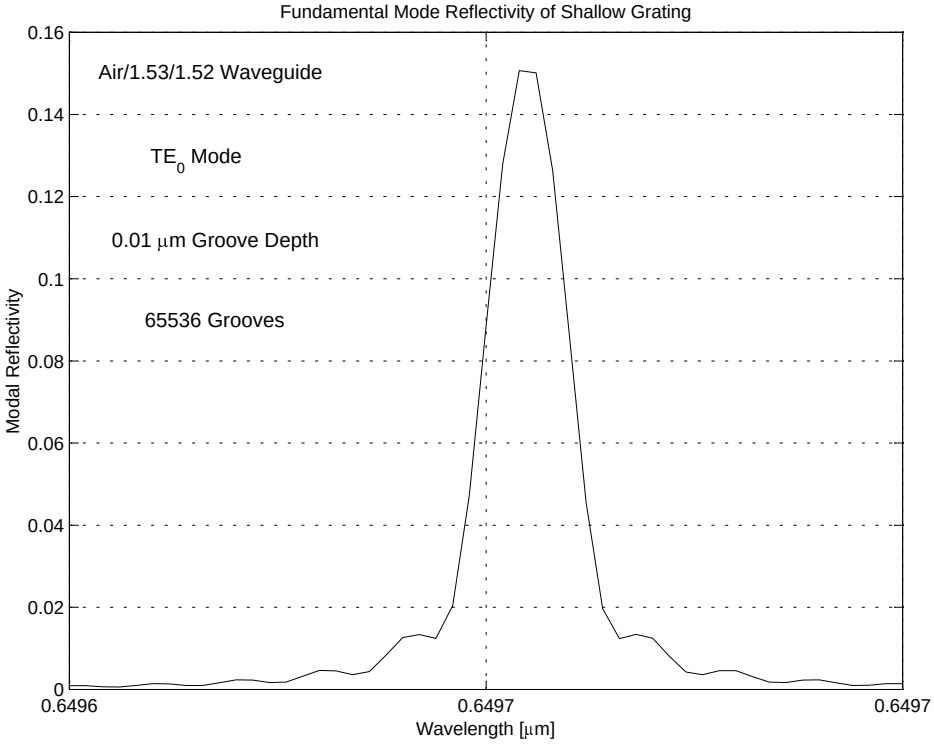

Figure 6.18: Modal Reflectivity of a Shallow Grating

the main lobe becomes wider and more asymmetric. The wavelength of peak reflectivity, often called the Bragg Wavelength λ_B shifts towards the shorter wavelength and the side lobe level increases.

6.6 Discussion

In this chapter, the cascading and doubling algorithm is used to model long gratings with a large number of grating periods. This algorithm is found to be fast and stable and its accuracy is verified against published results. This algorithm along with the MOL will be used to analyze the reflection mode polarizer in the next chapter.

It is concluded that the spectral reflectivity becomes asymmetric and the side lobes become more densely packed with the increase in the number of grating periods. The main lobe width and side lobe level depend on the groove depth and main lobe width and side lobe level increase with the groove depth.

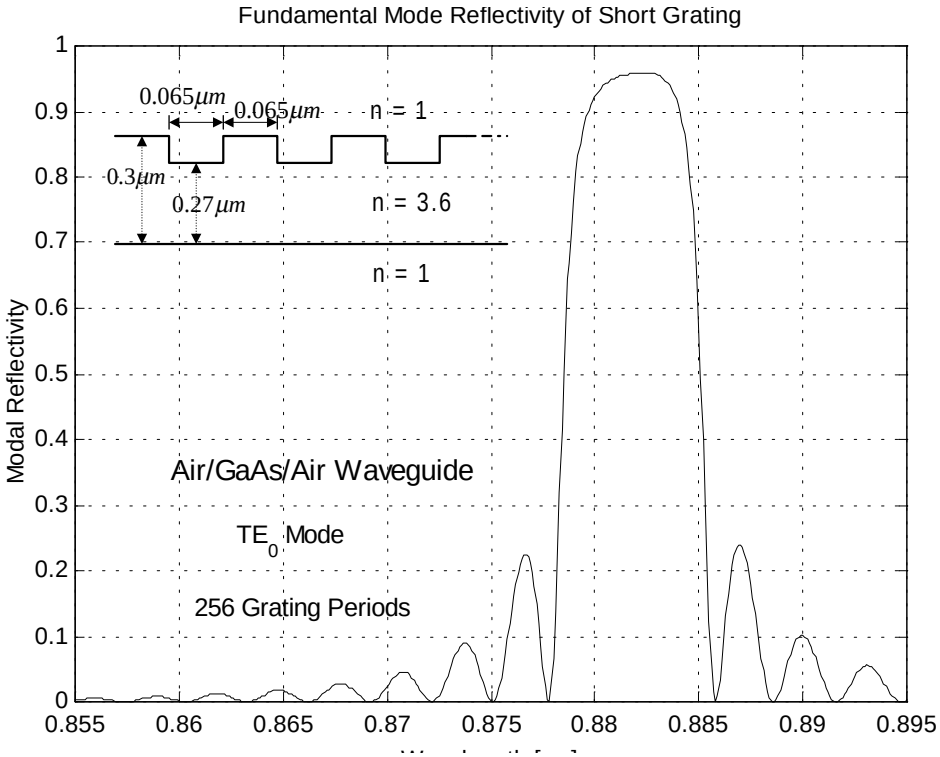

Figure 6.19: Short Grating Modal Reflectivity, 10% Grating Depth

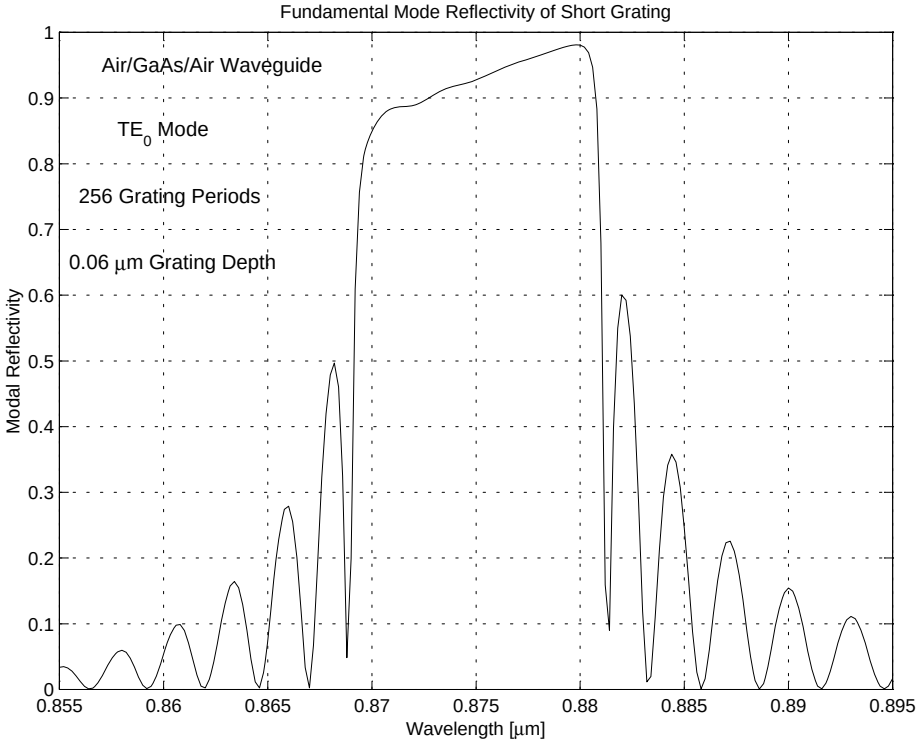

Figure 6.20: Short Grating Modal Reflectivity, 20% Grating Depth

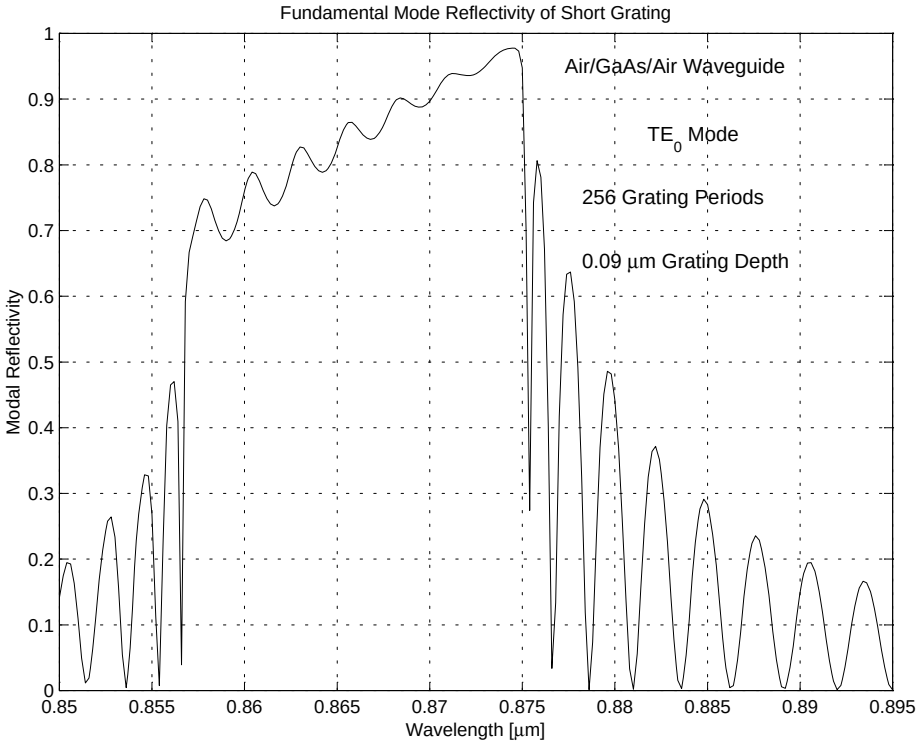

Figure 6.21: Short Grating Modal Reflectivity, 30% Grating Depth

Chapter 7

Analysis of TM-Pass Reflection Mode Polarizer

7.1 Introduction

In this chapter, periodic corrugations are introduced and combined with the high-index metal-clad waveguide to obtain a TM-pass reflection mode polarizer. The modal spectral response of this polarizer will be analyzed using the Method of Lines with seven-point formulation. The PML layer is used as an absorbing boundary condition. The TM-pass reflection mode polarizer structure itself is wavelength selective ($1.55\mu m$) as the resonance condition is satisfied only in a certain wavelength range. So for wavelength above or below the design wavelength, all modes will have higher loss.

7.2 Proposed Reflection Mode Polarizer

In the proposed reflection mode polarizer, periodic corrugations were first introduced in the waveguide core as shown in figure 7.1.

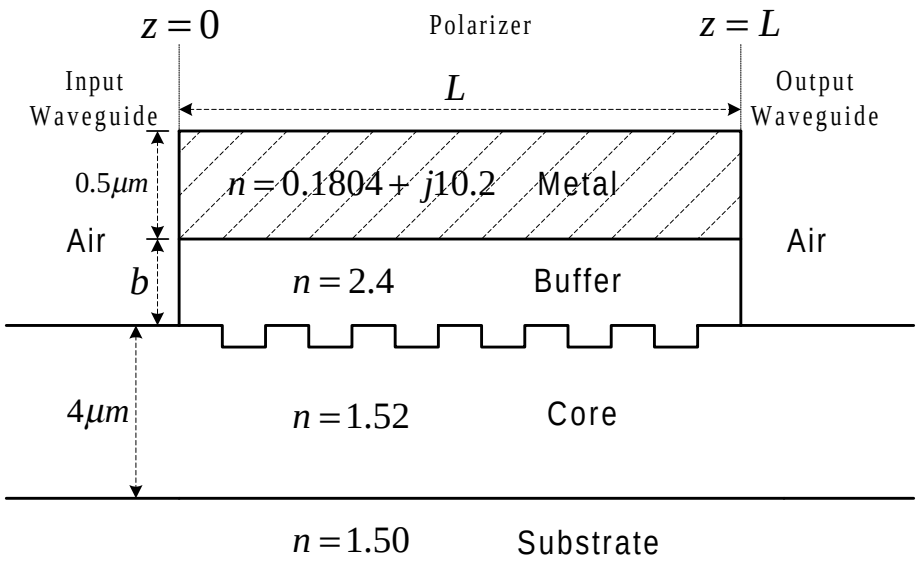

Figure 7.1: Proposed Reflection Mode Polarizer

The TE/TM modal spectral response of the proposed polarizer is analyzed for different high-index buffer thicknesses, different grating depths and different number of grating periods. Typical results are shown in figures 7.2 and 7.3. It can be concluded that this structure has a poor TE/TM discrimination and does not discriminate against the TE polarized waves, which is our aim. The poor performance of this structure is due to the fact that the presence of the TE_0 and TE_1 modes in the polarizer causes interference that leads to the high TE_0 modal reflectivity.

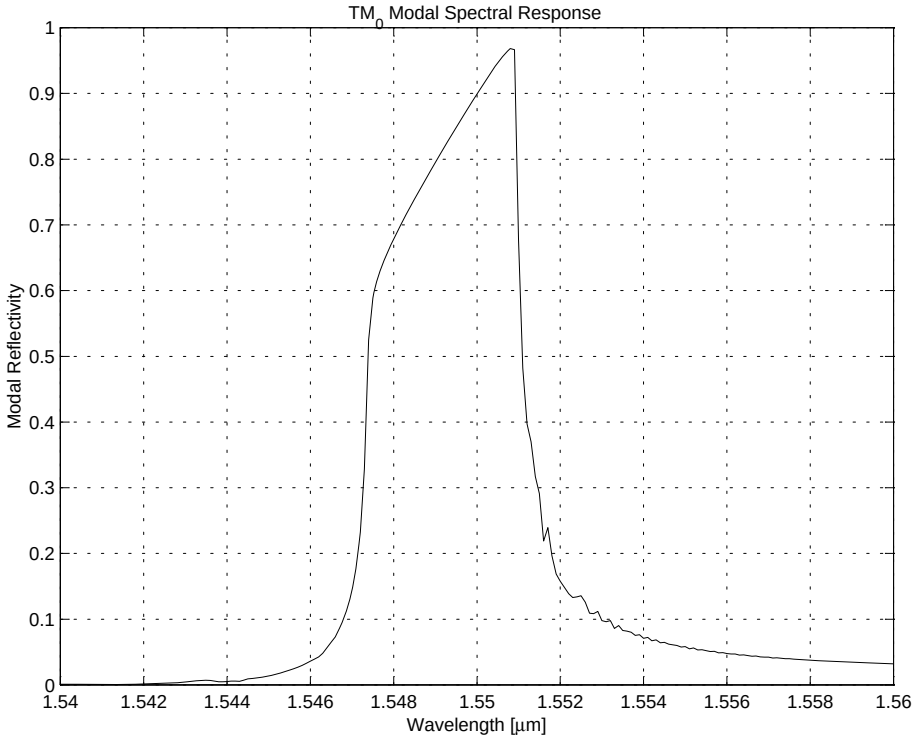

Figure 7.2: TM_0 Mode Spectral Response of the Proposed Reflection Mode Polarizer

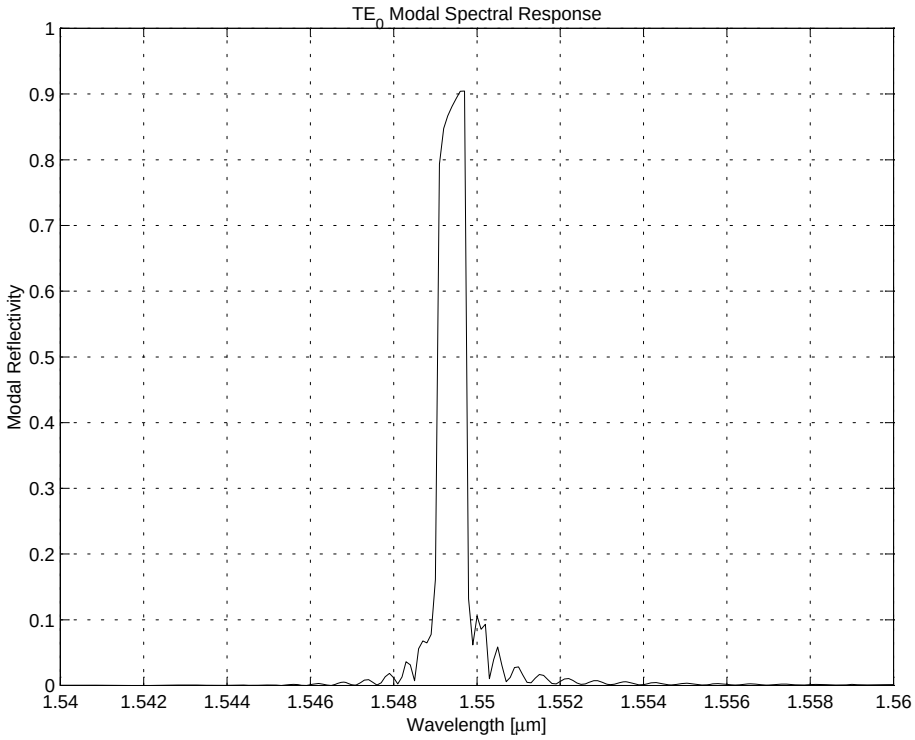

Figure 7.3: TE_0 Mode Spectral Response of the Proposed Reflection Mode Polarizer

7.3 TM-Pass Reflection Mode Polarizer

We then modified the above structure by putting the grating in series with the high-index metal-clad waveguide, rather that being within it. The structure of the modified TM-pass reflection mode polarizer is shown in figure 7.4. This device behaves as a wavelength selective filter due to multiple reflections from each discontinuity of the grating and their interaction with each other to cause resonance in the propagation direction. In this section, the modal spectral response of the reflection mode polarizer will be analyzed using the Method of Lines for different high-index buffer layer thicknesses (b), different groove depths, different number of grating periods, different polarizer lengths (L) and different spacings (L_s) between the high-index metal-clad waveguide and the grating.

Our main focus will be to cause the TM_0 mode to have high reflectivity with negligible TE reflection. It is found that the TM-pass reflection mode polarizer has very high loss for the TE_0 mode (see figure 7.5) and very low loss for TM_0 mode, (see figure 7.6). The peak TM_0 modal reflectivity is 0.92 with a very narrow bandwidth of 0.1 nm and the peak TE_0 modal reflectivity is very low that is 5.45e-4 which gives clear TE_0/TM_0 discrimination in favor of the TM_0 mode. In addition, there is a shift in the TE_0 Bragg wavelength (resonance wavelength) to the higher wavelength due to the higher value of the effective index of the TE_0 mode in the corrugated part. An approximate relation between the Bragg wavelength (λ_B), the grating period ($2d$) and the effective index (n_{eff}) is given approximately by $\lambda_B = 2d\ n_{eff}$ [86].

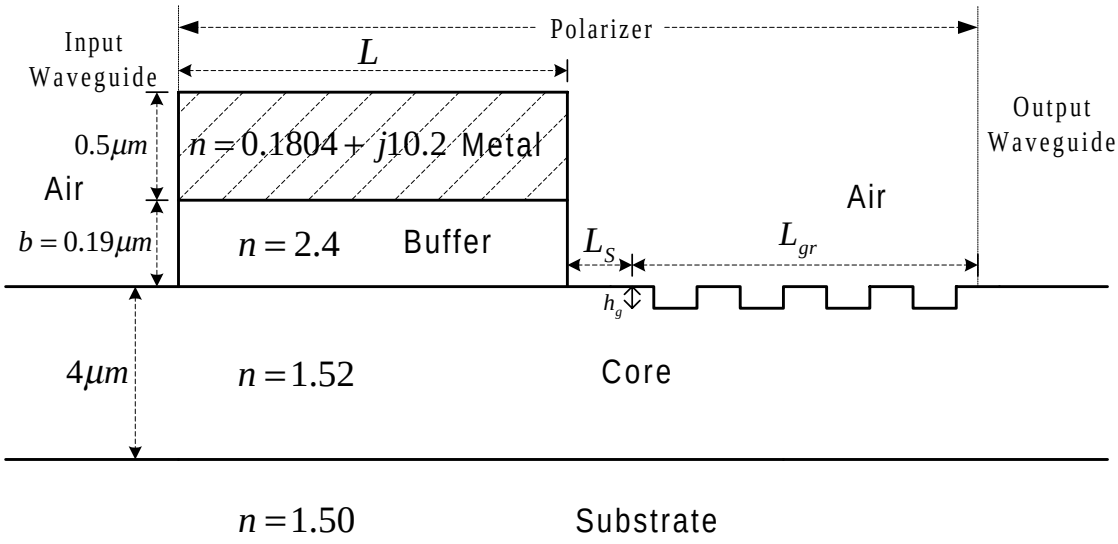

Figure 7.4: TM-Pass Reflection Mode Polarizer

The TM-pass reflection mode polarizer spectral width can be change by varying the grating depth. The polarizer spectral width can be lowered by reducing the grating depth while increasing the number of grating periods to achieve a higher peak reflectivity. If the grating is made deeper, its spectral width increases.

7.4 Effect of Polarizer Length and Buffer Thickness

The effect of the polarizer length and the high-index buffer layer thickness has been discussed in chapter 5. It is clear that there is one or more optimum polarizer

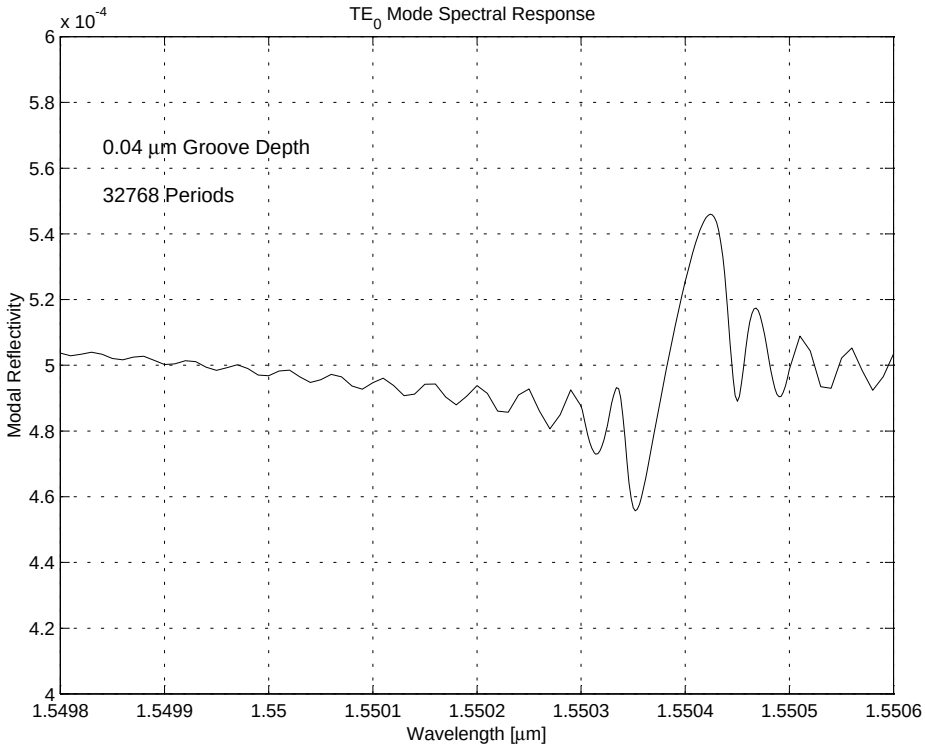

Figure 7.5: TE_0 Modal Refletivity

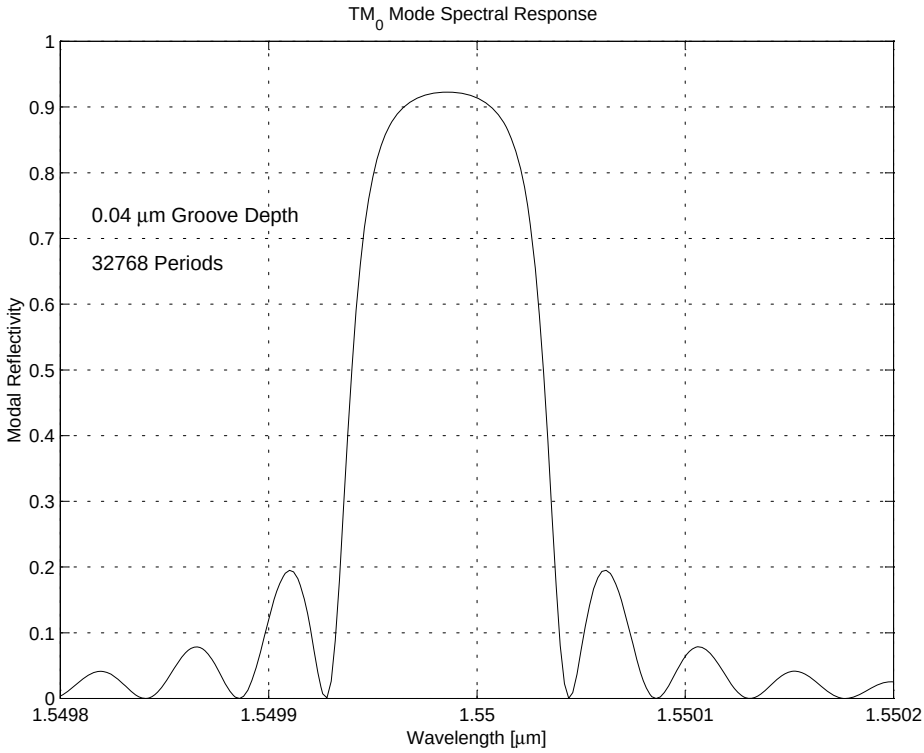

Figure 7.6: TM_0 Modal Reflectivity

lengths for each buffer layer thickness, where maximum TM_0 modal reflectivity and polarizer extinction ratio can be obtained. Here the buffer layer thicknesses and optimum polarizer lengths along with TM_0 and TE_0 peak modal reflectivities and TM-pass reflection mode polarizer extinction ratio are shown in table 7.1 while other polarizer parameters keep constant.

Buffer Thickness b (μm)	Optimum Polarizer Length L (mm)	Peak TM_0 Modal Reflectivity	Peak TE_0 Modal Reflectivity	Polarizer Extinction Ratio PER (dB)
0.185	1.97	0.822724	1.68277e-04	36.892
0.186	1.95	0.823363	6.26503e-05	41.187
0.187	1.93	0.823963	1.55571e-05	47.240
0.188	1.58	0.846295	1.46352e-05	47.621
0.189	0.91	0.891392	1.18196e-04	38.775
0.190	0.47	0.921921	5.45458e-04	32.279
0.191	0.15	0.945210	2.66215e-03	25.503
0.192	0.05	0.951437	2.72451e-03	25.431
0.193	0.05	0.950120	3.30968e-03	24.580

Table 7.1: Optimum Polarizer Lengths (L) for Different High-Index Buffer Layer Thicknesses (b) (Grating Depth=0.04μm, Periods=32768)

From table 7.1, it is evident that short polarizers give high TM_0 modal reflectivity and long polarizers give sufficiently high polarizer extinction ratio. With buffer layer thickness of 0.190 μm and polarizer length of 0.47 mm, we have 92 percent TM_0 modal reflectivity with 32 dB extinction ratio. This buffer layer thickness and polarizer length will be used for reflection mode polarizer analysis throughout the rest of this chapter.

7.5 Effect of the Polarizer Grating Separation (L_S)

The polarizer grating separation (L_S) is the distance between the metal-clad section and the corrugated part as shown in figure 7.4. We have found through numerical calculation that the L_S has a negligible effect on the overall device performance. Thus, we will fix L_S to $\lambda_B/4$ (approximately $0.1281\mu m$) throughout this work, and will not investigate the effect of L_S further.

7.6 Effect of Groove Depth

The variation of the TM_0 and TE_0 peak modal spectral reflectivity, reflection mode polarizer extinction ratio and spectral width (based on half power or 3-dB width) as a function of groove depths are presented in table 7.2. It is evident from table 7.2 that the spectral width increases with groove depth and the TM_0 modal reflectivity and polarizer extinction ratio reach maximum values for certain groove depths. If the grating depth is increased substantially, the TM_0 modal reflectivity decreases and TE_0 modal reflectivity increases, which results in lowering the value of extinction ratio.

In figure 7.7, the TM_0 modal spectral reflectivity and transmissivity of the TM-pass reflection mode polarizer with 1% groove depth is presented. The reflectivity spectrum has a small spectral width of about 0.1 nm, low side lobes level (about 7 dB) and a minimum modal transmissivity of about -14 dB. For the 2.5% groove

Groove Depth (μm)	Peak TM_0 Modal Reflectivity	Peak TE_0 Modal Reflectivity	Polarizer Extinction Ratio PER (dB)	Spectral Width (nm)
0.01	0.422948	3.42957e-04	30.910	0.040
0.02	0.612464	4.18016e-04	31.659	0.063
0.04	0.921921	5.45458e-04	32.279	0.100
0.06	0.952652	6.84628e-04	31.435	0.110
0.08	0.957105	8.41667e-04	30.558	0.130
0.10	0.958034	1.01873e-03	29.733	0.170
0.20	0.957450	2.21174e-03	26.364	0.290
0.40	0.952833	5.55657e-03	22.342	0.610
0.60	0.943497	8.87202e-03	20.267	0.890
0.80	0.928877	1.28800e-02	18.580	1.260

Table 7.2: Effect of Groove Depth (b=0.19 μm, Periods=32768 and L=0.47 mm)

depth case shown in figure 7.8, the spectral width increases to 0.15 nm and the transmissivity decreases to -36 dB. When the groove depth is increased to 5% (see figure 7.9), the spectral width of the polarizer is approximately doubled and the side lobes become higher and more closely packed. The minimum modal transmissivity is further reduced to a very low value of about -75 dB.

If the groove depth is increased further to 10%, the spectral width is again approximately doubled (see figure 7.10). The side lobes become higher and more closely packed. The minimum modal transmissivity curve is also plotted, and is seen to resemble a deep notch filter in the stop band of -165 dB.

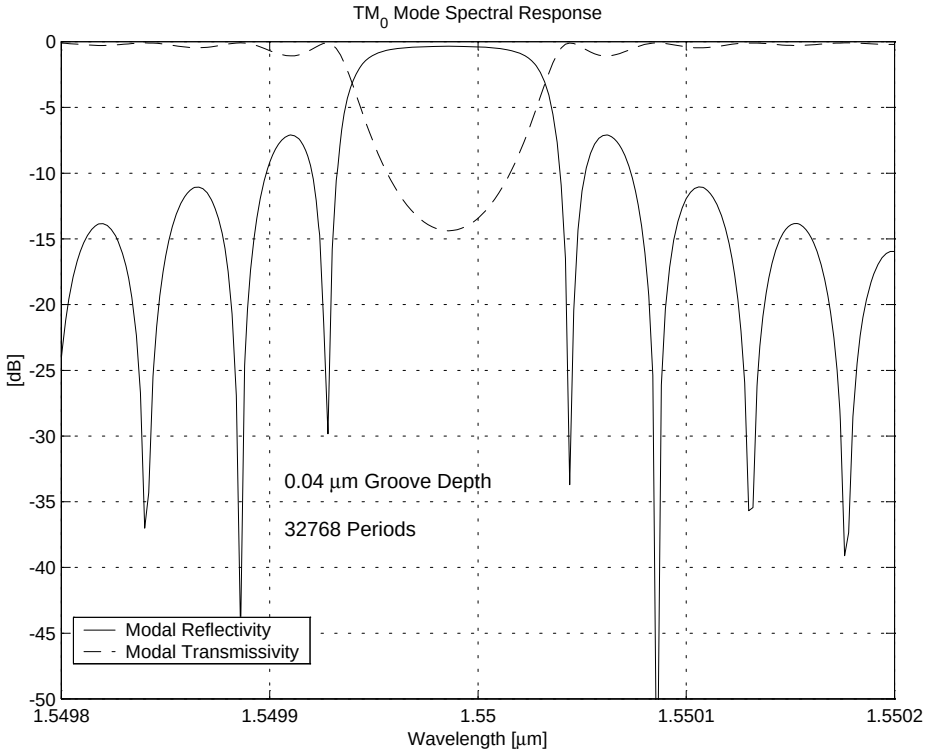

Figure 7.7: TM_0 Mode Response, 1% Groove Depth, 32768 Periods

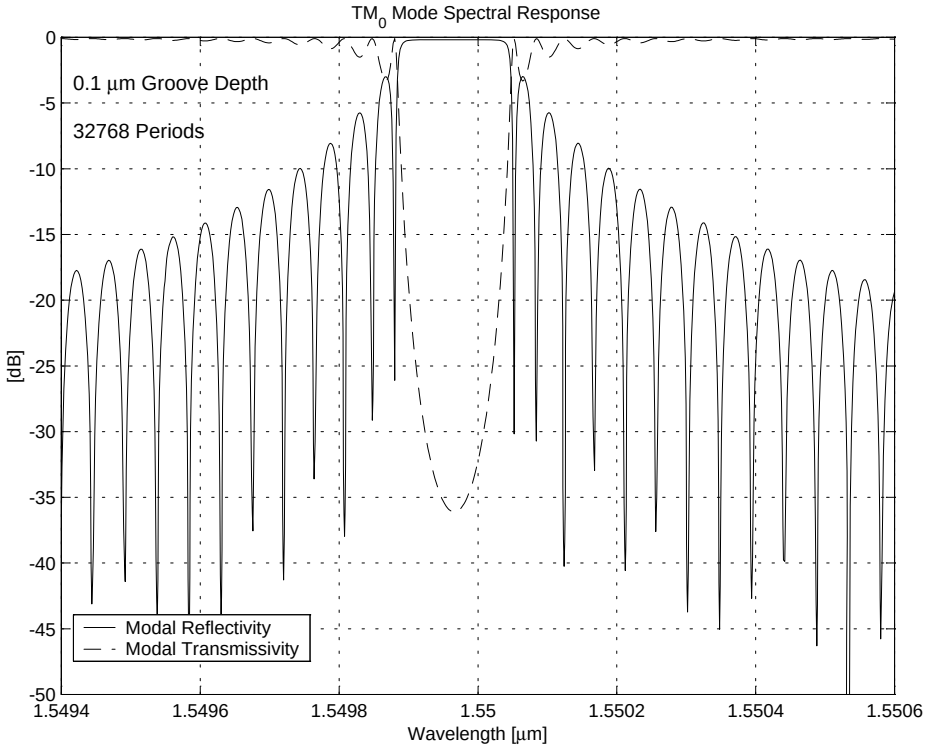

Figure 7.8: TM_0 Mode Response, 2.5% Groove Depth, 32768 Periods

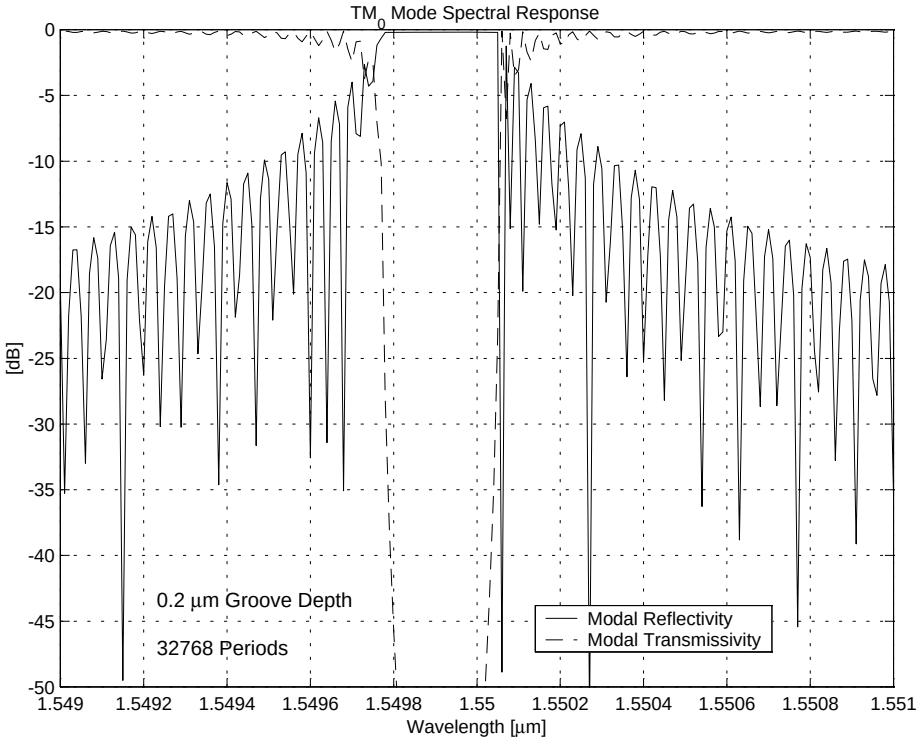

Figure 7.9: TM_0 Mode Response, 5% Groove Depth, 32768 Periods

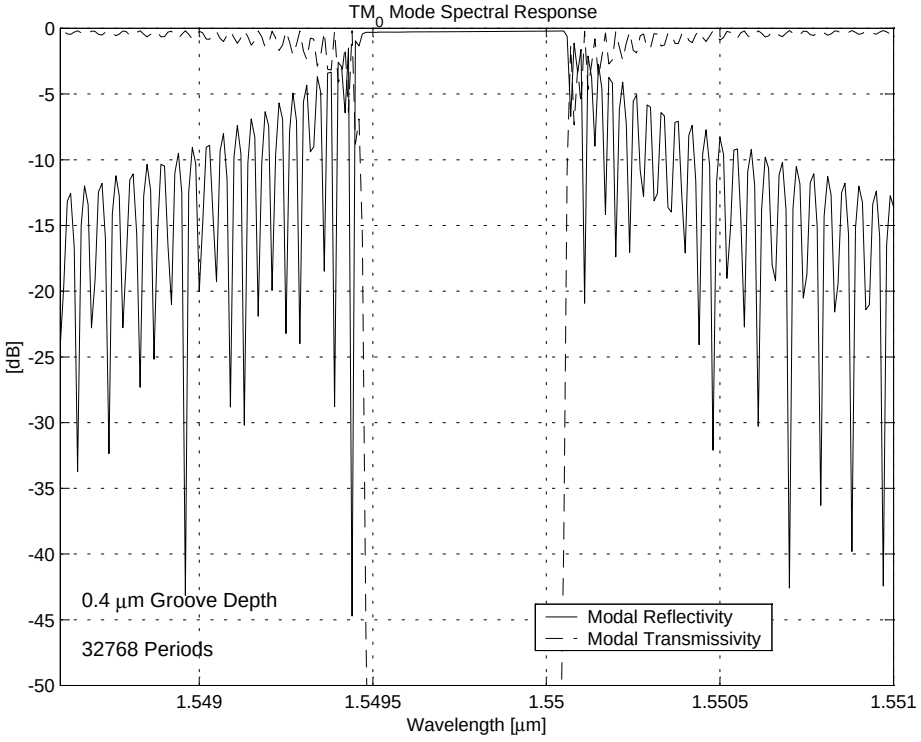

Figure 7.10: TM_0 Mode Response, 10% Groove Depth, 32768 Periods

7.7 Effect of the Number of Grating Periods

In this section, the modal spectral response of the TM-pass reflection mode polarizer is presented for different number of grating periods. It is evident from table 7.3 that for small number of grating periods the TM_0 modal reflectivity is low and spectral width is relatively high. Beyond a certain number of grating periods, adding extra periods does not affect the modal spectral reflectivity or spectral width.

Grating Period	Peak TM_0 Modal Reflectivity	Peak TE_0 Modal Reflectivity	Polarizer Extinction Ratio PER (dB)	Spectral Width (nm)
8192	0.652491	1.00545e-03	28.122	0.250
16384	0.938613	1.01134e-03	29.676	0.190
32768	0.958034	1.01873e-03	29.733	0.170
65536	0.977572	1.01220e-03	29.849	0.170
131072	0.977572	1.01220e-03	29.849	0.150
262144	0.977572	1.01220e-03	29.849	0.150

Table 7.3: Effect of Grating Periods (b=0.19 μm, Groove Depth=0.1 μm and L=0.47 mm)

In figure 7.11, the modal spectral reflectivity and transmissivity of the TM-pass reflection mode polarizer with 8192 periods is shown. The spectral reflectivity has width of 0.25 nm and a peak reflectivity of -2 dB and a minimum transmissivity of -5 dB. Thus, the TM-pass reflection mode polarizer having low number of grating periods has high reflection loss and transmission loss. If the number of grating periods is increased to 16384 and 32768 (see figures 7.12 and 7.8 respectively), the performance of the polarizer in terms of modal reflectivity and transmissivity im-

proves and the side lobes become higher and more closely packed while the spectral width nearly remains the same.

If the number of grating periods is further increased to 65536, the peak reflectivity remains the same and main lobe becomes flatter with higher and closely packed side lobes as shown in figure 7.13. The modal transmissivity plot has a deep notch in the stop band.

7.8 Discussion

The modal spectral response of the TM-pass reflection mode polarizer (see figure 7.4) is very similar to that of the conventional waveguide grating. As the number of grating periods is increased, the peak reflectivity also increases as there are more discontinuities to reflect the incident field backwards. The side lobes become densely packed and the main lobe becomes flatter. The side lobe level increases and the spectral width decreases slightly.

For shallow gratings, the response is symmetrical about the peak reflectivity wavelength. The main lobe has very narrow spectral width and the side lobes level is much lower. As the groove depth is increased, the response becomes asymmetric. The main lobe becomes broader and the side lobe level is increased.

The reflection mode polarizer is composed of two sections, the metal-clad section and the grating section. The total length of the reflection mode polarizer depends on the length of metal-clad and grating sections. The short polarizer

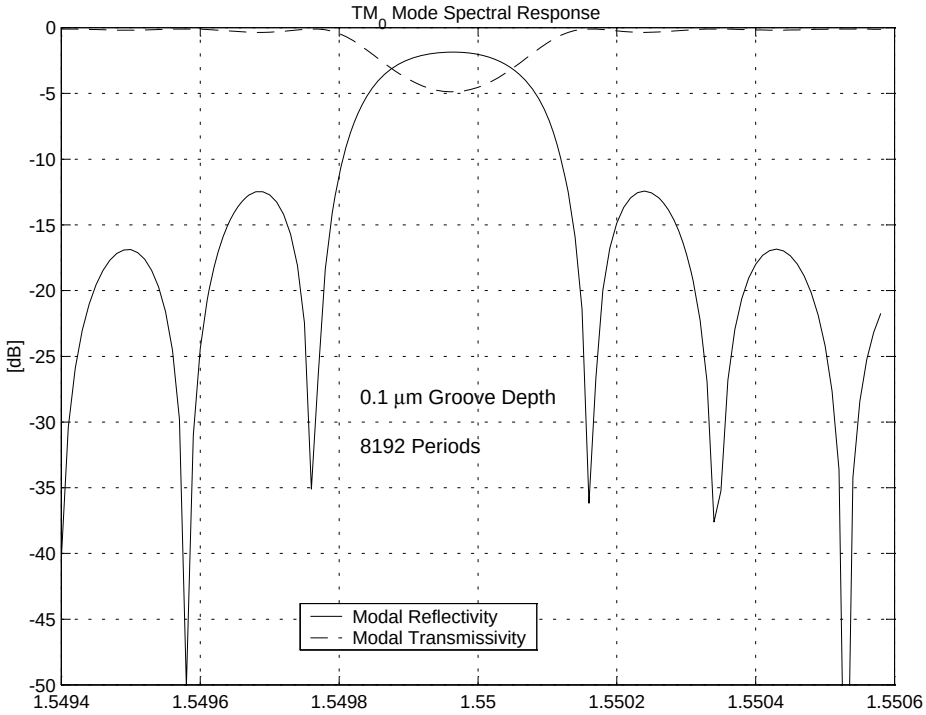

Figure 7.11: TM_0 Mode Response, 2.5% Groove Depth, 8192 Periods

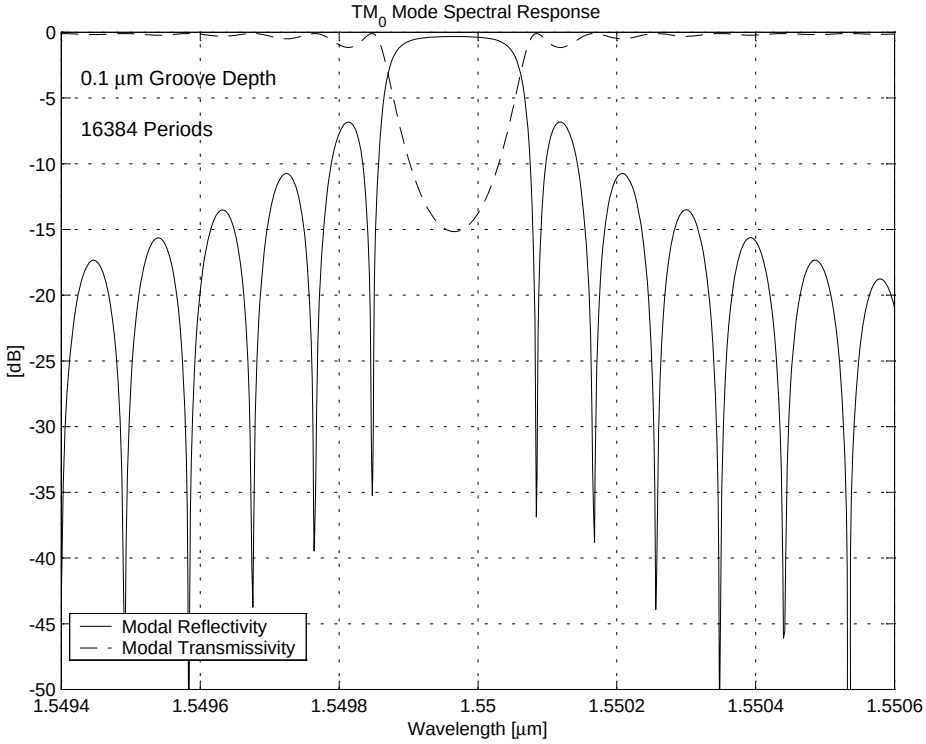

Figure 7.12: TM_0 Mode Response, 2.5% Groove Depth, 16384 Periods

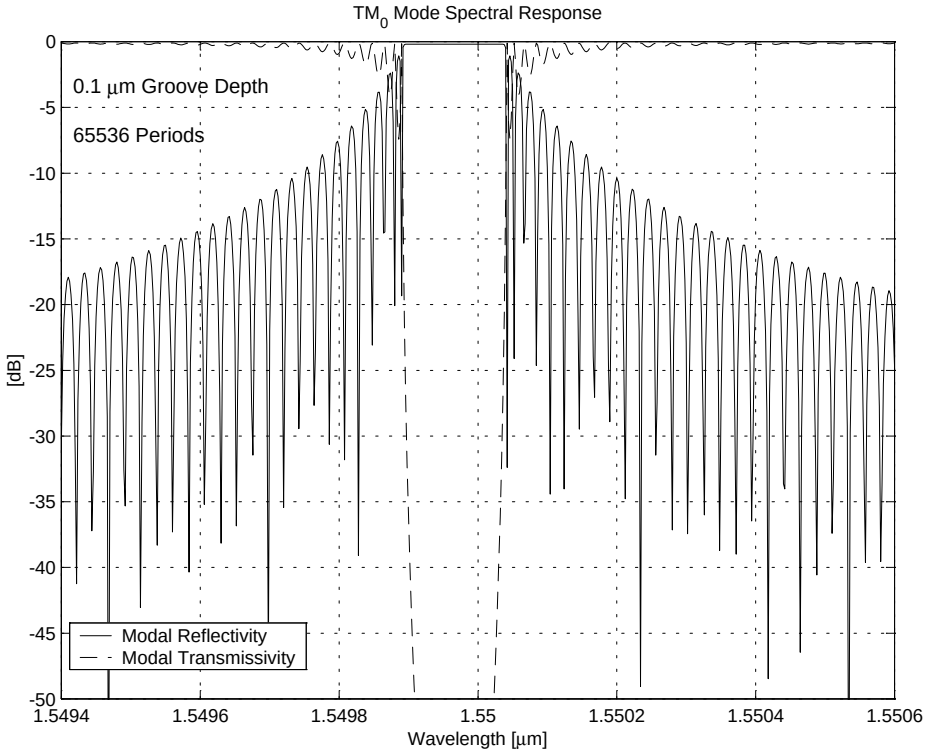

Figure 7.13: TM_0 Mode Response, 2.5% Groove Depth, 65536 Periods

with PER of 19.4 dB has the parameters; buffer layer thickness=0.192μm, grating depth=0.20μm, grating periods=8192, L_{gr}=4.2 mm, L=0.05 mm, peak TM_0 modal reflectivity=0.9525 and peak TE_0 modal reflectivity=0.011. The total length of this short polarizer is 4.25 mm. In order to obtain a polarizer with high extinction ratio the length of the polarizer is increased. The polarizer having the large length of 18.37mm has extinction ratio of 47.6 dB with parameters; buffer layer thickness=0.188μm, grating depth=0.04μm, grating periods=32768, L_{gr}=16.79 mm, L=1.58 mm, peak TM_0 modal reflectivity=0.8463 and peak TE_0 modal reflectivity=1.46e-5. Thus, the length of the polarizer can be chosen according to the particular application and requirement.

Chapter 8

Summary, Conclusions and Future Work

In this thesis, the Method of Lines (MOL) using higher-order approximations has been applied to find modal profiles and propagation constants of the eigen-modes of different multi-layer optical waveguide structures. It has been also used successfully to model the spectral responses of the TM-pass transmission and reflection mode polarizers. A brief summary of the work done, followed by conclusions and some future extensions of this work is given below.

8.1 Summary

- The MOL with higher-order approximations, five-point and seven-point approximations, is implemented for different structures and the results are veri-

fied against both published and analytical results.

- Perfectly Matched Layer (PML) absorbing boundary scheme has been used extensively in this research work. In chapter 4, single and multiple waveguide discontinuity problems are solved for different waveguide configurations. We have used the PML in each of these cases in order to absorb the radiative field.

- The MOL is used to find the modal fields and effective indices of the metal-clad waveguide without a buffer layer and with a buffer layer. These MOL results are verified against published as well as analytical results. The effect of varying high-index buffer layer thickness is studied. The metal-clad TE-pass and TM-pass polarizers performance is computed. The MOL has been used to account for the insertion loss as well as the coupling loss of the transmission mode TE and TM-pass polarizers. The optimum lengths of the TM-pass transmission mode polarizer is calculated for different high-index buffer layer thicknesses.

- The Cascading and Doubling Algorithm has been used to model periodic gratings with a large number of periods. This algorithm is found to be stable and its accuracy is verified against published results. Different conventional waveguide gratings are modeled and their spectral responses are calculated.

- The MOL is applied to model the TM-pass reflection mode polarizer. The modal spectral response of the polarizer is calculated using different device parameters. The polarizer with short length and long length is also analyzed.

8.2 Conclusions

- The three-point, five-point and seven-point approximations are used in the MOL to model a waveguide structure and it is found that the higher-order approximation requires relatively few discretization lines to sample the problem space. As shown in chapter 3, the higher-order approximation gives more accurate estimation of the modal field and the effective index. This results in a much reduced matrix size, faster computational speed and lower memory usage for stationary analysis as well as for multiple discontinuity problems. The higher-order scheme is highly favorable to waveguides with metallic layer, where large discretization lines are required to model the field in a metallic layer.

- The single and double discontinuity problems are solved and the perfectly matched layer (PML) absorber is used with MOL. The PML is easily incorporated into the MOL and the matrix size for the basic MOL is not increased substantially.

- The introduction of a high-index buffer layer of suitable thickness between the core and the metallic cladding converts a metal-clad three layer waveguide from a TE-pass to a TM-pass polarizer. With the optimum buffer layer thickness, the polarizer extinction ratio and the polarizer insertion loss of the TM-pass polarizer are found to reach high values.

- The Cascading and Doubling Algorithm is found to be highly efficient and numerically stable in modeling long gratings. It can model 2^n grating periods in n calculational steps. This algorithm gives improved accuracy and smaller memory requirement as compared to other methods. For N discretization lines in the problem space, its memory usage is $N \times N$ while some other algorithms require $2N \times 2N$ matrices.

- The modal spectral response of the TM-pass reflection mode polarizer is found to be very similar to that of the conventional waveguide grating. As the number of grating periods increased, the peak reflectivity also increases, the side lobes become more densely packed and the main lobe becomes flatter. For shallow gratings, the response is symmetrical about the peak reflectivity wavelength. The short length of the metal-clad section with suitable buffer layer thickness gives high peak TM_0 modal reflectivity. The polarizer extinction ratio can be increased using large length of the metal-clad section with suitable high-index buffer layer thickness.

8.3 Future Prospects

Scientific research is an ongoing process and there is always some room for improvement. The following is a brief list of suggestions for possible future work in this area.

- We have analyzed the spectral response of the TM-pass reflection mode po-

larizer in this thesis. The field variation within the grating and the metal-clad section of the TM-pass reflection mode polarizer can also be analyzed using the MOL.

- This planar TM-pass reflection mode polarizer can be extended to the cylindrical waveguide polarizer, so that it can be applied in fiber optic lasers.

- The scalar approximation of the electric field **E** or the magnetic field **H** has been used in this research work. This approximation is used for slab waveguides with large lateral dimension. However, it is not adequate for channel waveguides where guidance of the optical field is achieved in the two dimension of the transverse plane. In this case, it may be necessary to account for the full vectorial nature of the optical field. The Method of Lines may be extended in an efficient and stable way to model the full-vectorial nature of **E** or **H**, that is all six components E_x, E_y, E_z, H_x, H_y, H_z of the electromagnetic field in a waveguide are accounted for.

- The TM-pass reflection mode polarizer analyzed in this thesis behaves also as a very narrow band-pass filter. It would be desirable if a transmission mode TM mode polarizer with narrow band-pass characteristic is achieved. This type of device may be used in wavelength division multiplexing optical fiber communication systems.

- It would also be of interest to analyze a TM-pass polarizer that utilizes multilayers between the core and the metallic cover rather than just a single high-

index layer. This may lead to further enhancement of the TE/TM discrimination of the polarizer.

- Also an obvious extension of this work is to study the effects of different metals such as silver or copper on the polarizer performance.

Appendix A

Higher-Order Approximation

A.1 Five-Point Formulation

In this case, the field is expanded on either side of the interface in terms of the field at the interface using Taylor's series expansion, that is:

$$\psi_{+1} = \psi_{0^+} + h_2\psi'_{0^+} + \frac{h_2^2}{2!}\psi''_{0^+} + \frac{h_2^3}{3!}\psi'''_{0^+} + \frac{h_2^4}{4!}\psi''''_{0^+} + ... \quad \text{(A.1)}$$

$$\psi_{-1} = \psi_{0^-} - h_1\psi'_{0^-} + \frac{h_1^2}{2!}\psi''_{0^-} - \frac{h_1^3}{3!}\psi'''_{0^-} + \frac{h_1^4}{4!}\psi''''_{0^-} - ... \quad \text{(A.2)}$$

$$\psi_{+2} = \psi_{0^+} + 2h_2\psi'_{0^+} + \frac{(2h_2)^2}{2!}\psi''_{0^+} + \frac{(2h_2)^3}{3!}\psi'''_{0^+} + \frac{(2h_2)^4}{4!}\psi''''_{0^+} + ... \quad \text{(A.3)}$$

$$\psi_{-2} = \psi_{0^-} - 2h_1\psi'_{0^-} + \frac{(2h_1)^2}{2!}\psi''_{0^-} - \frac{(2h_1)^3}{3!}\psi'''_{0^-} + \frac{(2h_1)^4}{4!}\psi''''_{0^-} - ... \quad \text{(A.4)}$$

Using the interface conditions 3.26-3.30 and expressing the fields ψ_{+1} and ψ_{+2} in terms of the 0^- side derivatives of ψ, we obtain [58]:

$$\psi_{+1} = \left(1 + \frac{h_2^2\zeta_{12}}{2} + \frac{h_2^4\zeta_{12}^2}{24}\right)\psi_0 + \rho_{21}\left(h_2 + \frac{h_2^3\zeta_{12}}{6}\right)\psi'_{0^-}$$

$$+\left(\frac{h_2^2}{2}+\frac{h_2^4\zeta_{12}}{12}\right)\psi_{0^-}^{''}+\frac{h_2^3\rho_{21}}{6}\psi_{0^-}^{'''}+\frac{h_2^4}{24}\psi_{0^-}^{''''}+... \tag{A.5}$$

$$\psi_{+2}=\left(1+2h_2^2\zeta_{12}+\frac{2h_2^4\zeta_{12}^2}{3}\right)\psi_0+\rho_{21}\left(2h_2+\frac{4h_2^3\zeta_{12}}{3}\right)\psi_{0^-}^{'}$$

$$+\left(2h_2^2+\frac{4h_2^4\zeta_{12}}{3}\right)\psi_{0^-}^{''}+\frac{4h_2^3\rho_{21}}{3}\psi_{0^-}^{'''}+\frac{2h_2^4}{3}\psi_{0^-}^{''''}+... \tag{A.6}$$

Equations A.2, A.4, A.5 and A.6 can be put in matrix form, that is:

$$\begin{bmatrix}\psi_{+1}-a\cdot\psi_0\\ \psi_{+2}-b\cdot\psi_0\\ \psi_{-1}-c\cdot\psi_0\\ \psi_{-2}-d\cdot\psi_0\end{bmatrix}=\begin{bmatrix}a_{11}&a_{12}&a_{13}&a_{14}\\ a_{21}&a_{22}&a_{23}&a_{24}\\ a_{31}&a_{32}&a_{33}&a_{34}\\ a_{41}&a_{42}&a_{43}&a_{44}\end{bmatrix}\begin{bmatrix}\psi_{0^-}^{'}\\ \psi_{0^-}^{''}\\ \psi_{0^-}^{'''}\\ \psi_{0^-}^{''''}\end{bmatrix}$$

where a, b, c and d are the coefficients of ψ_0 in the previous equations. Inverting the above matrix equation to find the unknowns:

$$\begin{bmatrix}\psi_{0^-}^{'}\\ \psi_{0^-}^{''}\\ \psi_{0^-}^{'''}\\ \psi_{0^-}^{''''}\end{bmatrix}=\begin{bmatrix}b_{11}&b_{12}&b_{13}&b_{14}\\ b_{21}&b_{22}&b_{23}&b_{24}\\ b_{31}&b_{32}&b_{33}&b_{34}\\ b_{41}&b_{42}&b_{43}&b_{44}\end{bmatrix}\begin{bmatrix}\psi_{+1}-a\cdot\psi_0\\ \psi_{+2}-b\cdot\psi_0\\ \psi_{-1}-c\cdot\psi_0\\ \psi_{-2}-d\cdot\psi_0\end{bmatrix}$$

From which we have:

$$\psi_{0^-}^{''} = b_{22}\psi_{+2}+b_{21}\psi_{+1}-(a\cdot b_{21}+b\cdot b_{22}+c\cdot b_{23}+d\cdot b_{24})\psi_0+$$

$$b_{23}\psi_{-1}+b_{24}\psi_{-2} \tag{A.7}$$

This relation gives $\psi_i^{''}$ approximation at an interface in terms of the field samples

ψ_{i+2} , ψ_{i+1} , ψ_i , ψ_{i-1} and ψ_{i-2}. In this relation, the discontinuity in $\psi^{'}$, $\psi^{''}$, $\psi^{'''}$ and $\psi^{''''}$ at an index or mesh discontinuity are appropriately included. In regions of uniform index and mesh, this reduces to the familiar 5-point approximation, that is:

$$\psi_{0^-}^{''} \approx \frac{1}{12h^2}(-\psi_{+2} + 16\psi_{+1} - 30\psi_0 + 16\psi_{-1} - \psi_{-2}) \tag{A.8}$$

By using this five-point approximation, we get a penta-diagonal matrix of the form [36]:

$$\frac{1}{12h^2}\begin{bmatrix} -30 & 16 & -1 & & & & & \\ 16 & -30 & 16 & -1 & & & \mathcal{O} & \\ -1 & 16 & -30 & 16 & -1 & & & \\ & \ddots & \ddots & \ddots & \ddots & \ddots & & \\ & & & -1 & 16 & -30 & 16 & -1 \\ & \mathcal{O} & & & -1 & 16 & -30 & 16 \\ & & & & & -1 & 16 & -30 \end{bmatrix}$$

It is necessary to find the 5-point second-derivative formula at one sampling point *ahead* and one sampling point *before* the interface. In this derivation, it is assumed that the minimum number of samples in one layer is 3. With reference to figure 3.2, $\psi_0^{''}$ is to be expressed in terms of ψ_{-1} , ψ_0 , ψ_{+1} , ψ_{+2} and ψ_{+3}. Expanding the field samples on either side of the interface in terms of ψ_0:

$$\psi_{+1} = \psi_{0^+} + h_2\psi_{0^+}^{'} + \frac{h_2^2}{2!}\psi_{0^+}^{''} + \frac{h_2^3}{3!}\psi_{0^+}^{'''} + \frac{h_2^4}{4!}\psi_{0^+}^{''''} + ... \tag{A.9}$$

$$\psi_{+2} = \psi_{0^+} + 2h_2\psi_{0^+}^{'} + \frac{(2h_2)^2}{2!}\psi_{0^+}^{''} + \frac{(2h_2)^3}{3!}\psi_{0^+}^{'''} + \frac{(2h_2)^4}{4!}\psi_{0^+}^{''''} + ... \tag{A.10}$$

$$\psi_{+3} = \psi_{0+} + 3h_2\psi'_{0+} + \frac{(3h_2)^2}{2!}\psi''_{0+} + \frac{(3h_2)^3}{3!}\psi'''_{0+} + \frac{(3h_2)^4}{4!}\psi''''_{0+} + ... \quad \text{(A.11)}$$

$$\psi_{-1} = \psi_{0-} - h_1\psi'_{0-} + \frac{h_1^2}{2!}\psi''_{0-} - \frac{h_1^3}{3!}\psi'''_{0-} + \frac{h_1^4}{4!}\psi''''_{0-} - ... \quad \text{(A.12)}$$

Using the interface conditions 3.26-3.30, we express ψ_{0-} derivatives in terms of ψ_{0+} derivatives in equation A.12:

$$\begin{aligned}\psi_{-1} = \psi_0 &\left(1 - \frac{h_1^2}{2}\zeta_{12} + \frac{h_1^4}{24}\zeta_{12}^2\right) + \psi'_{0+}\left(\frac{-h_1}{\rho_{21}} + \frac{h_1^3}{6\rho_{21}}\zeta_{12}\right) \\ &+\psi''_{0+}\left(\frac{h_1^2}{2} - \frac{h_1^4}{12}\zeta_{12}\right) - \frac{h_1^3}{6\rho_{21}}\psi'''_{0+} + \frac{h_1^4}{24}\psi''''_{0+}\end{aligned} \quad \text{(A.13)}$$

In matrix form:

$$\begin{bmatrix} \psi_{+1} - \psi_0 \\ \psi_{+2} - \psi_0 \\ \psi_{+3} - \psi_0 \\ \psi_{-1} - a \cdot \psi_0 \end{bmatrix} = \begin{bmatrix} a_{11} & a_{12} & a_{13} & a_{14} \\ a_{21} & a_{22} & a_{23} & a_{24} \\ a_{31} & a_{32} & a_{33} & a_{34} \\ a_{41} & a_{42} & a_{43} & a_{44} \end{bmatrix} \begin{bmatrix} \psi'_{0+} \\ \psi''_{0+} \\ \psi'''_{0+} \\ \psi''''_{0+} \end{bmatrix}$$

where a is the coefficient of ψ_0 in equation A.13. Inverting the above matrix equation, we have [58]:

$$\begin{bmatrix} \psi'_{0+} \\ \psi''_{0+} \\ \psi'''_{0+} \\ \psi''''_{0+} \end{bmatrix} = \begin{bmatrix} b_{11} & b_{12} & b_{13} & b_{14} \\ b_{21} & b_{22} & b_{23} & b_{24} \\ b_{31} & b_{32} & b_{33} & b_{34} \\ b_{41} & b_{42} & b_{43} & b_{44} \end{bmatrix} \begin{bmatrix} \psi_{+1} - \psi_0 \\ \psi_{+2} - \psi_0 \\ \psi_{+3} - \psi_0 \\ \psi_{-1} - a \cdot \psi_0 \end{bmatrix}$$

Differentiating equation A.9 twice with respect to x:

$$\psi''_{+1} = \psi''_{0+} + h_2\psi'''_{0+} + \frac{h_2^2}{2}\psi''''_{0+} + ... \quad \text{(A.14)}$$

Putting the values of $\psi_{0^+}^{''}$, $\psi_{0^+}^{'''}$ and $\psi_{0^+}^{''''}$ in the above equation and simplifying, we have [58]:

$$\begin{aligned}\psi_{+1}^{''} = \quad & \psi_{+3}(b_{23} + h_2 b_{33} + 0.5h_2^2 b_{43}) + \psi_{+2}(b_{22} + h_2 b_{32} + 0.5h_2^2 b_{42}) + \\ & \psi_{+1}(b_{21} + h_2 b_{31} + 0.5h_2^2 b_{41}) - \psi_0(p_1 + h_2 p_2 + 0.5h_2^2 p_3) \\ & \psi_{-1}(b_{24} + h_2 b_{34} + 0.5h_2^2 b_{44}) \end{aligned} \tag{A.15}$$

where

$p_1 = b_{21} + b_{22} + b_{23} + a \cdot b_{24}$

$p_2 = b_{31} + b_{32} + b_{33} + a \cdot b_{34}$

$p_3 = b_{41} + b_{42} + b_{43} + a \cdot b_{44}$

This relation gives the five-point second-derivative approximation at one sample point ahead of an index or mesh discontinuity. The relation at one sample point before the interface can obtained by interchanging $h_2 \rightleftharpoons -h_1$, $\psi_{+2} \rightleftharpoons \psi_0$, $\psi_{+3} \rightleftharpoons \psi_{-1}$ and $n_1^2 \rightleftharpoons n_2^2$ [58].

A.2 Seven-Point Formulation

A similar procedure is adopted to find the 7-point second-derivative approximation with appropriate interface conditions.

$$\begin{aligned}\psi_{+1} &= \psi_{0^+} + h_2\psi_{0^+}^{'} + \frac{h_2^2}{2!}\psi_{0^+}^{''} + \frac{h_2^3}{3!}\psi_{0^+}^{'''} + \frac{h_2^4}{4!}\psi_{0^+}^{''''} + \\ &\quad \frac{h_5^4}{5!}\psi_{0^+}^{'''''} + \frac{h_2^6}{6!}\psi_{0^+}^{''''''} + ... \\ \psi_{+2} &= \psi_{0^+} + 2h_2\psi_{0^+}^{'} + \frac{(2h_2)^2}{2!}\psi_{0^+}^{''} + \frac{(2h_2)^3}{3!}\psi_{0^+}^{'''} + \frac{(2h_2)^4}{4!}\psi_{0^+}^{''''}\end{aligned} \tag{A.16}$$

$$+\frac{(2h_2)^5}{5!}\psi^{''''}_{0+} + \frac{(2h_2)^6}{6!}\psi^{''''''}_{0+} + ... \tag{A.17}$$

$$\psi_{+3} = \psi_{0+} + 3h_2\psi^{'}_{0+} + \frac{(3h_2)^2}{2!}\psi^{''}_{0+} + \frac{(3h_2)^3}{3!}\psi^{'''}_{0+} + \frac{(3h_2)^4}{4!}\psi^{''''}_{0+}$$
$$+\frac{(3h_2)^5}{5!}\psi^{''''}_{0+} + \frac{(3h_2)^6}{6!}\psi^{''''''}_{0+} + ... \tag{A.18}$$

$$\psi_{-1} = \psi_{0-} - h_1\psi^{'}_{0-} + \frac{h_1^2}{2!}\psi^{''}_{0-} - \frac{h_1^3}{3!}\psi^{'''}_{0-} + \frac{h_1^4}{4!}\psi^{''''}_{0-}$$
$$-\frac{h_1^5}{5!}\psi^{''''}_{0-} + \frac{h_1^6}{6!}\psi^{''''''}_{0-} - ... \tag{A.19}$$

$$\psi_{-2} = \psi_{0-} - 2h_1\psi^{'}_{0-} + \frac{(2h_1)^2}{2!}\psi^{''}_{0-} - \frac{(2h_1)^3}{3!}\psi^{'''}_{0-} + \frac{(2h_1)^4}{4!}\psi^{''''}_{0-}$$
$$-\frac{(2h_1)^5}{5!}\psi^{''''}_{0-} + \frac{(2h_1)^6}{6!}\psi^{''''''}_{0-} - ... \tag{A.20}$$

$$\psi_{-3} = \psi_{0-} - 3h_1\psi^{'}_{0-} + \frac{(3h_1)^2}{2!}\psi^{''}_{0-} - \frac{(3h_1)^3}{3!}\psi^{'''}_{0-} + \frac{(3h_1)^4}{4!}\psi^{''''}_{0-}$$
$$-\frac{(3h_1)^5}{5!}\psi^{''''}_{0-} + \frac{(3h_1)^6}{6!}\psi^{''''''}_{0-} - ... \tag{A.21}$$

Using the interface conditions 3.26-3.32, we express ψ_{0+} side derivatives in terms of ψ_{0-} derivatives:

$$\psi_{+1} = \psi_0\left(1 + \frac{\zeta_{12}h_2^2}{2!} + \frac{\zeta_{12}^2h_2^4}{4!} + \frac{\zeta_{12}^3h_2^6}{6!}\right) + \rho_{21}\psi^{'}_{0-}\left(h_2 + \frac{\zeta_{12}h_2^3}{3!} + \frac{\zeta_{12}^2h_2^5}{5!}\right)$$
$$+\psi^{''}_{0-}\left(\frac{h_2^2}{2!} + \frac{2\zeta_{12}h_2^4}{4!} + \frac{3\zeta_{12}^2h_2^6}{6!}\right) + \rho_{21}\psi^{'''}_{0-}\left(\frac{h_2^3}{3!} + \frac{2\zeta_{12}h_2^5}{5!}\right)$$
$$+\psi^{''''}_{0-}\left(\frac{h_2^4}{4!} + \frac{3\zeta_{12}h_2^6}{6!}\right) + \rho_{21}\psi^{''''}_{0-}\left(\frac{h_2^5}{5!}\right) + \psi^{''''''}_{0-}\left(\frac{h_2^6}{6!}\right) \tag{A.22}$$

Expressions for ψ_{+2} and ψ_{+3} are obtained by replacing h_2 by $2h_2$ and $3h_2$ in equation A.22 respectively. We then assimilate the final results in the matrix form :

$$\begin{bmatrix} \psi_{+1} - a \cdot \psi_0 \\ \psi_{+2} - b \cdot \psi_0 \\ \psi_{+3} - c \cdot \psi_0 \\ \psi_{-1} - \psi_0 \\ \psi_{-2} - \psi_0 \\ \psi_{-3} - \psi_0 \end{bmatrix} = \begin{bmatrix} a_{11} & a_{12} & a_{13} & a_{14} & a_{15} & a_{16} \\ a_{21} & a_{22} & a_{23} & a_{24} & a_{25} & a_{26} \\ a_{31} & a_{32} & a_{33} & a_{34} & a_{35} & a_{36} \\ a_{41} & a_{42} & a_{43} & a_{44} & a_{45} & a_{46} \\ a_{51} & a_{52} & a_{53} & a_{54} & a_{55} & a_{56} \\ a_{61} & a_{62} & a_{63} & a_{64} & a_{65} & a_{66} \end{bmatrix} \begin{bmatrix} \psi'_{0-} \\ \psi''_{0-} \\ \psi'''_{0-} \\ \psi''''_{0-} \\ \psi'''''_{0-} \\ \psi''''''_{0-} \end{bmatrix}$$

where a, b and c are the coefficients of corresponding ψ_0 terms in the previous equation. Inverting the above matrix equation, we have [36]:

$$\begin{bmatrix} \psi'_{0-} \\ \psi''_{0-} \\ \psi'''_{0-} \\ \psi''''_{0-} \\ \psi'''''_{0-} \\ \psi''''''_{0-} \end{bmatrix} = \begin{bmatrix} b_{11} & b_{12} & b_{13} & b_{14} & b_{15} & b_{16} \\ b_{21} & b_{22} & b_{23} & b_{24} & b_{25} & b_{26} \\ b_{31} & b_{32} & b_{33} & b_{34} & b_{35} & b_{36} \\ b_{41} & b_{42} & b_{43} & b_{44} & b_{45} & b_{46} \\ b_{51} & b_{52} & b_{53} & b_{54} & b_{55} & b_{56} \\ b_{61} & b_{62} & b_{63} & b_{64} & b_{65} & b_{66} \end{bmatrix} \begin{bmatrix} \psi_{+1} - a \cdot \psi_0 \\ \psi_{+2} - b \cdot \psi_0 \\ \psi_{+3} - c \cdot \psi_0 \\ \psi_{-1} - \psi_0 \\ \psi_{-2} - \psi_0 \\ \psi_{-3} - \psi_0 \end{bmatrix}$$

From which we have [36]:

$$\begin{aligned} \psi''_{0-} &= b_{23}\psi_{+3} + b_{22}\psi_{+2} + b_{21}\psi_{+1} - (a \cdot b_{21} + b \cdot b_{22} + c \cdot b_{23} + b_{24} + b_{25} + b_{26})\psi_0 \\ &\quad + b_{24}\psi_{-1} + b_{25}\psi_{-2} + b_{26}\psi_{-3} \end{aligned} \tag{A.23}$$

This relation gives approximation of ψ''_i at an interface point. In the regions of uniform index and uniform mesh, this relation reduces to the 7-point approximation

of the form:

$$\psi_{0^-}^{''} \approx \frac{1}{180h^2}(2\psi_{+3} - 27\psi_{+2} + 270\psi_{+1} - 490\psi_0 + 270\psi_{-1} - 27\psi_{-2} + 2\psi_{-3}) \quad \text{(A.24)}$$

By using this seven-point approximations, we get a hepta-diagonal matrix of the form [36]:

$$\frac{1}{180h^2}\begin{bmatrix} -490 & 270 & -27 & 2 & & & & & & \\ 270 & -490 & 270 & -27 & 2 & & & & \mathcal{O} & \\ -27 & 270 & -490 & 270 & -27 & 2 & & & & \\ 2 & -27 & 270 & -490 & 270 & -27 & 2 & & & \\ & \ddots & \ddots & \ddots & \ddots & \ddots & \ddots & \ddots & & \\ & & & 2 & -27 & 270 & -490 & 270 & -27 & 2 \\ & & & & 2 & -27 & 270 & -490 & 270 & -27 \\ & \mathcal{O} & & & & 2 & -27 & 270 & -490 & 270 \\ & & & & & & 2 & -27 & 270 & -490 \end{bmatrix}$$

To find the second-derivative formula at one sampling point before the interface, the procedure is similar to that followed in the previous section. With reference to the figure 3.2, $\psi_0^{''}$ is to be expressed in terms of ψ_{-1} , ψ_{-2} , ψ_{-3} , ψ_{-4} , ψ_{+1} and ψ_{+2}. Expanding the field samples on either side of the interface in terms of ψ_0:

$$\psi_{-1} = \psi_{0^-} - h_1\psi_{0^-}^{'} + ... + \frac{h_1^6}{6!}\psi_{0^-}^{''''''} + ... \quad \text{(A.25)}$$

$$\psi_{-2} = \psi_{0^-} - 2h_1\psi_{0^-}^{'} + ... + \frac{(-2h_1)^6}{6!}\psi_{0^-}^{''''''} + ... \quad \text{(A.26)}$$

$$\psi_{-3} = \psi_{0^-} - 3h_1\psi'_{0^-} + ... + \frac{(-3h_1)^6}{6!}\psi'''''_{0^-} + ... \quad (A.27)$$

$$\psi_{-4} = \psi_{0^-} - 4h_1\psi'_{0^-} + ... + \frac{(-4h_1)^6}{6!}\psi'''''_{0^-} + ... \quad (A.28)$$

$$\psi_{+1} = \psi_{0^+} + h_2\psi'_{0^+} + ... + \frac{h_2^6}{6!}\psi'''''_{0^+} + ... \quad (A.29)$$

$$\psi_{+2} = \psi_{0^+} + 2h_2\psi'_{0^+} + ... + \frac{(2h_2)^6}{6!}\psi'''''_{0^+} + ... \quad (A.30)$$

Replacing all $\psi^{(n)}_{0^+}$ derivatives with $\psi^{(n)}_{0^-}$ derivatives in the above equations. After simplifying, we obtain:

$$\begin{aligned}\psi_{+1} = \quad & \psi_0\left(1 + \frac{\zeta_{12}h_2^2}{2!} + \frac{\zeta_{12}^2h_2^4}{4!} + \frac{\zeta_{12}^3h_2^6}{6!}\right) + \rho_{21}\psi'_{0^-}\left(h_2 + \frac{\zeta_{12}h_2^3}{3!} + \frac{\zeta_{12}^2h_2^5}{5!}\right) \\ & + \psi''_{0^-}\left(\frac{h_2^2}{2!} + \frac{2\zeta_{12}h_2^4}{4!} + \frac{3\zeta_{12}^2h_2^6}{6!}\right) + \rho_{21}\psi'''_{0^-}\left(\frac{h_2^3}{3!} + \frac{2\zeta_{12}h_2^5}{5!}\right) \\ & + \psi''''_{0^-}\left(\frac{h_2^4}{4!} + \frac{3\zeta_{12}h_2^6}{6!}\right) + \rho_{21}\psi'''''_{0^-}\left(\frac{h_2^5}{5!}\right) + \psi'''''_{+1^-}\left(\frac{h_2^6}{6!}\right) \end{aligned} \quad (A.31)$$

For ψ_{+2}, replace h_2 by $2h_2$ in equation A.31. Assimilated the above equations in matrix form:

$$\begin{bmatrix} \psi_{+1} - a\cdot\psi_0 \\ \psi_{+2} - b\cdot\psi_0 \\ \psi_{-1} - \psi_0 \\ \psi_{-2} - \psi_0 \\ \psi_{-3} - \psi_0 \\ \psi_{-4} - \psi_0 \end{bmatrix} = \begin{bmatrix} a_{11} & a_{12} & a_{13} & a_{14} & a_{15} & a_{16} \\ a_{21} & a_{22} & a_{23} & a_{24} & a_{25} & a_{26} \\ a_{31} & a_{32} & a_{33} & a_{34} & a_{35} & a_{36} \\ a_{41} & a_{42} & a_{43} & a_{44} & a_{45} & a_{46} \\ a_{51} & a_{52} & a_{53} & a_{54} & a_{55} & a_{56} \\ a_{61} & a_{62} & a_{63} & a_{64} & a_{65} & a_{66} \end{bmatrix} \begin{bmatrix} \psi'_{0^-} \\ \psi''_{0^-} \\ \psi'''_{0^-} \\ \psi''''_{0^-} \\ \psi'''''_{0^-} \\ \psi''''''_{0^-} \end{bmatrix}$$

where a and b are the coefficients of the corresponding ψ_0 terms. Inverting the above

matrix equation, we obtain:

$$\begin{bmatrix} \psi'_{0-} \\ \psi''_{0-} \\ \psi'''_{0-} \\ \psi''''_{0-} \\ \psi'''''_{0-} \\ \psi''''''_{0-} \end{bmatrix} = \begin{bmatrix} b_{11} & b_{12} & b_{13} & b_{14} & b_{15} & b_{16} \\ b_{21} & b_{22} & b_{23} & b_{24} & b_{25} & b_{26} \\ b_{31} & b_{32} & b_{33} & b_{34} & b_{35} & b_{36} \\ b_{41} & b_{42} & b_{43} & b_{44} & b_{45} & b_{46} \\ b_{51} & b_{52} & b_{53} & b_{54} & b_{55} & b_{56} \\ b_{61} & b_{62} & b_{63} & b_{64} & b_{65} & b_{66} \end{bmatrix} \begin{bmatrix} \psi_{+1} - a \cdot \psi_0 \\ \psi_{+2} - b \cdot \psi_0 \\ \psi_{-1} - \psi_0 \\ \psi_{-2} - \psi_0 \\ \psi_{-3} - \psi_0 \\ \psi_{-4} - \psi_0 \end{bmatrix}$$

Differentiating Taylor's series expansion A.25 of ψ_{-1} twice with respect to x, we have:

$$\psi''_{-1} = \psi''_{0-} - h_1\psi'''_{0-} + \frac{h_1^2}{2!}\psi''''_{0-} - \frac{h_1^3}{3!}\psi'''''_{0-} + \frac{h_1^4}{4!}\psi''''''_{0-} - +... \tag{A.32}$$

Putting the values of ψ''_{0-} , ψ'''_{0-} , ψ''''_{0-} , ψ'''''_{0-} and ψ''''''_{0-} in equation A.32 and simplifying, we obtain:

$$\begin{aligned} \psi''_{-1} = \quad & \psi_{-4}\left(b_{26} - h_1 b_{36} + \frac{h_1^2}{2!}b_{46} - \frac{h_1^3}{3!}b_{56} + \frac{h_1^4}{4!}b_{66}\right) + \\ & \psi_{-3}\left(b_{25} - h_1 b_{35} + \frac{h_1^2}{2!}b_{45} - \frac{h_1^3}{3!}b_{55} + \frac{h_1^4}{4!}b_{65}\right) + \\ & \psi_{-2}\left(b_{24} - h_1 b_{34} + \frac{h_1^2}{2!}b_{44} - \frac{h_1^3}{3!}b_{54} + \frac{h_1^4}{4!}b_{64}\right) + \\ & \psi_{-1}\left(b_{23} - h_1 b_{33} + \frac{h_1^2}{2!}b_{43} - \frac{h_1^3}{3!}b_{53} + \frac{h_1^4}{4!}b_{63}\right) + \\ & \psi_0\left(p_1 - h_1 p_2 + \frac{h_1^2}{2!}p_3 - \frac{h_1^3}{3!}p_4 + \frac{h_1^4}{4!}p_5\right) + \\ & \psi_{+1}\left(b_{21} - h_1 b_{31} + \frac{h_1^2}{2!}b_{41} - \frac{h_1^3}{3!}b_{51} + \frac{h_1^4}{4!}b_{61}\right) + \end{aligned}$$

$$\psi_{+2}\left(b_{22}-h_1b_{32}+\frac{h_1^2}{2!}b_{42}-\frac{h_1^3}{3!}b_{52}+\frac{h_1^4}{4!}b_{62}\right) \tag{A.33}$$

where $p_1 = a\cdot b_{21}+b\cdot b_{22}+b_{23}+b_{24}+b_{25}+b_{26}$, $p_2 = a\cdot b_{31}+b\cdot b_{32}+b_{33}+b_{34}+b_{35}+b_{36}$, $p_3 = a\cdot b_{41}+b\cdot b_{42}+b_{43}+b_{44}+b_{45}+b_{46}$, $p_4 = a\cdot b_{51}+b\cdot b_{52}+b_{53}+b_{54}+b_{55}+b_{56}$ and $p_5 = a\cdot b_{61}+b\cdot b_{62}+b_{63}+b_{64}+b_{65}+b_{66}$. This relation gives the seven-point second derivative approximation at one sample point before the interface. The relation at one sample point ahead of the interface is obtained by interchanging $h_2 \rightleftharpoons -h_1$, $\psi_0 \rightleftharpoons \psi_{-2}$, $\psi_{+1} \rightleftharpoons \psi_{-3}$, $\psi_{+2} \rightleftharpoons \psi_{-4}$ and $n_1^2 \rightleftharpoons n_2^2$.

A similar procedure is followed to find the second-derivative formula at two sample points before the interface. With reference to figure 3.2, expanding the field on either sides of the interface in terms of ψ_0:

$$\psi_{-1} = \psi_{0^-} - h_1\psi_{0^-}^{'} + ... + \frac{h_1^6}{6!}\psi_{0^-}^{''''''} + ... \tag{A.34}$$

$$\psi_{-2} = \psi_{0^-} - 2h_1\psi_{0^-}^{'} + ... + \frac{(2h_1)^6}{6!}\psi_{0^-}^{''''''} + ... \tag{A.35}$$

$$\psi_{-3} = \psi_{0^-} - 3h_1\psi_{0^-}^{'} + ... + \frac{(3h_1)^6}{6!}\psi_{0^-}^{''''''} + ... \tag{A.36}$$

$$\psi_{-4} = \psi_{0^-} - 4h_1\psi_{0^-}^{'} + ... + \frac{(4h_1)^6}{6!}\psi_{0^-}^{''''''} + ... \tag{A.37}$$

$$\psi_{-5} = \psi_{0^-} - 5h_1\psi_{0^-}^{'} + ... + \frac{(5h_1)^6}{6!}\psi_{0^-}^{''''''} + ... \tag{A.38}$$

$$\psi_{+1} = \psi_{0^+} + h_2\psi_{0^+}^{'} + ... + \frac{(h_2)^6}{6!}\psi_{0^+}^{''''''} + ... \tag{A.39}$$

Replacing all $\psi_{0^+}^{(n)}$ derivatives with $\psi_{0^-}^{(n)}$ derivatives in above equations:

$$\begin{aligned}\psi_{+1} = \quad & \psi_{0^-}\left(1+\frac{\zeta_{12}h_2^2}{2!}+\frac{\zeta_{12}^2h_2^4}{4!}+\frac{\zeta_{12}^3h_2^6}{6!}\right)+\rho_{21}\psi_{0^-}^{'}\left(h_2+\frac{\zeta_{12}h_2^3}{3!}+\frac{\zeta_{12}^2h_2^5}{5!}\right)\\ & +\psi_{0^-}^{''}\left(\frac{h_2^2}{2!}+\frac{2\zeta_{12}h_2^4}{4!}+\frac{3\zeta_{12}^2h_2^6}{6!}\right)+\rho_{21}\psi_{0^-}^{'''}\left(\frac{h_2^3}{3!}+\frac{2\zeta_{12}h_2^5}{5!}\right)\end{aligned}$$

$$+\psi_{0^-}^{''''}\left(\frac{h_2^4}{4!}+\frac{3\zeta_{12}h_2^6}{6!}\right)+\rho_{21}\psi_{0^-}^{'''''}\left(\frac{h_2^5}{5!}\right)+\psi_{0^-}^{''''''}\left(\frac{h_2^6}{6!}\right) \tag{A.40}$$

Differentiating equation A.35 twice with respect to x:

$$\psi_{-2}^{''}=\psi_{0^-}^{''}-2h_1\psi_{0^-}^{'''}+\frac{(2h_1)^2}{2!}\psi_{0^-}^{''''}-\frac{(2h_1)^3}{3!}\psi_{0^-}^{'''''}+\frac{(2h_1)^4}{4!}\psi_{0^-}^{''''''}-... \tag{A.41}$$

Following the intermediate steps, we get the final relationship:

$$\begin{aligned}
\psi_{-2}^{''}= \quad & \psi_{-5}\left(b_{26}-2h_1b_{36}+\frac{(2h_1)^2}{2!}b_{46}-\frac{(2h_1)^3}{3!}b_{56}+\frac{(2h_1)^4}{4!}b_{66}\right)+\\
& \psi_{-4}\left(b_{25}-2h_1b_{35}+\frac{(2h_1)^2}{2!}b_{45}-\frac{(2h_1)^3}{3!}b_{55}+\frac{(2h_1)^4}{4!}b_{65}\right)+\\
& \psi_{-3}\left(b_{24}-2h_1b_{34}+\frac{(2h_1)^2}{2!}b_{44}-\frac{(2h_1)^3}{3!}b_{54}+\frac{(2h_1)^4}{4!}b_{64}\right)+\\
& \psi_{-2}\left(b_{23}-2h_1b_{33}+\frac{(2h_1)^2}{2!}b_{43}-\frac{(2h_1)^3}{3!}b_{53}+\frac{(2h_1)^4}{4!}b_{63}\right)+\\
& \psi_{-1}\left(p_1-2h_1p_2+\frac{(2h_1)^2}{2!}p_3-\frac{(2h_1)^3}{3!}p_4+\frac{(2h_1)^4}{4!}p_5\right)+\\
& \psi_{0}\left(b_{21}-2h_1b_{31}+\frac{(2h_1)^2}{2!}b_{41}-\frac{(2h_1)^3}{3!}b_{51}+\frac{(2h_1)^4}{4!}b_{61}\right)+\\
& \psi_{+1}\left(b_{22}-2h_1b_{32}+\frac{(2h_1)^2}{2!}b_{42}-\frac{(2h_1)^3}{3!}b_{52}+\frac{(2h_1)^4}{4!}b_{62}\right)
\end{aligned} \tag{A.42}$$

where $p_1=a\cdot b_{21}+b_{22}+b_{23}+b_{24}+b_{25}+b_{26}$, $p_2=a\cdot b_{31}+b_{32}+b_{33}+b_{34}+b_{35}+b_{36}$, $p_3=a\cdot b_{41}+b_{42}+b_{43}+b_{44}+b_{45}+b_{46}$, $p_4=a\cdot b_{51}+b_{52}+b_{53}+b_{54}+b_{55}+b_{56}$ and $p_5=a\cdot b_{61}+b_{62}+b_{63}+b_{64}+b_{65}+b_{66}$. This relation gives the seven-point second derivative approximation at two sample points before the interface. The relation at two sample points ahead of the interface is obtained by interchanging $h_2 \rightleftharpoons -h_1$, $\psi_{-1}\rightleftharpoons\psi_{-3}$, $\psi_0\rightleftharpoons\psi_{-4}$, $\psi_{+1}\rightleftharpoons\psi_{-5}$ and $n_1^2\rightleftharpoons n_2^2$.

Appendix B

STF1 Program : Zero Finding Routine, Eigenvalue Finding Routine

```
%-------------------------------------------------------------------------
% Written By : Dr. H. A. Al-Jamid
% Associate Professor, Electrical Engineering Department,
% King Fahd University, Dhahran 31261, Saudi Arabia.
%-------------------------------------------------------------------------
% zero.m is a zero-finding program based on Muller's method.
% to use it, define the function whos zero is to be found as an M-file
% ( i.e ftest.m) , then run zero.m with the initial guess.
% the ftest.m file may for example be:
%
%    function y=ftest(x);
%    y=x^2-2.001*x+1.001;
%
%    zero('ftest',1.9);
%
% where ftest is the fuction name (must be the same as the M-file name)
```

```
% 1.9 is the initial guess.

function b=zero(FunFcn,x2)

nm=30; %input('number of iterations required = ');

low=10^(-8);
h1=-1*10^(-6);
h2=.5*10^(-6);
x1=x2-h2;
x0=x1-h1;
f0=feval(FunFcn,x0);
f1=feval(FunFcn,x1);
f2=feval(FunFcn,x2);
fu=(f2-f1)/h2;
fd=(f1-f0)/h1;
%
%start loop
%
for m=1:nm;
f3=(fu-fd)/(h1+h2);
c=fu+h2*f3;
h1=h2;
pa=c-sqrt(c*c-4*f2*f3);
ma=c+sqrt(c*c-4*f2*f3);
paa=abs(pa);
maa=abs(ma);
if paa>maa
    h2=-2*f2/pa;
else
    h2=-2*f2/ma;
end%
x1=x2;
x2=x2+h2;
f1=f2;
f2=feval(FunFcn,x2);
fd=fu;%
fu=(f2-f1)/h2;
if abs(f2)<low
    zr=x2;
end
    low=min(low,abs(f2));
end
```

```
format long e
[zr feval(FunFcn,zr)]

%                              STF1
%
% This program computes the eigenvalues of guided
% TE and TM modes of a slab waveguide with an arbitrary number of
% layers.
% nps=superstrate refractive index squared. The superstrate is assumed
% to occupy the region x<0.
% nbs=substrate refractive index squared.
% ns=array containing the refractive index squared distribution of the
% layers between the superstrate and the substrate. The first entry
% corresponds to a layer next to the superstarate.
% d is similar to ns, but it contains the width distribution of the
% layers.
% Let TE=1 or any other non-zero number if TE modes are desired
% otherwise let TE=0 for TM modes.

function f=stf1(ne);
global co;
global lo;
global d;

TE = 1;
lambda = 1.55;
nps = [(0.1804+j*10.2)^2];
nbs = [1.5^2];
ns = [2.4^2 1.52^2];
d = [0.18 4];

% Start calculation.

nes=ne*ne;
k0=2*pi/lambda;
asp=k0*sqrt(nes-nps);
l1=k0*sqrt(ns(1)-nes);
rho=1;
if TE==0;rho=ns(1)/nps;end;
a=1;
b=rho*asp/l1;
co=[a b];
m=length(ns);
```

```
for s=2:m;
   l=k0*sqrt(ns(s-1)-nes);
   lp=k0*sqrt(ns(s)-nes);
   t=d(s-1);
   lt=l*t;
   rho=1;
   if TE==0;rho=ns(s)/ns(s-1);end;
   at=a*cos(lt)+b*sin(lt);
   b=rho*(-a*sin(lt)+b*cos(lt))*l/lp;
   a=at;
   co=[co a b];
   lo=[lo lp];
end;

   l=k0*sqrt(ns(m)-nes);
   asb=k0*sqrt(nes-nbs);
   t=d(m);
   lt=l*t;
   rho=1;
   if TE==0;rho=nbs/ns(m);end;

   at=a*cos(lt)+b*sin(lt);
   a=-rho*(-a*sin(lt)+b*cos(lt))*l/asb;
   f=at-a;

   co=[1 0 co a 0];
   lo=[asp lo asb];
```

Appendix C

MOL 3-Point Approximation

```
function C = threept(TE,EQ,lambda,n,h,ndp)

%   ***** Written by: Muhammmad Ajmal Khan *****
%   ***** This function calculates the Second Derivative Matrix C *****
%   ***** by using the Method of Lines (MOL), 3-Point.*****
%
%   Implements the correct B.Cs. at the Adjacent Points of Interface.
%   using Non-uniform Mesh
%   using Sparse Matrices
%   General Purpose for TE and TM mode.
%
%       C = threept(TE,EQ,lambda,n,h,ndp)
%
%   TE  Mode Selection,
%       TE=1 for TE mode, TE=0 for TM mode.
%
%   EQ  Selection for Mesh,
%       EQ=1 for Uniform Mesh, EQ=0 for Non-Uniform Mesh.
%
%   lambda  Wavelength (in micron, dont need to write with e-6).
%
%   n   Vector for Refractive Indices.
%       n(1) Refractive Index of Superstrate
```

```
%       n(2) Refractive Index of Core
%       n(3) Refractive Index of Substrate.
%
%   h   Vector array containing Mesh Size distribution in each layer.
%
%   ndp Vector array containing No. of Discretization points in each layer.

nlyr = length(n);   % No. of Layers.
tnp = sum(ndp); % Total number of discretization points

cdp = cumsum(ndp);  % Cumulative Sum of ndp.
ko = 2*pi/lambda; kos = ko*ko;

% ***** Matrix C *****
e = ones(tnp,1);

C = []; a = [];     b = [];

Ctmp = spdiags([+1*e -2*e +1*e], -1:1, tnp,tnp);

% ***** Dividing C by Mesh Size h^2 *****

C = Ctmp(1:ndp(1),:)/h(1)^2;

for m = 2:nlyr

   C = [C; Ctmp(cdp(m-1)+1:cdp(m),:)/h(m)^2];

end

% ***** Modification in the C Matrix. (Implementing B.Cs.) *****

for i=1:nlyr-1

   if EQ == 0
      t21=h(i+1)/h(i);      % For Non-uniform Mesh.
   else
      t21=1;                % For Uniform Mesh.
   end

   if TE == 1
      r21=1;            % for TE mode.
   else
```

```
      r21=(n(i+1)^2)/(n(i)^2);      % For TM Mode.
   end

   D=0.5*h(i+1)*(h(i)*r21+h(i+1));

   C(cdp(i),cdp(i)-1)=(1/D)*t21*r21;
   C(cdp(i),cdp(i))=(-1/D)*(t21*r21+1+0.5*h(i+1)^2*kos*(n(i)^2-n(i+1)^2));
   C(cdp(i),cdp(i)+1)=(1/D)*1;

end

% ***** End of Function Program *****
```

Appendix D

MOL 5-Point Approximation

```
function C = fivept(TE,EQ,lambda,n,h,ndp)

%   ***** Written by: Muhammmad Ajmal Khan *****
%   ***** This function calculates the Second Derivative Matrix C *****
%   ***** by using the Method of Lines (MoL), 5-Point.*****
%
%   Implements the correct B.Cs. at the Adjacent Points of Interface.
%   using Non-uniform Mesh
%   using Sparse Matrices
%   General Purpose for TE and TM mode.
%
%       C = fivept(TE,EQ,lambda,n,h,ndp)
%
%   TE  Mode Selection,
%       TE=1 for TE mode, TE=0 for TM mode.
%
%   EQ  Selection for Mesh,
%       EQ=1 for Uniform Mesh, EQ=0 for Non-Uniform Mesh.
%
%   lambda  Wavelength (in micron, dont need to write with e-6).
%
%   n   Vector for Refractive Indices.
%       n(1) Refractive Index of Superstrate
```

```
%       n(2) Refractive Index of Core
%       n(3) Refractive Index of Substrate.
%
%   h   Vector array containing Mesh Size distribution in each layer.
%
%   ndp Vector array containing No. of Discretization points in each layer.

nlyr = length(n);   % No. of Layers.
tnp = sum(ndp); % Total number of discretization points

cdp = cumsum(ndp);  % Cumulative Sum of ndp.
ko = 2*pi/lambda; kos = ko*ko;

% ***** Matrix C *****
e = ones(tnp,1);

C = []; a = [];     b = [];

div  = 12;

Ctmp = spdiags([-1/div*e 16/div*e -30/div*e 16/div*e -1/div*e],
-2:2, tnp,tnp);

% ***** Dividing C by Mesh Size h^2 *****

C = Ctmp(1:ndp(1),:)/h(1)^2;

for m = 2:length(ndp)

   C = [C; Ctmp(cdp(m-1)+1:cdp(m),:)/h(m)^2];

end


   % ***** Modification in the C Matrix. (Implementing I.C.) *****

   for i=1:nlyr-1

      h1 = h(i);            h2 = h(i+1);
      z12 = kos*(n(i)^2-n(i+1)^2);

      if EQ == 0
         t21=h(i+1)/h(i);       % For Non-uniform Mesh.
```

```
else
   t21=1;              % For Uniform Mesh.
end

if TE == 1
   r21=1;          % for TE mode.
else
   r21=(n(i+1)^2)/(n(i)^2);       % For TM Mode.
end

a0 = 1+h2^2*z12/2+h2^4*z12^2/24;
b0 = 1+2*h2^2*z12+2*h2^4*z12^2/3;

a(1,1) = r21*(h2+h2^3*z12/6);
a(1,2) = 1/2*h2^2+h2^4*z12/12;
a(1,3) = r21*h2^3/6;
a(1,4) = h2^4/24;

a(2,1) = r21*(2*h2+4*h2^3*z12/3);
a(2,2) = 2*h2^2+4*h2^4*z12/3;
a(2,3) = r21*4*h2^3/3;
a(2,4) = 2*h2^4/3;

a(3,1) = -h1;
a(3,2) = h1^2/2;
a(3,3) = -h1^3/6;
a(3,4) = h1^4/24;

a(4,1) = -2*h1;
a(4,2) = 2*h1^2;
a(4,3) = -4/3*h1^3;
a(4,4) = 2/3*h1^4;

b = inv(a);

% ***** On the Interface. *****

C(cdp(i),cdp(i)+2) = b(2,2);
C(cdp(i),cdp(i)+1) = b(2,1);
C(cdp(i),cdp(i)+0) = -(a0*b(2,1)+b0*b(2,2)+...
                       b(2,3)+b(2,4));
C(cdp(i),cdp(i)-1) = b(2,3);
C(cdp(i),cdp(i)-2) = b(2,4);
```

```
   % ***** ONE Sample Point Ahead of the Interface. *****

  a0 = 1-1/2*h1^2*z12+1/24*h1^4*z12^2;

  a(1,1) = h2;
  a(1,2) = h2^2/2;
  a(1,3) = h2^3/6;
  a(1,4) = h2^4/24;

  a(2,1) = 2*h2;
  a(2,2) = 2*h2^2;
  a(2,3) = 4*h2^3/3;
  a(2,4) = 2*h2^4/3;

  a(3,1) = 3*h2;
  a(3,2) = 9*h2^2/2;
  a(3,3) = 9*h2^3/2;
  a(3,4) = 27*h2^4/8;

  a(4,1) = (1/r21)*(-h1+1/6*h1^3*z12);
  a(4,2) = h1^2/2-1/12*h1^4*z12;
  a(4,3) = -h1^3/(6*r21);
  a(4,4) = h1^4/24;

  b = inv(a);

  p1 = b(2,1)+b(2,2)+b(2,3)+a0*b(2,4);
  p2 = b(3,1)+b(3,2)+b(3,3)+a0*b(3,4);
  p3 = b(4,1)+b(4,2)+b(4,3)+a0*b(4,4);

C(cdp(i)+1,cdp(i)+3) = b(2,3)+h2*b(3,3)+0.5*h2^2*b(4,3);
C(cdp(i)+1,cdp(i)+2) = b(2,2)+h2*b(3,2)+0.5*h2^2*b(4,2);
C(cdp(i)+1,cdp(i)+1) = b(2,1)+h2*b(3,1)+0.5*h2^2*b(4,1);
C(cdp(i)+1,cdp(i)+0) = -(p1+h2*p2+0.5*h2^2*p3);
C(cdp(i)+1,cdp(i)-1) = b(2,4)+h2*b(3,4)+0.5*h2^2*b(4,4);

  % ***** ONE Sample Point Before the Interface. *****

  a0 = 1+1/2*h2^2*z12+1/24*h2^4*z12^2;
  z12 = kos*(n(i+1)^2-n(i)^2);
```

```
      a(1,1) = -h1;
      a(1,2) = 1/2*h1^2;
      a(1,3) = -h1^3/6;
      a(1,4) = h1^4/24;

      a(2,1) = -2*h1;
      a(2,2) = 2*h1^2;
      a(2,3) = -4*h1^3/3;
      a(2,4) = 2*h1^4/3;

      a(3,1) = -3*h1;
      a(3,2) = 9*h1^2/2;
      a(3,3) = -9*h1^3/2;
      a(3,4) = 27*h1^4/8;

      a(4,1) =  r21*(h2-1/6*h2^3*z12);
      a(4,2) =  h2^2/2-1/12*h2^4*z12;
      a(4,3) =  1/6*h2^3*r21;
      a(4,4) =  h2^4/24;

      b = inv(a);

      p1 = b(2,1)+b(2,2)+b(2,3)+a0*b(2,4);
      p2 = b(3,1)+b(3,2)+b(3,3)+a0*b(3,4);
      p3 = b(4,1)+b(4,2)+b(4,3)+a0*b(4,4);

     C(cdp(i)-1,cdp(i)-3) = b(2,3)-h1*b(3,3)+0.5*h1^2*b(4,3);
     C(cdp(i)-1,cdp(i)-2) = b(2,2)-h1*b(3,2)+0.5*h1^2*b(4,2);
     C(cdp(i)-1,cdp(i)-1) = b(2,1)-h1*b(3,1)+0.5*h1^2*b(4,1);
     C(cdp(i)-1,cdp(i)+0)   = -p1+h1*p2-0.5*h1^2*p3;
     C(cdp(i)-1,cdp(i)+1) = b(2,4)-h1*b(3,4)+0.5*h1^2*b(4,4);

    end


% ***** End of Function Program *****
```

Appendix E

MOL 7-Point Approximation

```
function C = sevenpt(TE,EQ,lambda,n,h,ndp)

%   ***** Written by: Muhammmad Ajmal Khan *****
%   ***** This function calculates the Second Derivative Matrix C *****
%   ***** by using the Method of Lines (MoL), 7-Point.*****
%
%   Implements the correct B.Cs. at the Adjacent Points of Interface.
%   using Non-uniform Mesh
%   using Sparse Matrices
%   General Purpose for TE and TM mode.
%
%       C = sevenpt(TE,EQ,lambda,n,h,ndp)
%
%   TE  Mode Selection,
%       TE=1 for TE mode, TE=0 for TM mode.
%
%   EQ  Selection for Mesh,
%       EQ=1 for Uniform Mesh, EQ=0 for Non-Uniform Mesh.
%
%   lambda  Wavelength (in micron, dont need to write with e-6).
%
%   n   Vector for Refractive Indices.
%       n(1) Refractive Index of Superstrate
```

```
%       n(2) Refractive Index of Core
%       n(3) Refractive Index of Substrate.
%
%   h   Vector array containing Mesh Size distribution in each layer.
%
%   ndp Vector array containing No. of Discretization points in each layer.



nlyr = length(n);   % No. of Layers.
tnp = sum(ndp); % Total number of discretization points

cdp = cumsum(ndp);  % Cumulative Sum of ndp.
ko = 2*pi/lambda; kos = ko*ko;


    % ***** Matrix C *****
    e = ones(tnp,1);

    C = []; a = [];     b = [];

    div  = 180;

   Ctmp = spdiags([2/div*e -27/div*e 270/div*e -490/div*e,...
         270/div*e -27/div*e 2/div*e], -3:3, tnp,tnp);

   % ***** Dividing C by Mesh Size h^2 *****

   C = Ctmp(1:ndp(1),:)/h(1)^2;

   for m = 2:length(ndp)

      C = [C; Ctmp(cdp(m-1)+1:cdp(m),:)/h(m)^2];

   end


% ***** Modification in the C Matrix. (Implementing I.C.) *****

for i=1:nlyr-1

      h1 = h(i);            h2 = h(i+1);
      z12 = kos*(n(i)^2-n(i+1)^2);
```

```
if EQ == 0
   t21=h(i+1)/h(i);       % For Non-uniform Mesh.
else
   t21=1;             % For Uniform Mesh.
end

if TE == 1
   r21=1;         % for TE mode.
else
   r21=(n(i+1)^2)/(n(i)^2);       % For TM Mode.
end

% ***** ON the Interface. *****

a0 = 1+1/2*z12*h2^2+1/24*z12^2*h2^4+1/720*z12^3*h2^6;
b0 = 1+2*z12*h2^2+2/3*z12^2*h2^4+4/45*z12^3*h2^6;
c0 = 1+9/2*z12*h2^2+27/8*z12^2*h2^4+81/80*z12^3*h2^6;

a(1,1) = r21*(h2+1/6*z12*h2^3+1/120*z12^2*h2^5);
a(1,2) = 1/2*h2^2+1/12*z12*h2^4+1/240*z12^2*h2^6;
a(1,3) = r21*(1/6*h2^3+1/60*z12*h2^5);
a(1,4) = 1/24*h2^4+1/240*z12*h2^6;
a(1,5) = r21*1/120*h2^5;
a(1,6) = 1/720*h2^6;

a(2,1) = r21*(2*h2+4/3*z12*h2^3+4/15*z12^2*h2^5);
a(2,2) = 2*h2^2+4/3*z12*h2^4+4/15*z12^2*h2^6;
a(2,3) = r21*(4/3*h2^3+8/15*z12*h2^5);
a(2,4) = 2/3*h2^4+4/15*z12*h2^6;
a(2,5) = r21*4/15*h2^5;
a(2,6) = 4/45*h2^6;

a(3,1) = r21*(3*h2+9/2*z12*h2^3+81/40*z12^2*h2^5);
a(3,2) = 9/2*h2^2+27/4*z12*h2^4+243/80*z12^2*h2^6;
a(3,3) = r21*(9/2*h2^3+81/20*z12*h2^5);
a(3,4) = 27/8*h2^4+243/80*z12*h2^6;
a(3,5) = r21*81/40*h2^5;
a(3,6) = 81/80*h2^6;

a(4,1) = -h1;
a(4,2) = 1/2*h1^2;
a(4,3) = -1/6*h1^3;
```

```
a(4,4) = 1/24*h1^4;
a(4,5) = -1/120*h1^5;
a(4,6) = 1/720*h1^6;

a(5,1) = -2*h1;
a(5,2) = 2*h1^2;
a(5,3) = -4/3*h1^3;
a(5,4) = 2/3*h1^4;
a(5,5) = -4/15*h1^5;
a(5,6) = 4/45*h1^6;

a(6,1) = -3*h1;
a(6,2) = 9/2*h1^2;
a(6,3) = -9/2*h1^3;
a(6,4) = 27/8*h1^4;
a(6,5) = -81/40*h1^5;
a(6,6) = 81/80*h1^6;

b=inv(a);

C(cdp(i),cdp(i)+3) = b(2,3);
C(cdp(i),cdp(i)+2) = b(2,2);
C(cdp(i),cdp(i)+1) = b(2,1);
C(cdp(i),cdp(i)+0) = -(a0*b(2,1)+b0*b(2,2)+...
                       c0*b(2,3)+b(2,4)+b(2,5)+b(2,6));
C(cdp(i),cdp(i)-1) = b(2,4);
C(cdp(i),cdp(i)-2) = b(2,5);
C(cdp(i),cdp(i)-3) = b(2,6);


% ***** ONE Sample Point BEFORE the Interface. *****

a0 = 1+1/2*z12*h2^2+1/24*z12^2*h2^4+1/720*z12^3*h2^6;
b0 = 1+2*z12*h2^2+2/3*z12^2*h2^4+4/45*z12^3*h2^6;

% a(1,:) and a(2,:) remain same.

a(3,:) = a(4,:);
a(4,:) = a(5,:);
a(5,:) = a(6,:);

a(6,1) = -4*h1;
a(6,2) = 8*h1^2;
```

```
 a(6,3) = -32/3*h1^3;
 a(6,4) = 32/3*h1^4;
 a(6,5) = -128/15*h1^5;
 a(6,6) = 256/45*h1^6;

 b=inv(a);

 p1 = a0*b(2,1)+b0*b(2,2)+b(2,3)+b(2,4)+b(2,5)+b(2,6);
 p2 = a0*b(3,1)+b0*b(3,2)+b(3,3)+b(3,4)+b(3,5)+b(3,6);
 p3 = a0*b(4,1)+b0*b(4,2)+b(4,3)+b(4,4)+b(4,5)+b(4,6);
 p4 = a0*b(5,1)+b0*b(5,2)+b(5,3)+b(5,4)+b(5,5)+b(5,6);
 p5 = a0*b(6,1)+b0*b(6,2)+b(6,3)+b(6,4)+b(6,5)+b(6,6);

C(cdp(i)-1,cdp(i)-4) = b(2,6)-h1*b(3,6)+1/2*h1^2*b(4,6)-...
                       1/6*h1^3*b(5,6)+1/24*h1^4*b(6,6);
C(cdp(i)-1,cdp(i)-3) = b(2,5)-h1*b(3,5)+1/2*h1^2*b(4,5)-...
                        1/6*h1^3*b(5,5)+1/24*h1^4*b(6,5);
C(cdp(i)-1,cdp(i)-2) = b(2,4)-h1*b(3,4)+1/2*h1^2*b(4,4)-...
                        1/6*h1^3*b(5,4)+1/24*h1^4*b(6,4);
C(cdp(i)-1,cdp(i)-1) = b(2,3)-h1*b(3,3)+1/2*h1^2*b(4,3)-...
                        1/6*h1^3*b(5,3)+1/24*h1^4*b(6,3);
C(cdp(i)-1,cdp(i)+0) = -(p1-h1*p2+1/2*h1^2*p3-...
                        1/6*h1^3*p4+1/24*h1^4*p5);
C(cdp(i)-1,cdp(i)+1) = b(2,1)-h1*b(3,1)+1/2*h1^2*b(4,1)-...
                        1/6*h1^3*b(5,1)+1/24*h1^4*b(6,1);
C(cdp(i)-1,cdp(i)+2) = b(2,2)-h1*b(3,2)+1/2*h1^2*b(4,2)-...
                        1/6*h1^3*b(5,2)+1/24*h1^4*b(6,2);


 % ***** TWO Sample Points BEFORE the Interface. *****

 % a0 and a(1,:) remain same.

 a(2,:) = a(3,:);
 a(3,:) = a(4,:);
 a(4,:) = a(5,:);
 a(5,:) = a(6,:);

 a(6,1) = -5*h1;
 a(6,2) = 25/2*h1^2;
 a(6,3) = -125/6*h1^3;
 a(6,4) = 625/24*h1^4;
 a(6,5) = -625/24*h1^5;
```

```
   a(6,6) = 3125/144*h1^6;

   b = inv(a);

   p1 = a0*b(2,1)+b(2,2)+b(2,3)+b(2,4)+b(2,5)+b(2,6);
   p2 = a0*b(3,1)+b(3,2)+b(3,3)+b(3,4)+b(3,5)+b(3,6);
   p3 = a0*b(4,1)+b(4,2)+b(4,3)+b(4,4)+b(4,5)+b(4,6);
   p4 = a0*b(5,1)+b(5,2)+b(5,3)+b(5,4)+b(5,5)+b(5,6);
   p5 = a0*b(6,1)+b(6,2)+b(6,3)+b(6,4)+b(6,5)+b(6,6);

   C(cdp(i)-2,cdp(i)-5) = b(2,6)-2*h1*b(3,6)+2*h1^2*b(4,6)-...
                          4/3*h1^3*b(5,6)+2/3*h1^4*b(6,6);
   C(cdp(i)-2,cdp(i)-4) = b(2,5)-2*h1*b(3,5)+2*h1^2*b(4,5)-...
                          4/3*h1^3*b(5,5)+2/3*h1^4*b(6,5);
   C(cdp(i)-2,cdp(i)-3) = b(2,4)-2*h1*b(3,4)+2*h1^2*b(4,4)-...
                          4/3*h1^3*b(5,4)+2/3*h1^4*b(6,4);
   C(cdp(i)-2,cdp(i)-2) = b(2,3)-2*h1*b(3,3)+2*h1^2*b(4,3)-...
                          4/3*h1^3*b(5,3)+2/3*h1^4*b(6,3);
   C(cdp(i)-2,cdp(i)-1) = b(2,2)-2*h1*b(3,2)+2*h1^2*b(4,2)-...
                          4/3*h1^3*b(5,2)+2/3*h1^4*b(6,2);
   C(cdp(i)-2,cdp(i)+0) = -(p1-2*h1*p2+2*h1^2*p3-...
                          4/3*h1^3*p4+2/3*h1^4*p5);
   C(cdp(i)-2,cdp(i)+1) = b(2,1)-2*h1*b(3,1)+2*h1^2*b(4,1)-...
                          4/3*h1^3*b(5,1)+2/3*h1^4*b(6,1);

 % ***** ONE Sample Point AHEAD the Interface. *****

n1 = n(i+1); n2 = n(i);
h1 = -h(i+1); h2 = -h(i); r21 = 1/r21;
z21=ko^2*(n1^2-n2^2);

a0=1+1/2*h2^2*z21 +1/24*h2^4*z21^2+1/720*h2^6*z21^3;
b0=1+1/2*(2*h2)^2*z21 +1/24*(2*h2)^4*z21^2+1/720*(2*h2)^6*z21^3;

a(1,1) = r21*(h2+1/6*h2^3*z21+1/120*h2^5*z21^2);
a(1,2) = 1/2*h2^2+1/12*h2^4*z21+1/240*h2^6*z21^2;
a(1,3) = r21*(1/6*h2^3+1/60*h2^5*z21);
a(1,4) = 1/24*h2^4+1/240*h2^6*z21;
a(1,5) = r21*1/120*h2^5;
a(1,6) = 1/720*h2^6;

a(2,1) = r21*(2*h2+1/6*(2*h2)^3*z21+1/120*(2*h2)^5*z21^2);
a(2,2) = 1/2*(2*h2)^2+1/12*(2*h2)^4*z21+1/240*(2*h2)^6*z21^2;
```

```
    a(2,3) = r21*(1/6*(2*h2)^3+1/60*(2*h2)^5*z21);
    a(2,4) = 1/24*(2*h2)^4+1/240*(2*h2)^6*z21;
    a(2,5) = r21*1/120*(2*h2)^5;
    a(2,6) = 1/720*(2*h2)^6;

    a(3,1) = -h1;
    a(3,2) = 1/2*h1^2;
    a(3,3) = -1/6*h1^3;
    a(3,4) = 1/24*h1^4;
    a(3,5) = -1/120*h1^5;
    a(3,6) = 1/720*h1^6;

    a(4,1) = -2*h1;
    a(4,2) = 1/2*(2*h1)^2;
    a(4,3) = -1/6*(2*h1)^3;
    a(4,4) = 1/24*(2*h1)^4;
    a(4,5) = -1/120*(2*h1)^5;
    a(4,6) = 1/720*(2*h1)^6;

    a(5,1) = -3*h1;
    a(5,2) = 1/2*(3*h1)^2;
    a(5,3) = -1/6*(3*h1)^3;
    a(5,4) = 1/24*(3*h1)^4;
    a(5,5) = -1/120*(3*h1)^5;
    a(5,6) = 1/720*(3*h1)^6;

    a(6,1) = -4*h1;
    a(6,2) = 1/2*(4*h1)^2;
    a(6,3) = -1/6*(4*h1)^3;
    a(6,4) = 1/24*(4*h1)^4;
    a(6,5) = -1/120*(4*h1)^5;
    a(6,6) = 1/720*(4*h1)^6;

    b = inv(a);
    p1   = b(2,1)*a0+b(2,2)*b0+b(2,3)+b(2,4)+b(2,5)+b(2,6);
    p2   = b(3,1)*a0+b(3,2)*b0+b(3,3)+b(3,4)+b(3,5)+b(3,6);
    p3   = b(4,1)*a0+b(4,2)*b0+b(4,3)+b(4,4)+b(4,5)+b(4,6);
    p4   = b(5,1)*a0+b(5,2)*b0+b(5,3)+b(5,4)+b(5,5)+b(5,6);
    p5   = b(6,1)*a0+b(6,2)*b0+b(6,3)+b(6,4)+b(6,5)+b(6,6);

C(cdp(i)+1,cdp(i)+4) = b(2,6)-h1*b(3,6)+1/2*h1^2*b(4,6)-...
                       1/6*h1^3*b(5,6)+1/24*h1^4*b(6,6);
```

```
C(cdp(i)+1,cdp(i)+3) = b(2,5)-h1*b(3,5)+1/2*h1^2*b(4,5)-...
                       1/6*h1^3*b(5,5)+1/24*h1^4*b(6,5);

C(cdp(i)+1,cdp(i)+2) = b(2,4)-h1*b(3,4)+1/2*h1^2*b(4,4)-...
                       1/6*h1^3*b(5,4)+1/24*h1^4*b(6,4);

C(cdp(i)+1,cdp(i)+1) = b(2,3)-h1*b(3,3)+1/2*h1^2*b(4,3)-...
                       1/6*h1^3*b(5,3)+1/24*h1^4*b(6,3);

C(cdp(i)+1,cdp(i)+0) = -p1+h1*p2-1/2*h1^2*p3+1/6*h1^3*p4-...
                        1/24*h1^4*p5;

C(cdp(i)+1,cdp(i)-1) = b(2,1)-h1*b(3,1)+1/2*h1^2*b(4,1)-...
                       1/6*h1^3*b(5,1)+1/24*h1^4*b(6,1);

C(cdp(i)+1,cdp(i)-2) = b(2,2)-h1*b(3,2)+1/2*h1^2*b(4,2)-...
                       1/6*h1^3*b(5,2)+1/24*h1^4*b(6,2);

% ***** TWO Sample Points AHEAD the Interface. *****

   a(2,:) = a(3,:);
   a(3,:) = a(4,:);
   a(4,:) = a(5,:);
   a(5,:) = a(6,:);

   a(6,1) = -5*h1;
   a(6,2) = 1/2*(5*h1)^2;
   a(6,3) = -1/6*(5*h1)^3;
   a(6,4) = 1/24*(5*h1)^4;
   a(6,5) = -1/120*(5*h1)^5;
   a(6,6) = 1/720*(5*h1)^6;

   b = inv(a);

   p1   = b(2,1)*a0+b(2,2)+b(2,3)+b(2,4)+b(2,5)+b(2,6);
   p2   = b(3,1)*a0+b(3,2)+b(3,3)+b(3,4)+b(3,5)+b(3,6);
   p3   = b(4,1)*a0+b(4,2)+b(4,3)+b(4,4)+b(4,5)+b(4,6);
   p4   = b(5,1)*a0+b(5,2)+b(5,3)+b(5,4)+b(5,5)+b(5,6);
   p5   = b(6,1)*a0+b(6,2)+b(6,3)+b(6,4)+b(6,5)+b(6,6);


C(cdp(i)+2,cdp(i)+5) = b(2,6)-2*h1*b(3,6)+1/2*(2*h1)^2*b(4,6)-...
                       1/6*(2*h1)^3*b(5,6)+1/24*(2*h1)^4*b(6,6);
```

```
C(cdp(i)+2,cdp(i)+4) = b(2,5)-2*h1*b(3,5)+1/2*(2*h1)^2*b(4,5)-...
                       1/6*(2*h1)^3*b(5,5)+1/24*(2*h1)^4*b(6,5);

C(cdp(i)+2,cdp(i)+3) = b(2,4)-2*h1*b(3,4)+1/2*(2*h1)^2*b(4,4)-...
                       1/6*(2*h1)^3*b(5,4)+1/24*(2*h1)^4*b(6,4);

C(cdp(i)+2,cdp(i)+2) = b(2,3)-2*h1*b(3,3)+1/2*(2*h1)^2*b(4,3)-...
                       1/6*(2*h1)^3*b(5,3)+1/24*(2*h1)^4*b(6,3);

C(cdp(i)+2,cdp(i)+1) = b(2,2)-2*h1*b(3,2)+1/2*(2*h1)^2*b(4,2)-...
                       1/6*(2*h1)^3*b(5,2)+1/24*(2*h1)^4*b(6,2);

C(cdp(i)+2,cdp(i)+0) = -p1+2*h1*p2-1/2*(2*h1)^2*p3+...
                        1/6*(2*h1)^3*p4-1/24*(2*h1)^4*p5;

C(cdp(i)+2,cdp(i)-1) = b(2,1)-2*h1*b(3,1)+1/2*(2*h1)^2*b(4,1)-...
                       1/6*(2*h1)^3*b(5,1)+1/24*(2*h1)^4*b(6,1);

end

% ***** End of Function Program *****
```

Appendix F

TM-Pass Transmission Mode Polarizer

```
% ***** Written by: Muhammad Ajmal Khan *****
% ***** TM-PASS TRANSMISSION MODE POLARIZER *****

% ***** This Program calculates PER, PIL and FOM *****
% ***** using Method of Lines and STF1 *****
% ***** General Purpose for 3-pt, 5-pt and 7-pt Approximation *****
% ***** using Overlap Integral to calculate Modal Power *****

clear all
close all

lambda = 1.55;
ox = 2;     % Origin of X-axis.

% ***** Constants for Input Waveguide *****

n = [1 1 1 1.52 1.5 1.5 1.5 1.5];   % Refractive Indices of the layers.
wid = [1 0.5 0.190 4 4 4 1 1];
ndp = [7 25 10 40 40 20 7 7];
```

```
% ***** Constants for the Polarizer *****

clear j;
nm = 0.1804+j*10.2;     % Gold Cladding

n1 = [1 nm 2.4 1.52 1.5 1.5 1.5 1.5];

wid1 = [1 0.5 0.185 4 4 4 1 1];
ndp1 = [7 25 10 40 40 20 7 7];

% ***** Input Waveguide *****
% ***** PML/Air/Core/Substrate/PML/PML Structure *****

EQ = 0;     % Non-Uniform Mesh.
hh = wid./ndp;
nsq = n.^2;
nlyr = length(wid);
ko = 2*pi/lambda;
kos = ko*ko;
tnp = sum(ndp);
cdp = cumsum(ndp);  %Cumulative Sum of ndp Matrix.

% ***** Introducing Imaginary Distance *****
clear j;
hh(1) = hh(1)*(1+j*0.75);
hh(nlyr-1) = hh(nlyr-1)*(1+j*0.75);
hh(nlyr) = hh(nlyr)*(1+j*1);

% ***** Matrix for Refrective Indices. *****
N = [];     dx = [];
e = ones(tnp,1);
for k = 1:nlyr
   N = [N nsq(k)*ones(1,ndp(k))];
   dx = [dx hh(k)*ones(1,ndp(k))];
end
asp = 1:tnp;
N = sparse(asp,asp,N);

% ***** Matrix C *****

TE = 1;
Ce = fivept(TE,EQ,lambda,n,hh,ndp);
```

```
TE = 0;
Cm = fivept(TE,EQ,lambda,n,hh,ndp);

% ***** Calculationg Q Matrix. *****

% ***** FOR TE MODES *****

Qe = Ce + kos*N;
[Ue,Ve] = eig(full(Qe));
Ve = diag(Ve);
[vetmp,ie] = sort(real(Ve));
l = length(Ve);

Neffer = real(sqrt(Ve(ie(l)))/ko);
Neffei = imag(sqrt(Ve(ie(l)))/ko);
fs = Ue(:,ie(l));
FSe(:,1) = abs(fs)/max(abs(fs));

% ***** FOR TM MODES *****

Qm = Cm + kos*N;
req = kos*1.52^2;
[Um,Vm] = eigs(Qm,1,req);

Neffmr = real(sqrt(diag(Vm))/ko);
Neffmi = imag(sqrt(diag(Vm))/ko);
mx = max(abs(Um));
FSm(:,1) = abs(Um)/mx;

% ***** Setting X-axis. *****

ax = []; ox = cdp(2);
for y = 1:nlyr
   ax = [ax real(hh(y))*ones(1,ndp(y))];
end
ox = sum(ax(1:ox));
x = cumsum(ax);
x = x';
x = x-ox;

figure;plot(x,FSe(:,1),'b-'); hold on;plot(x,FSm(:,1),'r-');
hold on;stem(x(cdp(1)),1,'.');hold on;stem(x(cdp(2)),1,'.');
```

```
hold on;stem(x(cdp(3)),1,'.');hold on;stem(x(cdp(4)),1,'.');
grid on; xlabel('x [\mum]');ylabel('Field Strength');
title(['TE and TM Mode Patterns of Input Waveguide']);

% ***** For the Polarizer *****
% ***** PML/Metal/Buffer/Core/Substrate/PML/PML Structure *****

hh1 = wid1./ndp1;
nsq1 = n1.^2;
ko = 2*pi/lambda;
kos = ko*ko;
tnp1 = sum(ndp1);
cdp1 = cumsum(ndp1);  %Cumulative Sum of ndp Matrix.
nlyr1 = length(wid1);

% ***** Introducing Imaginary Distance *****
clear j;
hh1(1) = hh1(1)*(1+j*0.75);
hh1(nlyr1-1) = hh1(nlyr1-1)*(1+j*0.75);
hh1(nlyr1) = hh1(nlyr1)*(1+j*1);

% ***** Matrix for Refrective Indices. *****
N1 = [];
e = ones(tnp1,1);
for k = 1:nlyr1
   N1 = [N1 nsq1(k)*ones(1,ndp1(k))];
end
asp = 1:tnp1;
N1 = sparse(asp,asp,N1);

% ***** Matrix C *****

TE = 1;
Ce1 = fivept(TE,EQ,lambda,n1,hh1,ndp1);

TE = 0;
Cm1 = fivept(TE,EQ,lambda,n1,hh1,ndp1);

% ***** Calculationg Q Matrix. *****

% ***** FOR TE MODES *****

Qe1 = Ce1 + kos*N1;
```

```
[Ue1,Ve1] = eig(full(Qe1));
Ve1 = diag(Ve1);
[vetmp,ie1] = sort(real(Ve1));
l = length(Ve1);

fs = Ue1(:,ie1(l));
FSe1(:,1) = abs(fs)/max(abs(fs));
fs = Ue1(:,ie1(l-1));
FSe1(:,2) = abs(fs)/max(abs(fs));

% ***** FOR TM MODES *****

Qm1 = Cm1 + kos*N1;
req = kos*1.52^2;
[Um1,Vm1] = eigs(Qm1,1,req);

mx = max(abs(Um1(:,1)));
FSm1(:,1) = abs(Um1(:,1))/mx;

% ***** Setting X-axis. *****

ax = []; ox = cdp1(3);
for y = 1:nlyr1
   ax = [ax real(hh1(y))*ones(1,ndp1(y))];
end
ox = sum(ax(1:ox));
x = cumsum(ax);
x = x';
x = x-ox;

figure;plot(x,FSe1(:,1),'b-');hold on;plot(x,FSe1(:,2),'b--');
hold on;plot(x,FSm1(:,1),'r-');
hold on;stem(x(cdp1(1)),1,'.');hold on;stem(x(cdp1(2)),1,'.');
hold on;stem(x(cdp1(3)),1,'.');hold on;stem(x(cdp1(4)),1,'.');
hold on;stem(x(cdp1(5)),1,'.'); grid on;
xlabel('x [\mum]');ylabel('Field Strength');
title(['TE and TM Mode Patterns of the Polarizer']);

% ***** Relfection and Transmission Matrices *****

[Ue,Ve] = eig(full(Qe));
IUe = inv(Ue);
```

```
[Um,Vm] = eig(full(Qm));
IUm = inv(Um);

[Ue1,Ve1] = eig(full(Qe1));
IUe1 = inv(Ue1);

[Um1,Vm1] = eig(full(Qm1));
IUm1 = inv(Um1);

% ***** Making Imaginary Part of V to Positive *****

for i=1:tnp
   if imag(Ve(i,i)) < 0
      Ve(i,i) = Ve(i,i)';
   end

   if imag(Vm(i,i)) < 0
      Vm(i,i) = Vm(i,i)';
   end
end

for i=1:tnp1
   if imag(Ve1(i,i)) < 0
      Ve1(i,i) = Ve1(i,i)';
   end

   if imag(Vm1(i,i)) < 0
      Vm1(i,i) = Vm1(i,i)';
   end
end

% ***** LOOP FOR FINDING POWER LOSS *****

S0Ne = Ue*diag(diag(Ve).^(-0.5))*IUe;
S0Pe = Ue*diag(diag(Ve).^(0.5))*IUe;
S1Ne = Ue1*diag(diag(Ve1).^(-0.5))*IUe1;
S1Pe = Ue1*diag(diag(Ve1).^(0.5))*IUe1;
S2Ne = Ue*diag(diag(Ve).^(-0.5))*IUe;
S2Pe = Ue*diag(diag(Ve).^(0.5))*IUe;

S0Nm = Um*diag(diag(Vm).^(-0.5))*IUm;
S0Pm = Um*diag(diag(Vm).^(0.5))*IUm;
S1Nm = Um1*diag(diag(Vm1).^(-0.5))*IUm1;
```

```
S1Pm = Um1*diag(diag(Vm1).^(0.5))*IUm1;
S2Nm = Um*diag(diag(Vm).^(-0.5))*IUm;
S2Pm = Um*diag(diag(Vm).^(0.5))*IUm;

T1e = S1Ne*S0Pe;
T2e = S2Ne*S1Pe;

T1m = S1Nm*N1*N^(-1)*S0Pm;
T2m = S2Nm*N*N1^(-1)*S1Pm;

ind=1; PLosse(1) = 1; PLossm(1) = 1;

for lp=0.01:0.01:2
ind=ind+1
% ***** Transmitted Field A1 *****
d = lp*1000;

epS1de = Ue1*diag(exp(j.*(diag(Ve1)).^0.5.*d))*IUe1;

Im = eye(tnp);

VVe = inv(Im+T2e)*(T2e-Im)*epS1de;

S1e = inv(Im+epS1de*VVe);
S2e = inv(Im-epS1de*VVe)*T1e;
K3e = inv(S1e+S2e)*(S2e-S1e);
K4e = (Im+T1e)+(Im-T1e)*K3e;
Te = inv(Im+T2e)*T2e*epS1de*K4e;
Re = K3e;

epS1dm = Um1*diag(exp(j.*(diag(Vm1)).^0.5.*d))*IUm1;
Im = eye(tnp);
VVm = inv(Im+T2m)*(T2m-Im)*epS1dm;
S1m = inv(Im+epS1dm*VVm);
S2m = inv(Im-epS1dm*VVm)*T1m;
K3m = inv(S1m+S2m)*(S2m-S1m);
K4m = (Im+T1m)+(Im-T1m)*K3m;
Tm = inv(Im+T2m)*T2m*epS1dm*K4m;
Rm = K3m;

% ***** Transmitted and Reflected Fields *****
A2e = Te*FSe(:,1);      % Transmitted Field
B0e = Re*FSe(:,1);      % Reflected Field
```

```
A2m = Tm*FSm(:,1);
B0m = Rm*FSm(:,1);

% ***** Applying OVERLAP Integral *****

ModePowere = FSe(:,1)'*(FSe(:,1).*dx.');
alphae = (A2e'*(FSe(:,1).*dx.'))/ModePowere;
ModePowerm = (FSm(:,1)'*(diag(full(N^(-1))).*(FSm(:,1).*dx.')));
alpham = (A2m'*(diag(full(N^(-1))).*(FSm(:,1).*dx.')))/ModePowerm;
PLosse(ind) = (abs(alphae))^2;
PLossm(ind) = (abs(alpham))^2;

end

PLosse = 10*abs(log10(PLosse));
PLossm = 10*abs(log10(PLossm));

d = 0:0.01:lp;
% For buffer width=0.19
Neffer = 1.506161498503201;     % by STF1.
Neffei = 1.409655693340522e-004;        % by STF1.

Neffmr = 1.512428154445819;     % by STF1.
Neffmi = 4.883292030554847e-006;        % by STF1.

% ***** Power Loss for the Polarizer by STF1 *****
ind = 0;
for lp = 0:0.01:2
   d = lp*1000;
   ind = ind+1;
   PLstf1e(ind) = 20*ko*Neffei*d*log10(exp(1));
   PLstf1m(ind) = 20*ko*Neffmi*d*log10(exp(1));
end

figure plot(d,PLossm,'r-');grid on;
xlabel('Length of Polarizer (mm)');ylabel('TMo Loss (dB)');
title('Insertion Loss')

% ***** Figure of Merit (using dB values) *****
% ((TEo Loss - TMo Loss)*(TEo Loss / TMo Loss)) / Length of Polarizer

% ***** Figure of Merit by STF1 *****
```

```
FOMs = ((PLstf1e-PLstf1m).*(PLstf1e./PLstf1m))./d;

% ***** Figure of Merit by MoL *****
FOMmol = ((PLosse-PLossm).*(PLosse./PLossm))./d;

% ***** Extinction Ratio *****
% Extinction Ratio = TEo dB Loss - TMo dB Loss
% Extinction Ratio = 10*log10 (TMo Power at Output / TEo Power at Output)

% ***** by Using STF1 *****
ExtRs = PLstf1e-PLstf1m;

% ***** by using MoL *****
ExtRmol = PLosse-PLossm;

figure plot(d,FOMs,'b--');hold on;plot(d,FOMmol,'r-');grid on;
xlabel('Length of Polarizer (mm)');
ylabel('Figure of Merit (dB/mm)');
title('Figure of Merit')
legend ('by STF1','by MOL')

figure plot(d,ExtRs,'b--');hold on;plot(d,ExtRmol,'r-');grid on;
xlabel('Length of Polarizer (mm)');
ylabel('Extinction Ratio (dB)');
title('Extinction Ratio')
legend ('by STF1','by MOL')
```

Appendix G

TM-Pass Reflection Mode Polarizer

```
% ***** Written by: Muhammad Ajmal Khan *****
% ***** TM-PASS REFLECTION MODE POLARIZER *****

% ***** Using Cascading and Doubling Algorithm.
% ***** Using Overlap Integral.
% ***** General Purpose for TMo and TEo mode.

% ***** Using Method of Lines *****
% ***** General Purpose for 3-pt, 5-pt or 7-pt Approximation. *****

clear all
close all

lambda = 1.55;

%d = 0.512387;      % Core=4 and gh=0.01
%d = 0.512392;      % Core=4 and gh=0.02
d = 0.512402;       % Core=4 and gh=0.04
%d = 0.512421;      % Core=4 and gh=0.08
```

```
%d = 0.512431;      % Core=4 and gh=0.1
%d = 0.512482;      % Core=4 and gh=0.2
%d = 0.512536;      % Core=4 and gh=0.3
%d = 0.512594;      % Core=4 and gh=0.4
%d = 0.512654;      % Core=4 and gh=0.5
%d = 0.512718;      % Core=4 and gh=0.6
%d = 0.512858;      % Core=4 and gh=0.8

TE = 0; EQ = 0;

L = 0.47;       % Length of Polarizer in mm.
L = L*1000;
buf = 0.19;     % Buffer Layer Thickness.
grv = 15;       % Number of Grating Periods in terms of 2^n.
gh = 0.04;      % Groove Depth.

% ***** Constants for Metal-Clad Section *****
clear j;
nm = 0.1804+j*10.2;     % Gold Cladding at lambda=1.55

  n = [1   nm   2.4   1.52  1.52  1.5  1.5  1.5  1.5];
wid = [1  0.5   buf    gh   3.96   4    4    1    1];
ndp = [7 25    10    10   40    40   20    7    7];

% Heigher Width part of Core i-e. including Groove Height.

  n0 = [1    1    1   1.52  1.52  1.5  1.5  1.5  1.5];
wid0 = [1  0.5   buf  gh    3.96   4    4    1    1];
ndp0 = [7 25    10  10    40    40   20    7    7];

% Lower Width part of Core i-e. excluding Groove Height.

  n1 = [1    1   1     1    1.52  1.5  1.5  1.5  1.5];
wid1 = [1  0.5  buf    gh   3.96   4    4    1    1];
ndp1 = [7 25   10    10    40   40   20    7    7];

% Other Constants for Grating.

periods = 2^grv;    % Grooves (Periods).
Lgr = periods*d/1000;

d0 = d/2;       % Grating Half Width (in microns).
d1 = d/2;
```

```
% ***** For the Metal-Clad Section *****

EQ = 0;     % Non-Uniform Mesh.
hh = wid./ndp;
nsq = n.^2;
nlyr = length(wid);
tnp = sum(ndp);
cdp = cumsum(ndp);  %Cumulative Sum of ndp Matrix.

% ***** Introducing Imaginary Distance *****
clear j;
hh(1) = hh(1)*(1+j*0.75);
hh(nlyr-1) = hh(nlyr-1)*(1+j*0.75);
hh(nlyr) = hh(nlyr)*(1+j*1);

% ***** Matrix for Refrective Indices. *****
N = [];
e = ones(tnp,1);
for k = 1:nlyr
   N = [N nsq(k)*ones(1,ndp(k))];
end
asp = 1:tnp;
N = sparse(asp,asp,N);

% ***** INPUT and OUTPUT Waveguide *****

hh0 = wid0./ndp0;
nsq0 = n0.^2;
tnp0 = sum(ndp0);
cdp0 = cumsum(ndp0);  %Cumulative Sum of ndp Matrix.
nlyr0 = length(wid0);

nsq1 = n1.^2;
cdp1 = cumsum(ndp1);
tnp1 = sum(ndp1);
nlyr1 = length(wid1);

% ***** Introducing Imaginary Distance *****
clear j;
hh0(1) = hh0(1)*(1+j*0.75);
hh0(nlyr0-1) = hh0(nlyr0-1)*(1+j*0.75);
hh0(nlyr0) = hh0(nlyr0)*(1+j*1);
```

```
hh1 = hh0;      % Grid must be same in the grating part.

% ***** Matrix for Refrective Indices. *****

N0 = []; M0 = [];
e = ones(tnp0,1);
for k = 1:nlyr0
   N0 = [N0 nsq0(k)*ones(1,ndp0(k))];
   M0 = [M0 hh0(k)*ones(1,ndp0(k))];
end
asp = 1:tnp0;
N0 = sparse(asp,asp,N0);

N1 = [];
for k = 1:nlyr1
   N1 = [N1 nsq1(k)*ones(1,ndp1(k))];
end
asp = 1:tnp1;
N1 = sparse(asp,asp,N1);

% ***** START MAIN LOOP *****
% ***** START MAIN LOOP FOR REFLECTIVITY AND TRANSMISSIVITY *****

index = 0;

lamb = 1.5498:0.00001:1.5502;

for index = 1:length(lamb)

   lambda = lamb(index);
   ko = 2*pi/lambda;
   kos = ko*ko;

   disp (['Loop No. ',num2str(index)]);

% ***** Transmission Mode Polarizer *****
% ***** PML/Metal/Buffer/Core/Substrate/PML Structure *****

% ***** Matrix C *****

C = sevenpt(TE,EQ,lambda,n,hh,ndp);

% ***** Calculationg Q Matrix. *****
```

```
Q = C + kos*N;

% ***** Waveguide with Gratings for Ref and Trn *****
% ***** PML/Air/Core/Substrate/PML Structure *****

% ***** Matrix C0 *****

C0 = sevenpt(TE,EQ,lambda,n0,hh0,ndp0);

% ***** Calculationg Q Matrix. *****

% ***** FOR TE MODES *****
Q0 = C0 + kos*N0;
[U0,V0] = eig(full(Q0));
V0 = diag(V0);
[vtmp,ie] = sort(real(V0));
l = length(V0);
fs = U0(:,ie(l));
FS(:,1) = abs(fs)/max(abs(fs));

% ***** Matrix C1 *****

C1 = sevenpt(TE,EQ,lambda,n1,hh1,ndp1);

% ***** Calculationg Q Matrix. *****

Q1 = C1 + kos*N1;

% ***** Computing Eigen Values and Eigen Vectors for each *****

[U,V] = eig(full(Q));
IU = inv(U);

[U0,V0] = eig(full(Q0));
IU0 = inv(U0);

[U1,V1] = eig(full(Q1));
IU1 = inv(U1);

% ***** Making Imaginary Part of V to Positive *****
for i=1:tnp
   if imag(V(i,i)) < 0
```

```
      V(i,i) = V(i,i)';
   end
end

% ***** Making Imaginary Part of V0 to Positive *****
for i=1:tnp0
   if imag(V0(i,i)) < 0
      V0(i,i) = V0(i,i)';
   end
end

% ***** Making Imaginary Part of V1 to Positive *****
for i=1:tnp1
   if imag(V1(i,i)) < 0
      V1(i,i) = V1(i,i)';
   end
end

% ***** Reflected and Transmitted Field
%       from Gratings in the Polarizer *****

S0Ng = U0*diag(diag(V0).^(-0.5))*IU0;
S0Pg = U0*diag(diag(V0).^(0.5))*IU0;

S1Ng = U1*diag(diag(V1).^(-0.5))*IU1;
S1Pg = U1*diag(diag(V1).^(0.5))*IU1;

epS0d0g = U0*diag(exp(j.*(diag(V0).^0.5).*d0))*IU0;
epS1d1g = U1*diag(exp(j.*(diag(V1).^0.5).*d1))*IU1;

% ***** Single Interface *****

if TE == 1
   T1g = S0Ng*S1Pg;
else
   T1g = S0Ng*N0*N1^(-1)*S1Pg;
end

Im = eye(tnp0);
R1g = (Im-T1g)*inv(Im+T1g);

% ***** Double Interface *****
```

```
eReTg = inv(Im-(epS1d1g*R1g)^2)*epS1d1g*(Im+R1g);
Rg = R1g+(Im-R1g)*epS1d1g*(-R1g)*eReTg;
Tg = (Im-R1g)*eReTg;

% ***** Applying Doubling Algorithm *****

Rg = epS0d0g*Rg; Tg = epS0d0g*Tg;

for i = 1:grv

   eReTg = inv(Im-(Rg)^2)*Tg;
   Rg = Rg+Tg*Rg*eReTg;
   Tg = Tg*eReTg;

end

% ***** The Grating Part *****
RB1g = Rg; TB2g = Tg;

% ***** R & T of the Transmission Mode Polarizer *****
% ***** using Double Discontinuity Expression *****

SMN = U*diag(diag(V).^(-0.5))*IU;
SMP = U*diag(diag(V).^(0.5))*IU;

if TE == 1
   T1 = SMN*S0Pg;
   T2 = S0Ng*SMP;
else
   T1 = SMN*N*N0^(-1)*S0Pg;
   T2 = S0Ng*N0*N^(-1)*SMP;
end

epSMd = U*diag(exp(j.*(diag(V)).^0.5.*L))*IU;

Im = eye(tnp);

VV = inv(Im+T2)*(T2-Im)*epSMd;

S1 = inv(Im+epSMd*VV);
S2 = inv(Im-epSMd*VV)*T1;
K3 = inv(S1+S2)*(S2-S1);
K4 = (Im+T1)+(Im-T1)*K3;
```

```
TA2 = inv(Im+T2)*T2*epSMd*K4;
RA1 = K3;

% ***** Net R & T of First Interface and Polarizer *****
% ***** Using Cascading Algorithm *****

dd = d/4;

epSd1 = U0*diag(exp(j.*(diag(V0).^0.5).*dd))*IU0;
eReT1 = inv(Im-(epSd1*RA1*epSd1*RB1g))*epSd1*TA2;
R01 = RA1 + TA2*epSd1*RB1g*eReT1;
T02 = TB2g*eReT1;

% ***** Transmitted and Reflected Fields *****

A2 = T02*FS(:,1); B0 = R01*FS(:,1);

% ***** Applying OVERLAPPING Method *****
% ***** Modal Power Loss exactly at the Output z=0 *****

if TE == 1
   ModePower = FS(:,1)'*(FS(:,1).*M0.');
   alpha = (A2'*(FS(:,1).*M0.'))/ModePower;
   beeta = (B0'*(FS(:,1).*M0.'))/ModePower;
else

   ModePower = (FS(:,1)'*(diag(full(N0^(-1))).*(FS(:,1).*M0.')));
   alpha = (A2'*(diag(full(N0^(-1))).*(FS(:,1).*M0.')))/ModePower;
   beeta = (B0'*(diag(full(N0^(-1))).*(FS(:,1).*M0.')))/ModePower;
end

Ref(index) = (abs(beeta))^2;
Trn(index) = (abs(alpha))^2;

end     % end of Main Loop.


figure;plot(lamb,Ref,'b-'); grid on; xlabel('Wavelength [\mum]');
ylabel('Modal Reflectivity');
title(['TE_0/TM_0 Mode (Periods=',num2str(periods),...
      ,'Lgr=',num2str(Lgr),...
      'um, gh=',num2str(gh),'um, dd=',num2str(dd),...
      'um, buf=',num2str(buf),'um, L=',num2str(L/1000),'mm)']);
```

```
figure;plot(lamb,Trn,'r-'); grid on; xlabel('Wavelength [\mum]');
ylabel('Modal Transmissivity');
title(['TE_0/TM_0 Mode (Periods=',num2str(periods),...
      ', Lgr=',num2str(Lgr),...
      'um, gh=',num2str(gh),'um, dd=',num2str(dd),...
      'um, buf=',num2str(buf),'um, L=',num2str(L/1000),'mm)']);
```

Bibliography

[1] S. E. Miller, "Light propagation in generalized lenslike media," *Bell Syst. Tech. Journal*, vol. 44, pp. 2017–2064, 1965.

[2] S. E. Miller, "Integrated optics: an introduction," *Bell Syst. Tech. Journal*, vol. 48, pp. 2059–2069, 1969.

[3] T. Takano and J. Hamasaki, "Propagation modes of a metal-clad dielectric-slab waveguide for integrated optics," *IEEE Journal of Quantum Electronics*, vol. 8, pp. 206–212, Feb. 1971.

[4] E. M. Garmire and H. Stoll, "Propagation losses in metal-film-substrate optical waveguides," *IEEE Journal of Quantum Electronics*, vol. 8, pp. 763–766, Oct. 1972.

[5] I. P. Kaminow, W. L. Mammel, and H. P. Weber, "Metal-clad optical waveguides: Analytical and Experimental study," *Applied Optics*, vol. 13, pp. 396–405, Feb 1974.

[6] J. N. Polky and G. L. Mitchell, "Metal-clad planar dielectric waveguide for integrated optics," *Journal of Optical Society of America*, vol. 64, pp. 274–279, Mar 1974.

[7] A. Reisinger, "Characteristics of optical guided modes in lossy waveguides," *Applied Optics*, vol. 12, pp. 1015–1025, May 1973.

[8] A. Reisinger, "Attenuation properties of optical waveguides with a metal boundary," *Applied Physics Letters*, vol. 23, pp. 237–239, Sep 1973.

[9] M. F. Khodr, J. J. Sluss, and T. E. Batchman, "Modal analysis of PbSe-clad optical waveguides," *Lasers Appl.*, pp. 143–147, 1982.

[10] S. Ohke, Y. Cho, and T. Okabe, "TM-mode selective filter using a high refractive index lossy layer cladded optical waveguide," *Japanese Journal of Applied Physics*, vol. 25, pp. 1266–1269, 1986.

[11] M. C. McWright and T. E. Batchman, "A thin-film waveguide photodetector using hydrogenated amorphous silicon," *IEEE Journal of Lightwave Technology*, vol. 6, pp. 1854–1860, 1988.

[12] H. A. Jamid, *Absorption Loss in graded-index metal-clad optical waveguides.* PhD thesis, King Fahd University of Petroleum and Minerals, Saudi Arabia, August 1986.

[13] S. J. Al-Bader, "Ohmic loss in metal-clad graded-index optical waveguides," *IEEE Journal of Quantum Electronics*, vol. QE-22, pp. 8–11, Jan 1986.

[14] S. J. Al-Bader and H. A. Jamid, "Comparison of absorption loss in metal-clad optical waveguides," *IEEE Transactions on Microwave Theory and Techniques*, vol. MTT-34, pp. 310–314, Feb. 1986.

[15] M. Masuda, "Propagation losses of guided modes in an optical graded-index slab waveguide with metal-cladding," *IEEE Trans. on Microwave Theory and Techniques*, vol. MTT-25, pp. 773–776, Sept 1977.

[16] T. E. Batchman and S. C. Rashleigh, "Mode-selective properties of a metal-clad-dielectric-slab waveguide for integrated optics," *IEEE Journal of Quantum Electronics*, vol. QE-8, pp. 848–850, Nov. 1972.

[17] A. Shahar and A. Zussman, "Optical properties of metal-clad/$\mathrm{Pb1}-x\mathrm{Sn}_x\mathrm{Te}$ waveguides," *IEEE Proceedings*, vol. 135, pp. 349–354, October 1988.

[18] J. Ctyroky and H. J. Henning, "Thin film polarizer for Ti: LiNbO_3 waveguides at $\lambda = 1.3$ μm," *IEEE Electronics Letters*, vol. 22, pp. 756–757, July 1986.

[19] Y. Yamamoto, T. Kamiya, and H. Yanai, "Characteristics of optical guided modes in multilayer metal-clad planar optical guide with low-index dielectric buffer layer," *IEEE Journal of Quantum Electronics*, vol. QE-11, pp. 729–736, September 1975.

[20] T. Takano and J. Hamasaki, "Approximate solutions of propagating modes of a metal-clad-dielectric-slab optical waveguide," *Trans. Inst. Electron. Commun. Eng. Japan*, vol. 56-A, pp. 385–392, July 1973.

[21] G. R. Chakravarty, V. Priye, B. P. Pal, and K. Thyagarajan, "Polarizer based on a pbse-clad optical waveguide in the infrared wavelength: The role of a buffer layer," *IEEE Proc. Optoelectronics*, vol. 145, pp. 223–226, Aug. 1998.

[22] H. A. Jamid and S. J. Al-Bader, "TM-Pass polarizer using metal-clad waveguide with high index buffer layer," *Electronics Letters*, vol. 24, pp. 229–230, Feb. 1988.

[23] L. Sun and G. L. Yip, "Analysis of metal-clad optical waveguide polarizers by the vector beam propagation method.," *Applied Optics*, vol. 33, pp. 1047–1050, Feb. 1994.

[24] C. L. Xu and W. P. .Huang, *Finite-Difference Beam-Propagation Methods for Guided Wave optics*. Progress in Electromagnetics Research (PIER) 11, Elsevier Science Publishing Co., Inc., 1995.

[25] H. M. Masoudi, M. Al-Sunaidi, and J. M. Arnold, "Time-domain finite-difference beam propagation method," *IEEE Photonics Technology Letters*, vol. 11, pp. 1274–1276, Oct. 1999.

[26] S. T. Chu and S. K. Chaudhrui, *Finite-Difference-Time-Domain Methods for Optical Waveguide Analysis*. Progress in Electromagnetics Research (PIER) 11, Elsevier Science Publishing Co., Inc., 1995.

[27] A. K. Taneja and A. Sharma, "Reflection characteristics of guided wave bragg gratings using the collocation method," *SPIE Proceedings, Internationl conference on fiber optics and photonics*, vol. 3666, pp. 112–119, April 1999.

[28] Q.-H. Liu and W. C. Chew, "Analysis of discontinuities in planar dielectric waveguides : An eigenmode propagation method," *IEEE Transactions on Microwave Theory and Techniques*, vol. 39, pp. 422–430, Mar. 1991.

[29] J. Gerdes and R. Pregla, "Beam-propagation algorithm based on the method of lines," *Optical Society of America (B)*, vol. 8, pp. 389–394, Feb. 1991.

[30] U. Rogge and R. Pregla, "Method of lines for the analysis of strip-loaded optical waveguides," *Optical Society of America (B)*, vol. 8, pp. 459–463, Feb. 1991.

[31] K. S. Chiang, "Review of numerical and approximate methods for the modal analysis of general optical dielectric waveguides," *Optical and Quantum Electronics*, vol. 26, pp. 113–134, 1994.

[32] H. J. W. M. Hoekstra, "On beam propagation methods for modelling in integrated optics," *Optical and Quantum Electronics*, vol. 29, pp. 157–171, 1997.

[33] A. Sharma, *Collocation Method For Wave Propagation Through Optical Waveguiding Structures*. Progress in Electromagnetic Research, (PIER) 11, Elsevier Science Publishing Co., Inc., 1995.

[34] M. A. A. Pudensi and L. G. Ferreira, "Method to calculate the reflection and transmission of guided modes," *Journal of Optical Society of America*, vol. 72, pp. 126–130, 1982.

[35] M. J. Al-Majid, "Method of lines analysis of gaussian beam coupling to the dielectric slab waveguide," Master's thesis, King Fahd University of Petroleum and Minerals, Saudi Arabia, February 1994.

[36] M. N. Akram, "Analysis of anti-resonant reflecting optical waveguide (ARROW) grating using the method of lines," Master's thesis, King Fahd University of Petroleum and Minerals, Saudi Arabia, April 2000.

[37] S. J. Al-Bader and H. A. Jamid, "Perfectly matched layer absorbing boundary conditions for the method of lines modeling scheme," *IEEE Microwave and Guided Waves Letters*, vol. 8, pp. 357–359, November 1998.

[38] H. A. Al-Jamid, "Cascading and doubling algorithm to model long gratings." personal notes.

[39] M. J. Adams, *An Introduction to Optical Waveguides.* John Wiley and Sons Inc., 1981.

[40] A. Yariv, *Optical Electronics.* Saunders College Publishing, 4 ed., 1991.

[41] J. A. Kong, *Electromagnetic Wave Theory.* John Wiley and Sons Inc., 1986.

[42] T. Tamir, ed., *Guided-Wave Optoelectronics*, vol. 26. Springer Series, 2nd ed., 1990.

[43] D. Marcuse, *Theory of Dielectric Optical Waveguides.* Academic Press Inc., 1974.

[44] Y. P. Chiou and H. C. Chang, "Analysis of optical waveguide discontinuities using pade approximation," *IEEE Photonics Technology Letters*, vol. 9, pp. 964–966, 1997.

[45] J. Gerdes, B. Lunitz, D. Benish, and R. Pregla, "Analysis of slab waveguide discontinuities including radiation and absorption effects," *Electronics Letters*, vol. 28, p. 1013, May 1992.

[46] W. D. Yang and R. Pregla, "Method of lines for analysis of waveguide structures with multidiscontinuities," *Electronics Letters*, vol. 31, p. 892, May 1995.

[47] R. Pregla and W. Yang, "Method of lines for analysis of multilayered dielectric wavegides with bragg gratings," *Electronics Letters*, vol. 29, p. 1962, October 1993.

[48] R. Pregla and E. Ahlers, "Method of lines for analysis of discontinuities in optical waveguides," *Electronics Letters*, vol. 29, p. 1845, October 1993.

[49] A. A. Shittu, *Study of periodic waveguides by the finite-difference time-domain method and the Method of Lines.* PhD thesis, King Fahad University of Petroleum and Minerals, Dhahran 31261, Saudi Arabia, September 1994.

[50] T. Itoh, ed., *Numerical Techniques for Microwave and Millimeter-Wave Passive Structures.* John Wiley and Sons Inc., 1989.

[51] S. J. Al-Bader and H. A. Jamid, "Method of lines applied to non-linear guided waves," *Electronics Letters*, vol. 31, pp. 79–85, Feb. 1995.

[52] M. Imtaar and S. J. Al-Bader, "Analysis of diffraction from abruptly-terminated optical fibers by the method of lines," *Journal of Lightwave Technology*, vol. 13, pp. 137–141, Feb. 1995.

[53] E. Ahlers and R. Pregla, "3-D modeling of concatenations of straight and curved waveguides by MoL-BPM," *Optical and Quantum Electronics*, pp. 151–156, 1997.

[54] W. D. Yang and R. Pregla, "The method of lines for analysis of integrated optical waveguide structures with arbitrary curved interfaces," *Journal of Lightwave Technology*, vol. 14, pp. 879–884, May 1996.

[55] F. H. Al-Harbi, "Implementation of a full vectorial method of lines analysis in the study of metal clad rib waveguide," Master's thesis, King Fahd Univeristy of Petroleum and Minerals, Saudi Arabia, December 2000.

[56] H. Diestel, "Analysis of planar multiconductor transmission line systems with the method of lines," *Arch. Elektron Ueber*, vol. 41, pp. 169–175, 1987.

[57] H. Diestel and S. Worm, "Analysis of hybrid field problems by the method of lines with nonequidistant discretization," *IEEE Trans. Microwave Theory Tech.*, vol. MTT-32, no. 6, pp. 633–638, 1984.

[58] H. A. Jamid and M. N. Akram, "A new higher-order finite-difference approximation scheme for the method of lines," *IEEE Journal of Lightwave Technology*, March 2001. accepted for publication.

[59] R. Syms and J. Cozens, *Optical Guided Waves and Devices.* Shopenhangers Road, Maidenhead, Berkshire, SL6 2QL, England: McGraw-Hill Book Company Europe, 1992.

[60] B. Engquist and A. Majda, "Abosrbing boundary conditions for the numerical simulation of waves," *Math. Comput.*, vol. 31, pp. 629–651, July 1977.

[61] J. P. Berenger, "A perfectly matched layer for the absorption of electromagnetic waves," *Journal of Computational Physics*, pp. 185–200, Oct. 1994.

[62] H. A. Jamid, "Frequency-Domain PML layer based on the complex mapping of space boundary condition treatment," *IEEE Microwave and Guided Wave Letters*, vol. 10, pp. 356–358, Sep. 2000.

[63] W. C. Chew and J. M. Jin, "Perfectly matched layers in the discretized space: an analysis and optimization," *Electromagnetics*, vol. 16, no. 4, pp. 325–340, 1996.

[64] J. J. Gerdes, "Bidirectional eigenmode propagation analysis of optical waveguides based on method of lines," *Electronics Letters*, vol. 30, p. 550, March 1994.

[65] S. T. Peng and T. Tamir, "TM mode perturbation analysis of dielectric gratings," *Applied Physics*, vol. 7, no. 35, pp. 35–38, 1975.

[66] J. Rodriguez, R. D. Crespo, and S. Fernandez, "Radiation losses on discontinuities in integrated optical waveguides," *Optical Engineering*, vol. 38, pp. 1896–1906, Nov. 1999.

[67] S. J. Al-Bader and H. A. Jamid, "Mode scattering by a non-linear step-discontinuity in dielectric optical waveguides," *IEEE Transactions on Microwave theory and Techniques*, vol. 44, pp. 218–224, Feb. 1996.

[68] H. A. Jamid and S. J. Al-Bader, "Reflection and transmission of surface plasmon mode at a step discontinuity," *IEEE Photonics Technology Letters*, vol. 9, pp. 220–222, Feb. 1997.

[69] H. A. Jamid and S. J. Al-Bader, "Diffraction of surface plasmon-polaritons in an abruptly terminated dielectric-metal interface," *IEEE Photonics Technology Letters*, vol. 7, pp. 321–323, Mar. 1995.

[70] G. Grand and S. Valette, "Optical polarizers of high extinction ration integrated on oxidised silicon substrate," *Electronics Letters*, vol. 20, pp. 730–731, 1984.

[71] J. P. G. Bristow, A. C. G. Nutt, and P. J. R. Laybourn, "Novel integrated optical polarizers using surface plasma waves and ion milled grooves in lithium niobate," *IEEE Electronics Letters*, vol. 20, no. 25/26, pp. 1047–1048, 1984.

[72] K. H. Rollke and W. Sohler, "Metal-clad waveguide as a cutoff polarizer for integrated optics," *IEEE Journal of Quantum Electronics*, vol. QE-13, no. 141-145, 1977.

[73] J. J. Veselka and G. A. Bogert, "Low-loss TM-Pass polarizer fabricated by proton exchange for Z-cut Ti: $LiNbO_3$ waveguides," *Electronics Letters*, vol. 23, pp. 29–30, 1987.

[74] D. E. Muller, "A method for solving algebraic equations using an automatic computer," *MTAC*, vol. 10, pp. 208–215, 1956.

[75] T. Nakano, K. Baba, and M. Miyagi, "Insertion loss and extinction ration of a surface plasmon-polariton polarizer: theoretical analysis," *Journal of Optical Society of America B*, vol. 11, pp. 2030–2035, October 1994.

[76] C. Elachi, "Waves in active and passive periodic structures: A Review," *IEEE Proceedings*, vol. 64, pp. 1666–1698, Dec. 1976.

[77] T. Tamir and S. T. Peng, "Analysis and design of grating couplers," *Applied Physics*, vol. 14, pp. 235–254, 1977.

[78] M. T. Wlodarczyk and S. R. Seshadri, "Analysis of grating couplers for planar dielectric waveguides," *Journal of Applied Physics*, vol. 58, pp. 69–87, July 1985.

[79] A. Yariv, "Periodic structures for integrated optics," *IEEE Journal of Quantum Electronics*, vol. 14, pp. 233–253, Apr. 1977.

[80] W. Streifer, D. R. Scifres, and R. D. Burnham, "Coupling coefficients for distributed feedback single- and double-hetrostructure diode lasers," *IEEE Journal of Quantum Electronics*, vol. 11, pp. 867–873, Nov. 1975.

[81] W. Streifer, D. R. Scifres, and R. D. Burnham, "Coupled wave analysis of dfb and dbr lasers," *IEEE Journal of Quantum Electronics*, vol. 13, pp. 134–141, Apr. 1977.

[82] Y. Yamamoto, T. Kamiya, and H. Yanai, "Improved coupled mode analysis of corrugated waveguides and lasers.," *IEEE Journal of Quantum Electronics*, vol. 14, pp. 245–258, Apr. 1978.

[83] H. Nishihara, M. Haruna, and T. Suhara, *Optical Integrated Circuits*. McGraw-Hill, 1989.

[84] D. C. Flanders and H. Kogelnick, "Grating filters for thin-film optical waveguides," *Applied Physics Letters*, vol. 24, pp. 194–196, Feb. 1974.

[85] K. A. Winick, "Effective-index method and coupled-mode theory for almost-periodic waveguide gratings: a comparison," *Applied Optics*, vol. 31, pp. 757–764, Feb. 1992.

[86] J. Ctyroky, S. Helfert, and R. Pregla, "Analysis of deep waveguide bragg gratings," *Optical and Quantum Electronics*, pp. 343–358, 1998.

Vita

1973/12 : Born in Karachi, Islamic Republic of Pakistan.

1989 : Matriculation with Science Major.

1991 : H.Sc. (with distinction) Pre-Engineering.

1992-1997 : B.E. Electrical Engineering, N.E.D. University of Engineering and Technology, Karachi, Pakistan, Major : Communication, Electronics and Power Systems. First Class First Position.

1997-1999 : Teaching in N.E.D. University of Engineering and Technology, Karachi, Pakistan, as Lecturer.

1999-2001 : M.S. Electrical Engineering, King Fahd University of Engineering and Technology, Dhahran, Saudi Arabia. Worked on integrated optics modeling, waveguide discontinuities, gratings and Metal-Clad waveguide using numerical Method of Lines (MOL). Worked on Finite-Difference Time-Domain (FDTD) method to model electro-magnetic wave propagation. **Thesis Advisor :** Dr. Hussain A. Al-Jamid.

Worked as a Research/Teaching Assistant in the Electrical Engineering department. Have been member of Computer Utilization Committee (CUC) of the EE department and involved in system and network administration and web page designing.